Excessive iron accumulation mediated oxidative stress and β-cell dysfunction via perturbations of insulin secretion in MIN6 cells

Blesia, V.

Excessive iron accumulation mediated oxidative stress and β-cell dysfunction via perturbations of insulin secretion in MIN6 cells

By

Voni Blesia

School of Life Sciences
University of Westminster, London

A thesis submitted to the University of Westminster in candidature for the award of the degree of Doctor of Philosophy

April 2020

Acknowledgment

With love and appreciation, I would like to extend my profound gratitude to Jesus Christ, the one who makes everything works together for my good. Blessings and favours have been mine and given freely during the year of studies.

This thesis simply would not have been finished without the following people who provided enthusiastic help and support.

My supervisor, Dr. Mohammed Gulrez Zariwala whose countless support, guidance, and constant advice that helped in finishing the project strongly. I am deeply indebted to him for the encouragement and advice that made a strong, compassionate, and hard-working person.

My extended supervisors, Dr. Vinood Patel & Dr. Hisham Al-Obaidi whose sincere help made it possible for me to complete this project.

I humbly extend my gratitude to Mr. Thakor Tandel as one of the technicians who helped with invaluable guidance for running few experiments.

All colleagues at PhD office, especially Priya Mani, Thula Ganeshan, and Leah Mursaleen who provided me with passionate encouragement and thoughtful ideas throughout the course.

My phenomenal father, Robert Blesia and siblings, Leni, Michael and Jhon, and entire family whose prayers, love and overwhelming encouragement have been constant in pushing me to reach the potential beyond limit. Every effort, tear, and joy of this work is dedicated to the memory of my loving mother who is in heaven.

To Indonesia Endowment Fund for Education (LPDP), the financial support of Indonesia scholarship that funded me throughout my course.

Declaration

I, Voni Blesia, do hereby declare that the thesis entitled **Excessive iron accumulation mediated oxidative stress and β-cell dysfunction via perturbations of insulin secretion in MIN6 cells** has been undertaken by me for the award of Doctor of Philosophy. I have completed this study under the guidance of **Dr. Mohammed Gulrez Zariwala, B.Pharm, MSc, PhD, CMgr MCMI, FHEA, Assistant Head of School & Reader in Translational Physiology, School of Life `sciences, University of Westminster, London**.

I also declare that this thesis has not been submitted for the award of any Degree, Diploma, Master, Associate-ship or Fellowship or any other title in this University or any other University.

Place : London

Date : 16th of April 2020

Voni Blesia

W1564070

Abstract

Type 2 diabetes mellitus (T2DM) is the predominant form of diabetes, with prevalence increasing steadily both in developed and developing countries. Defects in both insulin action and insulin secretion are known to contribute to the development of T2DM. Reactive oxygen species (ROS) mediated cellular oxidative damage has been implicated in cellular dysfunction in various organs and disease states. Exposure to high level of glucose during hyperglycaemia has been co-related to ROS generation and oxidative stress in β-cells. In the initial series of experiments MIN6 pseudoislets were cultured under standard conditions and exposed to a range of iron concentrations (20 µM – 100 µM; signifying low to high iron exposure) at predefined glucose levels (5.5 mM and 11 mM) in a static incubation experiment. These series of experiments were categorised into two type of timelines in which experiments were carried. These timelines were at 24 and 48 h and 48 and 72 h. Within the timeline of 24 & 48 h, insulin secretion & content, expression of SNAP-25, mitochondrial oxygen consumption rate (OCR), mitochondrial membrane potential (Δψm), and protein carbonylation were estimated. In addition, antioxidant activity (cellular/non-cellular), cytotoxicity, and cellular ferritin were assessed using the shell of nanocarriers composed of (i) potato protein (PP) - potato dextrin (PD), (ii) PP - modified citrus pectin (MCP) used to formulate Fe and hesperetin in the presence/absence of EGCG. These experiments were followed by assessments of cellular iron content, lipid peroxidation, and cell viability at 48 & 72 h. Our results suggest that presence of 100 µM iron exerted the most detrimental effect on MIN6 β-cell viability and this alteration was consistent with the data from cellular iron uptake analysis, lipid peroxidation, protein carbonyl, OCR, Δψm, SNAP-25, and insulin secretion and its content. All nanocarrier formulations coated antioxidant especially MCP demonstrated higher stability and robustness compared to dextrin control and the ability to resist the inhibitory effect of a potent iron inhibitor highlight its potential as an iron delivery vehicle. These data indicate that excessive iron and glucose accumulation, and consequent oxidative stress results in cellular membrane and

mitochondrial damage and disruption. The perturbations in mitochondria functionality correlate with diminishing of MIN6 β-cell insulin secretion, suggesting a mechanistic role for iron overload in the development and progression of type 2 diabetes. These nanoformulations may be potentially used as a model to counter oxidative stress in pancreatic β-cell.

Table of Contents

LIST OF FIGURES

LIST OF TABLES

Abbreviation

ABAP: 2,2’-azobis(2-aminopropane)

ADP: Adenosine diphosphate

APS: Ammonium persulphate

ATP: Adenosine triphosphate

AUC: Area under curve

BCA: bicinchoninic acid

BSA: Bovine serum albumin

CAA: Cellular antioxidant activity

cAMP: cyclic adenosine monophosphate

CAT: Catalase

C-peptide: Connecting peptide

DCFH: 2′,7′-Dichlorofluorescin

DCFH-DA: Dichlorofluorescin diacetate

Dcyt-b: Duodenal cytochrome-b

dH_2O: Distilled water

DI: Diabetes insipidus

DMEM: Dulbecco's Modified Eagle Medium

DMSO: dimethyl sulfoxide

DMT1: Divalent metal transporter 1

DNA: Deoxyribonucleic acid

DNP: Dinitrophenylhydrazine

DPBS: Dulbecco's Phosphate Buffered Saline

DPP-4: Dipeptidyl peptidase-4

DTT: Dithiothreitol

ECL: Enhanced chemiluminescence

EGCG: Epigallocatechin gallate

ELISA: Enzyme-linked immunosorbent assay

EPAC2/cAMP: Exchange protein is activated by cAMP2

ETC: electron transport chain

FBS: Foetal bovine serum

FCCP: carbonyl cyanide p-trifluoromethoxy-phenylhydrazone

Fe^{+2}: Ferrous iron

Fe^{+3}: Ferric iron

$FeSO_4$: Ferrous sulfate

FFA: Free fatty acid

Fig: Figure

FPN1: Ferroprotein 1

FRAP: Ferric reducing antioxidant power

GEF II: Guanine nucleotide exchange factor II

GIP: Glucose-dependent insulinotropic peptide

GIPR: GIP receptor

GLP-1: Glucagon-like peptide- 1

GLP-1R: GLP-1 receptor

GLUTs: Glucose transporters

GLUT2: Glucose transporter 2

GLUT4: Glucose transporter 4

GPx: Glutathione peroxidase

HAMP: hepcidin gene

HBSS: Hanks' Balanced Salt Solution

HCP1: Haem carrier protein 1

HEPES: 4-(2-hydroxyethyl)-1-piperazineethanesulfonic acid

HH: Hereditary hemochromatosis

HNE: 4-hydroxy-2-nonenal

HO1: Haem oxygenase 1

H_2O_2: Hydrogen peroxide

IDF: International Diabetes Federation

IDDM: Insulin-dependent diabetes mellitus

IMM: Inner mitochondrial membrane

IMS: Inter membrane space

IREs: Iron-responsive elements

IRPs: Iron-regulatory proteins

ISC: Iron sulfur cluster

K_{ATP}: ATP-sensitive K

Kir6.2: Inwardly rectifying K_+ channel 6.2 subunits

KRBB: Krebs-Ringer Bicarbonate Buffer

LIP: Labile iron pool

LOOH: lipid hydroperoxides

LVDCC: L-type voltage-dependent calcium channel

PKA: protein kinase A

MCPD: Modified citrus pectin dextran

MDA: Malondialdehyde

MEM: Minimum Essential Medium

MIN6: Mouse insulinoma 6

mM: millimolar

mPTP: mitochondrial permeability transition pore

mRNA: Messenger ribonucleic acid

Mtf: Mitoferrin

MtFt: mitochondrial ferritin

MTT: 3- (4,5- dimethylthiazol-2-yl) -2,5-diphenyl tetrazolium bromide

NF: nanoformulation

NaCl: Sodium chloride

NADPH: Nicotinamide adenine dinucleotide phosphate hydrogen

NO: Nitric oxide

OCR: Oxygen consumption rate

•OH: Hydroxyl radical

OMM: Outer mitochondrial membrane

OS: Oxidative stress

OXPHOS: Mitochondrial oxidative phosphorylation

O_{2-}.: Superoxide anion

PC: Pyruvate carboxylase

PDH: Pyruvate dehydrogenase

PFA: Paraformaldehyde

PIC: Protease inhibitor cocktail

PKA: Protein kinase A

PP: Potato protein

PUFA: Polyunsaturated fatty acid

RER: Rough endoplasmic reticulum

RIPA: Radioimmunoprecipitation assay

RNS: Reactive nitrogen species

ROS: Reactive oxygen species

rpm: Revolutions per minute

SDS: Sodium dodecyl sulphate

SDS-PAGE: Sodium dodecyl sulphate - polyacrylamide gel electrophoresis

SEM: Standard error of the mean

SGLT2: Sodium/glucose cotransporter 2

SLNs: Solid lipid nanoparticles

SNAP23 or SNAP25: Soluble N-ethylmaleimide sensitive factor 23/25

SNARE: Soluble N-ethylmaleimide-sensitive factor attachment protein receptor

SOD: Superoxide dismutase

SU: Sulfonylurea receptor 1

SUR1: Sulfonylurea receptor 1

TBARS: Thiobarbituric acid reactive substances

TCA: Tricarboxylic acid

TEMED: N,N,N’,N’, Tetramethylethylenediamine

Tf: Apotransferrin

TfR1: Transferrin receptor 1

TPTZ: Tripyridyl triazine

t-SNARE: Target-SNARE

T1D: Type 1 diabetes

T2DM: Type 2 diabetes mellitus

UTRs: Untranslated regions

V: Volts

VAMP2: Vesicle-associated membrane protein 2

VDCC: Voltage-dependent Ca^{2+} channels

v-SNARE: Vesicle-SNARE

WHO: World Health Organisation

[4Fe-4S]: Iron-sulfur

β-cell: Beta cell

μM: Micromolar

$\Delta\psi m$: Mitochondrial membrane potential

Δp: Protonmotive force

CHAPTER 1
INTRODUCTION

1. Introduction

Type 2 diabetes mellitus (T2DM), also known as insulin-dependent diabetes mellitus (IDDM) is a common and global health problem with incidence that has been increasing rapidly. As per the International Diabetes Federation (IDF) there were more than 425 million people affected in 2017, with numbers increasing every year and projected to reach 629 million by 2045 (IDF, 2017). As per World Health Organisation (WHO), diabetes will be the 7th leading cause of death worldwide by 2030. Besides being a leading cause of mortality, TD2M is associated with severe complications known to be major causes of disabilities, including nephropathies, retinopathies and neuropathies, thus placing a severe financial burden on the resources of modern societies. T2DM represents a serious disease that has its prevalence in both developed and developing countries (Wild et al., 2004).

In 2000, Indonesia ranks fourth as the prevalence country in the world with 8.4 million people with diabetes. This rank is after India, China, and the United States. This number is assumed to reach a threefold increase by 2030 (WHO, 2014). The UK is reported to count more than 2.7 million people affected with T2DM, although those presenting the symptoms and as yet not diagnosed are not accounted for, representing an additional 750,000 people to this number (Diabetes.co.uk). T2DM is a metabolic disorder that is caused by various factors, both genetic and environmental conditions associated with pathogenesis of T2DM. Genetic factors, such as identical twins are 60-100% likely to be sufferers of T2DM (Jun et al., 1999). In addition, developing countries have shown that T2DM is rapidly rising presumably due to a shift to relatively affluent lifestyles, energy–dense low-nutrient diet and lesser physical activity (Wild et al., 2004).

Defects in both insulin action and insulin secretion contribute to the development of T2DM (Weir, 1994). Insulin is a key regulator of blood glucose in the body to keep the glucose in a homeostasis state. Pancreatic β-cells have a crucial role to synthesise and secrete insulin at appropriate rates. Due to its important functions, β-cell has few antioxidant enzymes, such as catalase and glutathione peroxidase that are able to function as protection. Unfortunately, since β-cell has few and relatively weak defense system, it is highly sensitive to oxidative stress. The higher concentration of reactive

oxygen species (ROS) could raise oxidative stress, which leads to cellular toxicity (Jezek & Hlavata, 2005). Recent studies have shown that iron over accumulation in the β-cell leads to increased mitochondrial iron transport, which induces mitochondria to dysfunction (Ma et al., 2011). The mitochondrion is essential because it produces adenosine triphosphate (ATP) through electron transport chain (ETC) by utilising glucose metabolism in order for the numerous chemical reactions to occur, and its dysfunction may be a primary cause to insulin secretory dysfunction.

Iron is a trace metal that has a pivotal role in the body due to its function in numerous physiological reactions. It is an essential mineral that is required for many functions, such as oxygen transport, ATP production, and deoxyribonucleic acid (DNA) synthesis. However, when it is present at high levels, its accumulation could lead to cell toxicity. As iron is crucial to life, this metal is required to be well regulated and the body needs to have sufficient iron levels. When the amount of free ferrous iron is elevated, it is believed to lead to the generation of ROS through Fenton and Haber-Weiss chemistry (Hansen et al., 2014). Hydroxyl radical (•OH) is the most reactive oxygen radical that can readily react with biological molecules in its immediate vicinity, which explains its great destructive power (Lenzen, 2008). •OH is a major species that attacks cell membrane lipids, proteins, and DNA and causes tissue damage leading to insulin resistance and eventually β-cell failure (Jiang et al., 2004).

There are 3 major types of diabetes mellitus (DM), Type 1 diabetes, Type 2 diabetes and gestational diabetes mellitus. T1D or known as insulin dependent diabetes mellitus is a result of β-cells destruction by autoimmune in the islet of Langerhans. This type of diabetes leads to gradual loss of insulin secretion, causing a deficiency of insulin. T2D is the most common type of diabetes and is characterised by hyperglycaemia in the context of insulin resistance and β-cells dysfunction (Unger, 2003). Gestational diabetes manifests during pregnancy term in women with hyperglycaemia and insulin resistance. Insulin resistance is a pathological condition in which cells are not functioning properly in response to insulin. In peripheral tissue where insulin resistance exists, it can lead to severe consequences. Resistance of this hormone may cause defects in its secretion, which impairs the regulation of blood glucose levels.

Another type of diabetes called diabetes insipidus (DI) was also found and first introduced in 1794 by Johann Peter Frank (Frank, 1832). Diabetes insipidus (DI) is a rare disorder characterised by excretion of large volumes of urine that is “insipid,” or dilute and odourless (Kalra et al., 2016). Normally, the kidneys produce about 1 to 2 quarts of urine a day. However, in people with DI, the kidneys can produce 3 to 20 quarts of urine a day (NIDDK, 2015). Diabetes mellitus and DI are two different disorders that share similarities in its name and particular conditions that cause frequent urination (polyuria) and constant thirst (polydipsia) (NIDDK, 2015). Diabetes mellitus is a metabolic disease that results from defects in insulin secretion, insulin action, or both, leading to high levels of blood glucose (Alberti & Zimmet, 1998). On the other hand, people with DI produce normal levels of blood glucose, but their kidneys are unable to balance fluid in the body (NIDDK, 2015).

Mitochondria have a pivotal role in regulating the secretion of insulin by managing the level of ATP, which responsible for providing membrane depolarisation and the release of insulin granule (Maechler, 2013). Lewis et al, 2002 observed that there was a rapid change in mitochondrial morphology upon insulin secretion stimulated by glucose (Lewis et al., 2002). In addition, this secretion also promoted certain changes in mitochondrial metabolism and calcium homeostasis. It is thus crucial to study mitochondria in details to observe the link between iron and diabetes mediated by ROS.

1.1 Structure and function of endocrine pancreas

The pancreas lies inferior to the stomach with an elongated gland about 15 cm (6 inch) long. It comprises of islet of Langerhans, representing 1% of the pancreas (Jain, 2012). This organ contains two types of tissues, termed exocrine and endocrine, which also have distinct roles. The exocrine pancreas produces digestive enzymes that are secreted into the small intestine, whereas the endocrine pancreas primarily secretes hormones, notably insulin and glucagon (Longnecker, 2014). In addition, five cell types have been identified in the islets, producing various hormones with particular actions. Alpha (α) cells secrete glucagon in response to low blood glucose levels. These cells are located in surrounding β-cells or on the peripheral side of islet of Langerhans. The most abundant cells, β-cells secrete insulin, found on the centre of this islet. Delta (δ)

cells secrete somatostatin acting as the universal inhibitor hormones of most of peptide hormones. PP cells produce pancreatic polypeptide and epsilon cells produce ghrelin (Lawlor et al., 2017).

1.1.1 Insulin and glucose-stimulated insulin secretion

Diabetes mellitus is an epidemic disease that has been rapidly progressed worldwide. It is crucial to understand the hormone, its role and other mechanisms related to this disease that can have significant implications in various chronic diseases. Insulin is a hormone that is synthesised and released by pancreatic β-cells and is functioned in regulating the metabolism of blood glucose. The structure of this hormone consists of two chains, notably as A and B chains and is linked by disulphide bridges. In 1921, this 51-amino acid-contained protein was isolated and preceded on the market by early 1923 (Papaspyros, 1964). Banting accompanied by his assistant Best under a supervision of Professor McLeod were the first to discover insulin which earned them the Nobel Prize in 1923 (Seale, 1946).

Insulin is synthesised in β-cells of islets of Langerhans with the insulin gene located on chromosome 11 in humans (Schroder & Zuhlke, 1982). Several steps are involved in the production of insulin. The synthesis of insulin is initiated with formation of pre-proinsulin (mw: 11,500) in the rough endoplasmic reticulum (RER). Pre-proinsulin is then cleaved to yield proinsulin by removal of the signal peptide to be finally transferred to the Golgi apparatus. This organelle contains an environment of aqueous zinc and calcium, creating soluble zinc-containing proinsulin hexamers (Dodson & Steiner, 1998). Moreover, the immature secretory vesicles are assembled within this organelle before being docked out to be converted from this precursor resulting in insulin and its peptide fragment, termed connecting peptide (C-peptide) (Malaisse, 1997). When the granules are mature and stimulus triggers, they are secreted into the circulation, releasing the same molar ratio of insulin and C-peptide.

In response to blood glucose as a stimulus, there are two phases involved in the secretion of insulin, and the secretory profile is thus biphasic (Grodsky, 2000). The first phase begins with a rapid phase, in which insulin secretion lasts within 5-10 min, while the second phase can take longer up to hours if glucose level is elevated persistently (Curry et al., 1968; Grodsky, 2000). β-cells are constantly exposed to

particular stimulatory signals within the body. Besides glucose as the main fuel secretagogue, several factors can cause insulin secretion, such as GIP, GLP-1, parasympathetic inputs, FFA, amino acids, hormones, and neural inputs (Bratanova-Tochkova et al., 2002).

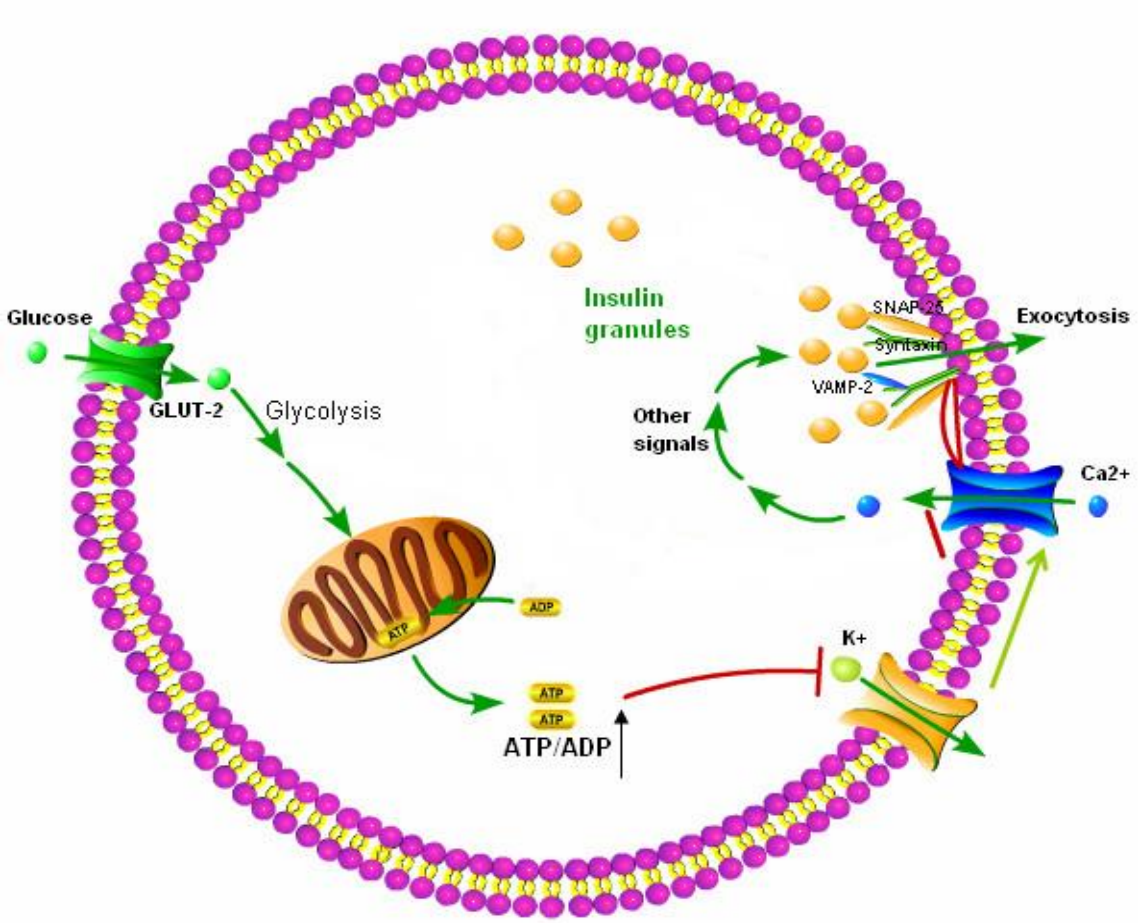

Fig. 1.1.1. Glucose-stimulated insulin secretion.
Glucose enters the pancreatic β-cells via glucose transporters, termed GLUT2 in which is located on the plasma membrane and undergoes glycolysis. These cells are equipped with K_{ATP} channels, which are crucial to affect its closure due to an elevation of ATP/ADP ratio in the cytoplasm. Following this closure, the membrane undergoes depolarisation and subsequently opening of L-type of voltage-dependent Ca^{2+} channels (VDCC). Increase of cytosolic calcium, which in turn, triggers exocytosis. SNARE complex proteins; syntaxin, SNAP-25, and VAMP-2/synaptobrevin-2, play a crucial role in insulin granule secretion. (Taken from Ren et al., 2007)

In a condition of high circulating plasma glucose concentration, glucose enters the pancreatic β-cells via glucose transporters, termed GLUT2 in which is located on the plasma membrane. Subclasses of GLUTs have been established, however GLUT4 has been considered as a key regulator of the whole-body glucose homeostasis

(Huang & Czech, 2007). GLUT4 is a major mediator of glucose disposal from circulation and transporting it into the skeletal muscles and adipose tissue where it can be suitably applied (Huang & Czech, 2007). Following insulin mediated cellular uptake, glucose is phosphorylated by glucokinase and undergoes glycolysis, generating the production of two molecules of pyruvate located in the cytoplasm. Before entering the matrix of mitochondria, pyruvate is equally metabolised by pyruvate dehydrogenase (PDH) and pyruvate carboxylase (PC) (Patterson et al., 2014). The generation of ATP from these processes have become an important molecule that signals insulin to be secreted from β-cells. These cells are equipped with K_{ATP} channels, which are crucial to affect its closure due to an elevation of ATP/ADP ratio in the cytoplasm. Following this closure, the membrane undergoes depolarisation and subsequently opening of L-type of voltage-dependent Ca^{2+} channels (VDCC). Sulfonylureas (SU) and glinide are insulin secretagogues used in the treatment of T2D. These two drugs target and bind to K_{ATP} channels particularly sulfonylurea receptor 1 (SUR1), which affects the closure of this channel. Hibino and colleagues (2010) identified the structure of this channel as a tetra-octamer consisting of four SUR1 and inwardly rectifying K^+ channel 6.2 subunits (Kir6.2) (Hibino et al., 2010). Insulin is then rapidly increasing because of the subsequent Ca^{2+} influx, which causes elevation of cytosolic free Ca^{2+} concentration (Jewel et al., 2010) (Fig.1.1.1).

1.1.2 Calpain 10

Calpains are calcium-dependent intracellular nonlysosomal proteases that are believed to hydrolyse specific substrates involved in calcium-regulated signalling pathways. As a consequence of partial proteolysis, these proteins result in either activation or inhibition of substrate function. Calpain 10 is an atypical member of calpain family that has been associated with an increased risk of T2DM in humans. Calpain 10 is one of three other type calpain family, which has certain domains have been replaced or deleted (Barnes & Hodgkin, 1996). A study performed by Ma and colleagues in 2001 concluded that calpain 10 seems to be ubiquitous in all tissues and its expression level as well as subcellular distribution are influenced by calcium (Ma et al., 2001). Due to their wide range of substrate specificities, numerous diseases, such as ischemic stroke, Alzheimer's disease, rheumatoid arthritis, and T2D have developed as implications of these calpain family members (Machado et al., 2015). In

T2D, calpain inhibition has been affecting some tissues involved in T2D such as adipocytes, skeletal muscle, and pancreatic islets. The highest expression of calpain 10 mRNA is found in human heart, followed by the pancreas (Emori et al., 1986).

Calpain-10 was positively identified to be localised in insulin secreting cells both in the cytosol and cell compartments and its expression was found to increase in response to glucose concentrations by Marshall and colleagues (Marshall et al., 2005). It was also shown that an isoform of calpain-10 acts as a Ca^{2+} sensor to trigger soluble N-ethylmaleimide-sensitive factor attachment protein receptor (SNARE) complex rearrangement, granule fusion and insulin exocytosis. The study thus identified calpain-10 as central to stimulus-secretion coupling in the β-cells.

1.1.3 SNARE-facilitated insulin exocytosis

SNARE is a core complex protein that mediates exocytosis of insulin from β-cells. Syntaxin, SNAP23 or SNAP25, and VAMP2 (synaptobrevin) are three proteins that compose this SNARE complex core, which is forming a stable bundle (Fig.1.1.3). This complex protein consists of the three different proteins with equal 1:1:1 ratio, docked at the plasma membrane (Jewell et al., 2010). The SNARE bundle is made of the common secondary structure of proteins named alpha helices that comprises of four helices, with contributions from each trimeric protein, in which one alpha-helix from VAMP, one from syntaxin, and the remaining two from SNAP23/25. SNARE's are categorised into two types depending upon the location of the component proteins. Vesicle (v-SNARE) SNARE comprises of VAMP2, whereas target (t-SNARE) SNARE consists of syntaxin and SNAP23 or SNAP25 (Jahn & Scheller, 2006).

The SNARE core complex was discovered a decade ago, which was initially identified in the yeast Sec1 protein in 1990 (Rizo & Sudhof, 2002). This discovery established this particular protein as the regulator of SNARE mediated exocytotic function, directly interacting with syntaxin (Jewell et al., 2010). This protein superfamily has been found to be involved not only in neurotransmitter release at the synapse, but also in most intracellular membrane fusion reaction (Chen & Scheller, 2001). Besides being involved directly in membrane

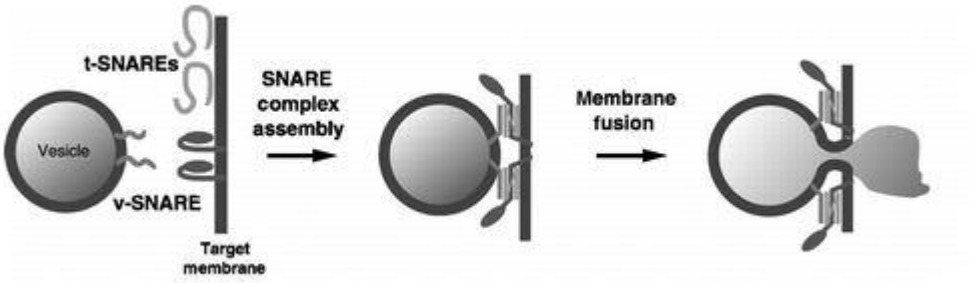

Fig.1.1.3. A general SNARE-mediated fusion reaction. (Ungar & Hughson, 2003).

fusion, the fundamental function of this core complex protein is engaging the membrane substrates (Ungar & Hughson, 2003). Intracellularly, SNARE protein contains multiple isoforms required in exocytotic events related to insulin-secreting β-cells and insulin-responsive muscle and adipose cells. In pancreatic β-cells, syntaxin isoforms of 1A, 2, 3, and 4 are expressed, albeit only isoforms 1A and 4 are known to be required for the insulin exocytosis (Ohara-Imaizumi et al., 2007). The principal neuronal isoform, SNAP 25 has been established to be present in β-cells. Though SNAP23 and SNAP29 are reported as isoforms of SNAP25 (Jewell et al., 2010). SNAP23 is expressed in skeletal muscle and adipose tissues (Araki et al., 1997). In addition to these isoforms, there are seven isoforms identified belong to VAMP proteins. Of these, three isoforms (VAMP2, VAMP3, & VAMP8) are required for GSIS with VAMP2 as the predominant isoform (Nagamatsu et al., 2001).

1.1.4 Glucagon: another glucose regulator

It is known that glucose is a major fuel for muscles and organs use to work and stay healthy. Unfortunately, glucose can cause a serious problem when its balanced is out of proportion. Glucagon and insulin are two major hormones that responsible for the homeostasis of blood sugar. Glucagon was first discovered in 1922 by Murlin from the University of Rochester. It was found that besides the glucose lowering hormone insulin, the pancreas also produces another factor with the ability to raise glucose. This putative substance was named the glucagon and is known to act along with insulin in maintaining glucose homeostasis (Kimball & Murlin, 1923). This characteristic was presented by Sutherland and de Duve with their studies, which provided the evidence that glucagon is an islet hormone produced in alpha cells. Like insulin, glucagon is synthesised from a precursor molecule, proglucagon. Besides

being released from alpha cells during hypoglycaemia and starvation, glucagon was shown to be secreted as part of mechanisms involving both autonomic nerves, namely sympathetic and parasympathetic nervous system (Ahren & Taborsky, 1986). This was particularly evidenced in a clinical experiment where glucagon secretion was inhibited during a hypoglycaemic state due to ganglionic blockade (Havel et al., 1993). In parallel, other factors are known to impair its secretion, including insulin and somatostatin, respectively produced in β and δ cells.

1.1.5 Incretins

Incretins cannot be released without any response to glucose or nutrients, which is considerably working in a dependent manner. Two major incretin hormones have been observed in humans that are synthesised by endocrine cells. These two hormones are GLP-1 and glucose-dependent insulinotropic peptide (GIP) or also known as gastric inhibitory peptide. GIP was considered to be the first incretin identified and is secreted from K cells of the upper small intestine (Brown et al., 1970). This hormone consists of 42 amino acids with a direct effect on pancreatic islets to promote insulin secretion (Adrian et al., 1978). The second incretin releasing from L cells of the lower intestine and colon was termed GLP-1 (Schmidt et al., 1985).

Both GIP and GLP-1 amplify similar functions on insulin by binding to their receptors, through the GIP receptor (GIPR) and the GLP-1 receptor (GLP-1R) (Gremlich et al., 1995; Dillon et al., 1993). These receptors belong to the G-protein coupled receptor family, promoting stimulation of insulin secretion in pancreatic β-cells via activating adenylate cyclase, which increases the level of intracellular cyclic adenosine monophosphate (cAMP). In addition to this increase, protein kinase A (PKA) is activated (Fehmann et al., 1995) and exchange protein is activated by cAMP2 (EPAC2)/cAMP-guanine nucleotide exchange factor (GEF) II (Holz, 2004). Although sharing common properties as incretins, these two hormones can exert different biological functions depending on the organ involved. In the bone, GIP increases bone formation (Tsukiyama et al., 2006), which is in contrast with GLP-1, inhibiting the resorption of bone (Yamada et al., 2008). Whereas in adipose tissue, GIP facilitates fat deposition (Carr et al., 2008) and GLP-1 has no effect at all. However, in the brain, both are involved in memory formation and regulation of appetite.

Like other proteins, GIP and GLP-1 both undergo proteolytic degradation catalysed particularly by the enzyme DPP-4 (dipeptidyl peptidase-4), suppressing the insulinotropic effects of GIP and GLP-1 (Deacon et al., 1995). Fortunately, many DPP-4 inhibitors, also known as gliptins, have been used successfully to block this protein that is encoded by DPP4 gene in humans. DPP-4 inhibitors (e.g. sitagliptin and vildagliptin) and incretins and GLP-1 receptor agonists have been developed and shown to improve glycaemic control (Zander et al., 2002) and are used in T2DM therapy (Nathan et al., 2009).

1.1.6 Tolbutamide as an insulin secretagogue

Tolbutamide is one of the first generation of sulphonylureas class that has been extensively used for treatment of T2DM. The main effect of tolbutamide is similar to other sulfonylureas agents, which is too increase the concentration of plasma insulin. This drug promotes insulin secretion in a physiological manner by binding to the specific sulfonylureas receptors (SUR1) in the pancreatic β-cells. SUR1 is highly expressed in pancreatic islets and also in the brain. Tolbutamide blocks the inflow of potassium (K_+) associated with ATP-dependent channel, Kir6.2. The complex binding of SUR1-Kir6.2 results in the closure of this channel, which is subsequently depolarized the membrane, causing calcium (Ca^{2+}) influx into the cells and subsequently triggering insulin undergoes exocytosis from insulin vesicles (Jewel et al., 2010).

Sulfonylureas may provide glycaemic control in the short term, but this could worsen in a long-term period. The most common side effect is hypoglycaemia due to an excessive dosage. In addition, weight gain and skin rash may also occur. Although an association with other drugs such as metformin may help mitigate these effects, particularly weight gain, this drug is no longer used considering the wide spectrum of off target effects. However, its use in research has been extensively explored due to successful outcomes in cultured cells (Sola et al., 2015).

1.2 Iron related oxidative stress in pancreatic β-cell

Iron is the most important of all the trace elements, found in many essential enzymes and proteins. This transition metal exists in two valency states, Fe^{+2} (ferrous iron) and

Fe^{+3} (ferric iron) and has various essential functional roles in the body including a vital contribution to the redox reactions of oxidative phosphorylation by accepting and donating electrons (Andrews, 1999).

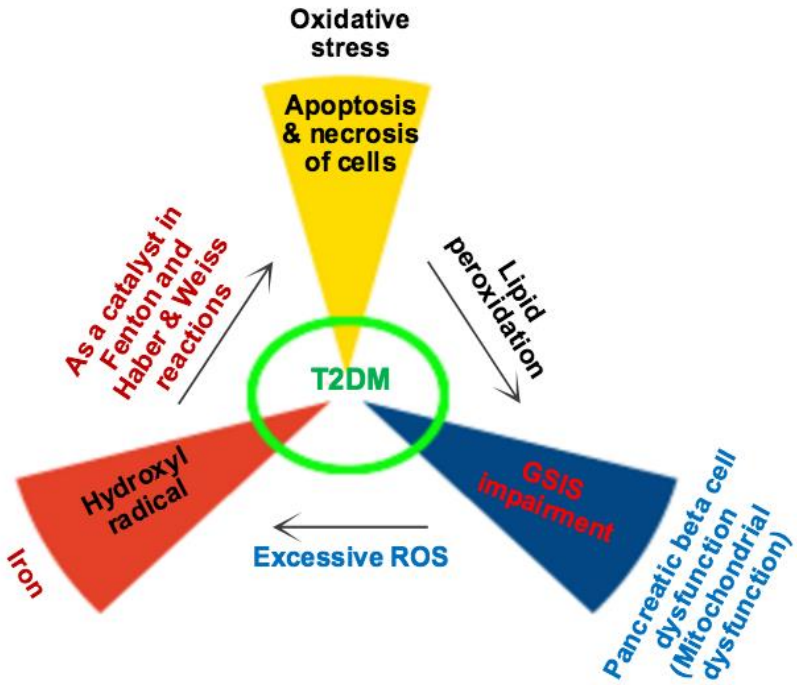

Fig. 1.2. A Model for relationships between iron, oxidative stress, and pancreatic β-cell in type 2 diabetes mellitus patients (T2DM).

Oxygen transport, DNA synthesis, and respiration require iron. Unfortunately, the same properties that make iron useful can also make it be toxic (Fig.1.2). Through the generation of free radicals, iron can damage essential biologic components such as DNA, proteins, and lipids (Fairweather-Tait, 2004). Thus, an organism must pay attention over the amount of iron that is consumed daily and the amount of iron that is excreted.

1.2.1 Metabolism of iron

Iron is an essential trace metal requisite for normal cellular functions. It functions as the crucial component in oxygen transport and exchange, cytochromes, and enzymes that transfer electrons (Andrews & Schmidt, 2007). Unfortunately, this vital component could be potentially harmful when its levels are exceeded. Several studies suggest

that iron is a key pathogenetic factor in T2DM diabetes due to its generation of free radicals (Hansen et al., 2014). Thus, the amount of iron uptake and the amount of iron that is excreted needs to be maintained properly to avoid inappropriate responses lead to anaemia or iron overload **(**Roy & Enns, 2000**)**.

1.2.1.1 Iron absorption

Iron plays a pivotal role in the body and is an essential mineral, which can only be obtained from the diet due to the inability of the body to manufacture its own supply. The body absorbs 1-2 mg of dietary iron in a day with apical membrane of duodenal enterocytes being a critical role in iron homeostasis, where first absorption of iron takes place (Siah et al., 2006).

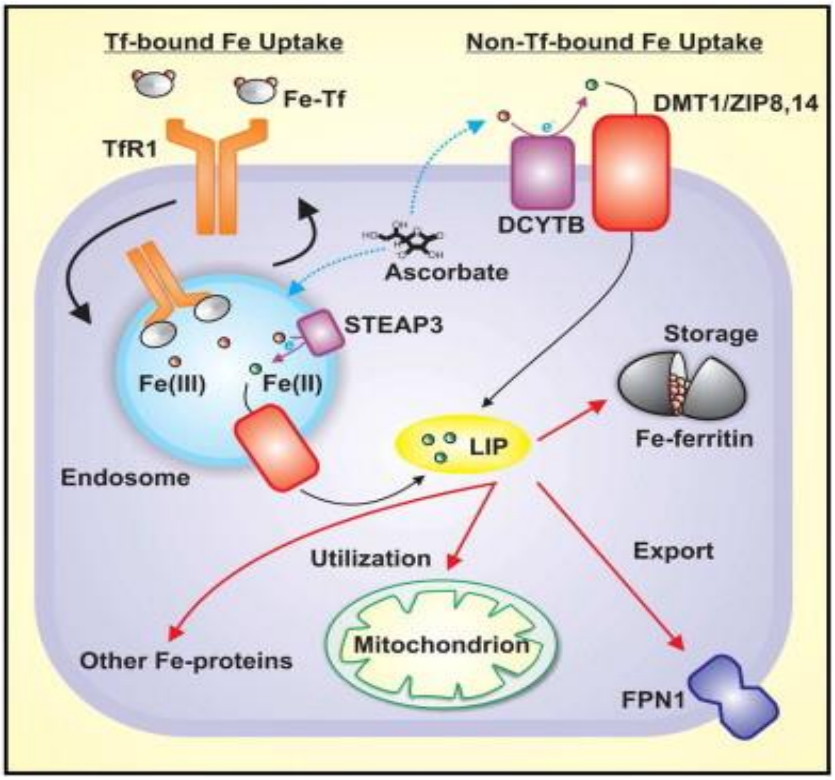

Fig. 1.2.1.1 The above image represents two major pathways of iron uptake into the cells (particularly pancreatic β-cell), called Tf-bound Fe uptake and non-Tf-bound Fe (NTBI) uptake. Physiologically, Tf-bound Fe binds to TfR1 on the cell surface, which mediates endocytosis where Fe is being released from Tf due to a decrease in endosomal pH. Endosomal reductase; STEAP3 (or potentially ascorbate) reduces Fe (III) into Fe (II) and is transported across the endosomal membrane by DMT1. Within the cytosol, iron is transported to LIP, used for storage in ferritin, or used for synthesis of heme and Fe-S clusters in the mitochondrion. Iron can exit the cells via FPN1. Under iron overload conditions, NTBI exists in the blood and can involve the contribution of DCYTB to reduce Fe (III) into Fe (II), which can be transported across the cells by DMT1. (Taken from Lane at al., 2015)

Organic or non-haem iron (90% of total daily iron intake) is the form of most dietary iron that is consumed in the body and prior to absorption, ferric iron must be reduced to ferrous iron by ferrireductase duodenal cytochrome-b (Dcyt-b). Ferrous iron is transported across the apical membrane by divalent metal transporter 1 (DMT1), which also transports other metal ions, such as zinc, copper and cobalt (Gunshin et al., 1997).

Dietary inorganic or haem iron (10% of total daily iron intake) is transported into the enterocyte through the haem carrier protein 1 (HCP1) (Hansen et al., 2014). Within the enterocyte, iron liberated from haem by the enzyme haem oxygenase 1 (HO1) or transported through DMT1 enters labile iron pool (LIP), which could consist of chelates or chaperone proteins that bind and transport iron (Dunn et al., 2006). Prior to being externalised to the interstitial fluid, iron has two possible fates - it may be stored as within the protein ferritin, or it may be transferred across the basolateral membrane to reach circulation. Iron is delivered to the basolateral membrane where the exporter ferroportin 1 (FPN1) is located via which it exits the enterocyte. Hephaestin is a transmembrane copper - dependent ferroxidase that oxidises ferrous iron into the ferric iron state in order to bind to apotransferrin (Tf) to form di-ferric transferrin which acts as the primary plasma iron carrier protein (Andrews et al., 2007) (Fig.1.2.1.1).

1.2.1.2 Iron distribution

The total human body iron content is 3000-5000 mg or 45 and 55 mg/kg of body weight in adult women and men respectively. Ironically, total iron in men is higher than that in women, but women require more dietary iron due to menstruation, which results in loss of iron with blood (Arora & Kapoor, 2012). About 65-70% of total body iron is located in haem group of haemoglobin in circulating red blood cells. In addition, iron is also present abundantly in organs, such as liver and muscles. Besides distribution to other organs, iron is stored in ferritin as the major iron storage protein. Hepatocytes and reticuloendothelial macrophages become cells that store approximately 20-30% of body iron. The remaining iron is found in myoglobin, cytochromes, and iron-containing enzymes (Papanikolaou & Pantopoulo, 2005).

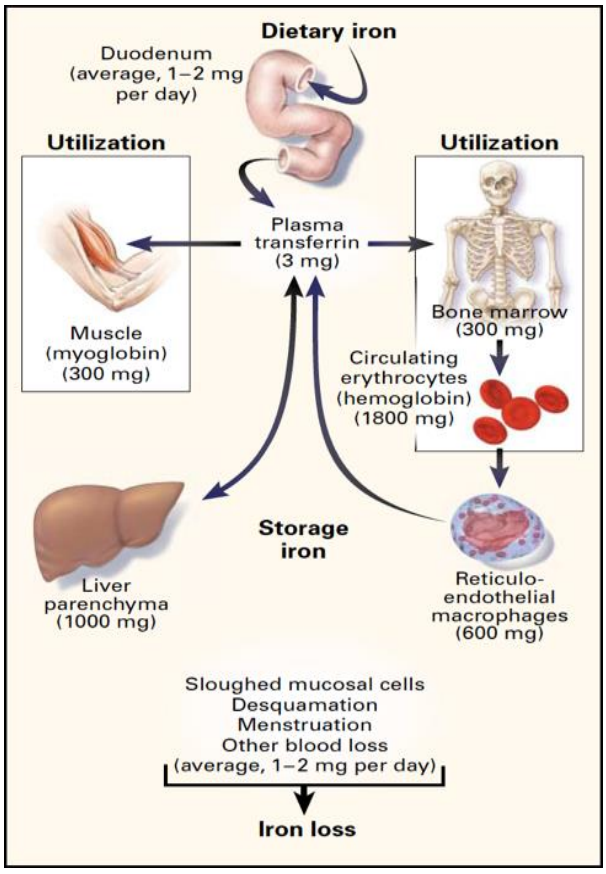

Fig. 1.2.1.2. Iron distribution in adults. (Andrews, 1999).

As described above, iron is transported across multiple cell membranes to reach its site of utilisation. Following exit via duodenal FPN1 into plasma iron is then transported into various target organs (Fig.1.2.1.2). Pancreatic β-cells uptake the extracellular iron as the Tf-bound iron through transferrin receptor 1 (TfR1) - mediated process (Aisen, 2004). This Tf-bound iron is internalised into the cells and the iron is released by low pH from the receptor-ligand complex. Following iron release, TfR1 and Tf are cycled back to the plasma membrane. Tf then cycles back to the plasma and TfR1 remains on the surface membrane ready to take up next cycle of iron (Ganz & Nemeth, 2006).

It is known that iron-regulatory proteins (IRPs) 1 and 2 are key controllers of vertebrate iron metabolism and iron homeostasis genes (Cairo & Stefania, 2007). As iron must be tightly bound by specific proteins to minimise free iron levels, the responsible proteins must work efficiently. The expression of genes controlled by these proteins is involved in iron uptake, utilisation, storage, and export (Cairo & Stefania, 2007). Iron-

responsive elements (IREs) were identified as proteins that control gene expression in response to changes in the iron level (Aziz & Munro, 1987). IRP1 and IRP2 belong to aconitase superfamily, which specifically bind to conserved IREs in the UTRs of mRNA. Under the condition of iron deficiency, IRPs bind to IREs located in either 5' or 3' UTRs of the indicated mRNAs, causing translation or degradation of mRNA respectively. In contrast, increased iron levels decrease IRE-binding activity, inducing mRNA ferritin translation to sequester iron rather than release it.

IRP1 is an intriguing protein as it performs dual functions depending on its structure. In a state of its apoform, this protein is able to bind to IRE, controlling the expression of gene. Conversely, IRP1 can also assemble a [4Fe-4S] cluster and become the cytosolic counterpart of mitochondrial aconitase (Beinert & Kennedy, 1993). These functions are mainly regulated by the availability of iron within LIP (Breuer & Cabantchik, 2008). Thus, IRP1 is considered as both a sensor of iron levels intracellularly and a regulator of cellular iron homeostasis (Hentze & Kühn, 1996).

1.2.2 Hepcidin

Hepcidin is a hepatic antimicrobial peptide that regulates iron entry into systemic circulation as well as various organs. This hormone is synthesised by the liver and comprises of 25-amino acid peptides. Prior to its discovery in involvement of iron metabolism, hepcidin was initially identified as a novel antimicrobial peptide (Park et al., 2001). It has been established that hepcidin plays a key role in regulating iron homeostasis. Nicolas and his colleagues identified that iron overload was observed in mice due to disruption of hepcidin gene (*HAMP*) (Nicolas et al., 2001). In addition to inhibit iron absorption in enterocytes by binding to and inducing the internalisation and degradation of ferroportin transporter located in basolateral membrane, hepcidin also inhibits ferroportin expression in macrophages as recycled iron of senescent erythrocytes, and as well as the release of stored iron from hepatocytes (Ganz & Nemeth, 2012).

Hepatocytes are the main place for hepcidin synthesise, but at low level it is expressed in other cells and tissues including macrophages, adipocytes and brain cells (Nemeth & Ganz, 2009). Hepcidin is regulated by iron and erythropoietic activity. The stimuli

that can regulate the level of hepcidin to rise include inflammatory cytokine, predominantly IL-6. In contrast, a wide range of stimuli that can suppress hepcidin synthesis such as iron deficiency anaemia, haemolytic anaemia, and hypoxia (Ganz, 2003). Iron that is bound to transferrin and intracellular ferritin can regulate the synthesis or secretion of hepcidin by hepatocytes. In response to elevated iron levels, the synthesis of hepcidin by the liver is increased. Thus, hepcidin is the key central regulator of systemic iron homeostasis.

1.2.3 Hereditary hemochromatosis and risk of type 2 diabetes

Hereditary hemochromatosis (HH) is an autosomal recessive disorder that disrupts the absorption of iron, leading to iron overload associated with secondary tissue damage in different types of organs (Allen et al., 2008). Hemochromatosis was first identified in the 1800s and was considered to be an inherited disease in 1935 (Hopkins Medicine, 2001). This disorder is characterised by mutations in the *HFE* gene located on the chromosome 6 (Cherfane et al., 2013). *HFE* gene is a product of HFE protein that functions to modulate the uptake of transferrin-bound iron into intestinal epithelial cells. The mutation on this specific chromosome leads to the substitution of the 282nd amino acid in which cysteine becomes tyrosine called C282Y (National Institute of Health, 1998). This substitution affects the interaction between HFE protein and TFR1 as an important protein involved in iron homeostasis (National Institute of Health, 1998). The body undergoes many mutations linked to proteins responsible for iron homeostasis, causing hemochromatosis. However, *HFE* gene mutation has been considered to be the most common cause found in myriad cases. HH is the most common genetic disorder among Caucasian population in the United States as one in nine people carry the gene and one in three hundred people are being affected (Hopkins Medicine, 2001).

As previously mentioned, the body - particularly in the proximal small intestine absorbs iron at the rate of 1-2 mg per day. However, people with hereditary hemochromatosis could absorb iron at 4-5 mg per day, with accumulation to 15-40 grams of iron in the body (Hopkins Medicine, 2001). In addition to the lack of an excretory system of excess iron, this metal tends to be stored in the most notable organs, such as the liver, pancreas, and heart. Excess iron in the liver causes cirrhosis, which may develop into

liver cancer or liver failure (Hopkins Medicine, 2001). Excess iron stored in pancreas and heart may lead to diabetes and cardiomyopathy, respectively (National Institute of Health, 1998). In addition to HH, other genetic disorders-related iron overload has been identified. African iron overload, sickle cell disease, thalassemia, and X-linked sideroblastic anaemia are several disorders, which result in increase of iron absorption and increased iron deposition (Iron disorders institute, 2009).

Increased intracellular iron causes multiple damages including peroxidative injury towards organelle membranes i.e. mitochondria, lysosomes, and microsomes. As discussed earlier, Excess free iron has been established to be a crucial component in the formation of several free radicals, which can result in cell death due to lipid peroxidation. Iron level has been linked to increased risk of type 2 diabetes as this metal is an important determinant of insulin secretion and insulin action (Abraham et al., 2006). Furthermore, People with hemochromatosis demonstrated decreased insulin secretion, which increased the risk of this metabolic disease (McClain et al., 2006; Dymock et al., 1972).

Treatments include regular blood donations and therapy venesection may reduce the body's iron levels. Furthermore, early recognition of this disorder is advised to take place to prevent irreversible complications as mentioned previously above (NHSUK, 2019).

1.3 Cellular oxidative damage

Oxidative stress has become a considerable interest due to several related pathogenesis including cancer, T2DM (Fig.1.1.1), Parkinson's disease, Alzheimer's disease, inflammation, neurogenerative disease, atherosclerosis, and many other diseases (Droge, 2002). The body undergoes a disturbance in the balance between oxidants (free radicals) and antioxidant defenses, this condition then could lead to potential damage, which is defined as oxidative stress (Betteridge, 2000). In addition, oxidative stress could be described as the accumulation of ROS/RNS, which leads to oxidative damage to biomolecules, including DNA, proteins, and lipids (Jezek & Hlavata, 2005). Ironically, the generation of ROS is not always a harmful process due to its function for some biological responses (Finkel, 2003; Buetler et al., 2004), such

as ion transport, redox-dependent transcriptional regulation, and protein phosphorylation.

Under non-stress condition, mitochondria are considered as one of the primary sources of ROS (Turrens, 2003). The Oxygen is very vital to the body for survival, but like iron it could be a causative agent in a wide variety of diseases. Once the two unpaired electrons derived from molecular oxygen start spinning in opposing directions, it could quickly react with other pairs of electrons.

This reaction would produce superoxide anion (O_2^{-}.), which could be resulted in hydroxyl radical (OH•) as one of the strongest and dangerous oxidants in nature. O_2^{-}. is then enzymatically dismutated to yield hydrogen peroxide (H_2O_2) by mitochondrial electron transport chain (ETC) (Singh et al., 2004). Hydroxyl radical can be generated by two different reactions as a result of different speed of reaction (Kehrer, 2000). In the Fenton reaction ferrous iron reacts with hydrogen peroxide to generate hydroxyl radical, which is a much faster set of reactions (I). In the Haber Weiss reaction iron generates hydroxyl radicals from hydrogen peroxide and superoxide, which leads to a very slow reaction (II) (McKenna, 2009). These reactions are considered to be the genesis of a number of diseases (Ames, 1993).

(I) $\mathbf{Fe^{2+} + H_2O_2 \rightarrow Fe^{3+} + OH^- + \bullet OH}$

(II) $\mathbf{\bullet O_2^- + H_2O_2 \rightarrow \bullet OH + OH^- + O_2}$

O_2^{-}. can be produced both enzymatically and non-enzymatically *in vivo*. Enzymatically, O_2^{-}. is produced through NADPH oxidase specifically by Complex I, which is found in the presence of succinate as the substrate of Complex II (Liu et al., 2002). Complex I and III are linked by ubiquinone, an electron transfer agent in cell respiration. In addition to Complex I, ubiquinone is linked Complex II and III, thereby makes Complex III as a primary player in the formation of O_2^{-}. (Zorov et al., 2014) (Fig.1.3.1).

As described above that ROS clearly possess the capacity to behave as destructive agents, the only key element to defend against this toxicity is the induction of antioxidant. Unfortunately, chronic oxidative stress could lead to progression of

pancreatic β-cell dysfunction due to the lack of protective agents (Wang & Wang, 2017). Thus, different strategies are required to use in early intervention of metabolic syndrome and T2DM.

1.3.1 Mitochondrial structure and function

The mitochondrion is essential due to a myriad of pivotal functions for various cellular processes. This organelle is considered as a distinct organelle since it consists of two membranes with four compartments: the matrix, inner membrane, inter membrane space (IMS), and outer membrane (Fig.1.3.1).

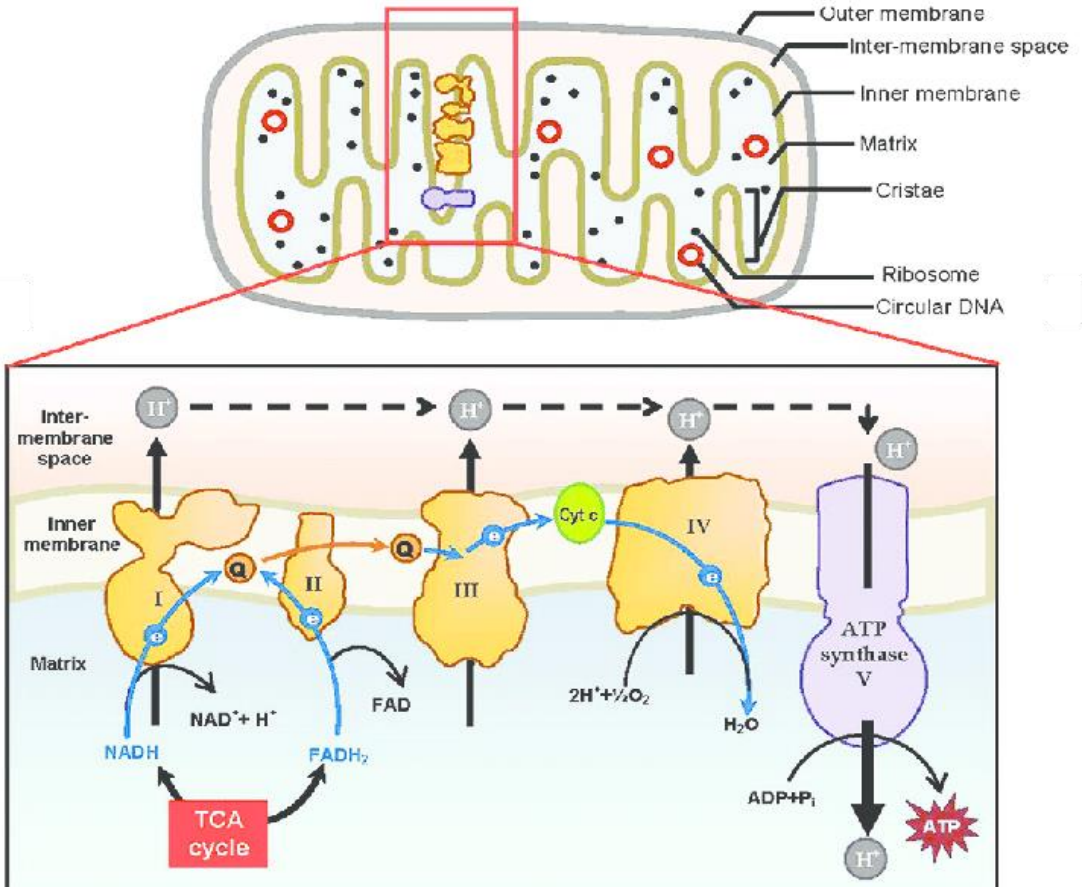

Fig. 1.3.1 Structure of a mitochondrion and the human electron transport chain on the inner mitochondrial membrane. (a) A representation of mitochondrion structure. (b) Schematised complexes I-IV of electron transport chain and ATP synthase. Protons are pumped out of the matrix through complex I, III, and IV due to electrons flow along the ETC. Protons then flow back into the matrix via ATP synthase, resulting in ATP production. (Taken from Yusoff, 2015).

The outer mitochondrial membrane (OMM) is more permeable to ions and small-uncharged metabolites as large porins channels (Bayrhuber et al., 2008). Many proteins are expressed in this power-house organelle, but 95% of proteins found in

this organelle are imported from the cytosol (Pfanner & Geissler, 2001). Mitochondrial electron transport chain is composed of four multiprotein complexes called complex 1-IV. Ubiquinone site in complex III and an unknown site in complex I are identified as the major sites to generate ROS. However, the ubiquinone site of complex III is still controversial due to production of ROS at this site is usually artificially induced with the complex III inhibitor antimycin A (Forman and Azzi, 1997). Various ROS are generated in this organelle, such as superoxide anion, hydrogen peroxide, and the hydroxyl radical. Of these, hydrogen peroxide is the most stable and abundant ROS. In addition, this particular species is the by-product of superoxide scavenging by superoxide dismutase (SOD) enzymes. Since mitochondria are considered as the major generator of free radicals, this organelle is most prone to oxidative damage. Other ROS which also cause oxidation include nitric oxide (NO), peroxynitrite, lipid hydroperoxides (LOOH), nitrogen-centred radical, sulfate radical (SO_{4}^{-}), and metal oxygen complexes.

In the mitochondrion iron metabolism has three major pathways which are utilized in heme synthesis, iron-sulfur clusters, and storage called mitochondrial ferritin (MtFt). MtFt has a similar function with antioxidant due to its role as a defense against the interaction between ROS and free iron. Moreover, MtFt is also potentially functions as a regulator of local iron trafficking. However, it remains a complex topic since it hasn't been identified yet whether and when this potential function is used by cells in physiological conditions. Of these proteins, heme and ISCs are involved in the biogenesis of electron transport chain (ETC). Iron-sulfur (Fe-S) protein is essential to human body due to its variety of functions such as enzyme catalysis, electron carriers, homeostatic regulation, and sulfur activation (Stehling and Lill, 2013). Mitochondria assemble Fe-S proteins to regulate cellular iron homeostasis. Eukaryotic Fe-S proteins are located in mitochondria, cytosol, and nucleus. These proteins have diverse function relating to their performance in metabolism and regulation of cellular. Maturation of Fe-S proteins both inside and outside mitochondria is directed by the cytosolic iron-sulfur protein assembly (CIA) machinery. CIA can use its function depending on the core of mitochondrial ISC assembly system.

This mitochondrion plays a pivotal role in ISC synthesis as it is then main site of ISC assembly. These clusters perform several processes, which contain different vital

functions such as electron transport, redox reactions, metabolic catalysis, etc. (Lill & Mühlenhoff, 2006). In eukaryotic cells, maturation of ISC proteins require some molecules involved, which are found in mitochondria, cytosol, and nucleus. A study performed by Lill et al (1999) in yeast showed defects in Fe-S enzymes cluster. Consequently, yielding in the iron accumulation in mitochondria with local enzymatic damage and reduction of mitochondrial functionality. Heme is the iron-containing prosthetic groups at the catalytic centre of many critical metabolic enzymes. This protein is synthesised by the ferrochelatase enzyme inserting ferrous iron inside protoporphyrin located within mitochondrial matrix (Ponka, 1997). Like ISCs, iron is also vital in the heme synthesis, which is imported from the cytosol. Various mitochondrial proteins, particularly in ETC depends on the function of ISCs and heme to have correct folding, which result in an efficient activity (Lin et al., 1983). In mitochondrial ETC, there are eight molecules of three different types of heme and 10-11 ISCs (Tyler, 1992). As ISCs and heme play a crucial role in the assembly of a variety of apoproteins, it is necessary to understand their metabolism in tissues to expand some understanding of mitochondrial dysfunction.

1.3.2 Dual functions of mitochondria: survival and death

Since a mitochondrion is a major source of reactive oxygen species, iron is one of the examples of an ion that should be regulated tightly. Thus, iron transportation from cytosol is required to be generated tightly due to its uptake to the mitochondria. Although iron transporters in inner mitochondrial membrane have been identified, the pathways that use iron in the outer mitochondrial membrane are still not elucidated. If ROS production is not compensated with endogenous antioxidants, this condition will lead to the rise of ROS beyond normal threshold levels. This condition could result in further damage such as cell death (loss of function), and consequently the whole organ failure. Mitochondria have a notable role as the house production of energy, which undergo through some complex metabolisms. In addition, mitochondria also participate in the regulation of cell death (apoptosis), signalling, metabolic pathways involving lipids, amino acids, and maintenance of calcium and iron homeostasis (Cheng et al., 2013).

ETC in mitochondria plays a crucial role as one of the steps to generate ATP production. Heme and ISCs, the main form of iron in mitochondria are involved in reducing oxygen to water and generating the proton gradient across the inner membrane (Ly et al., 2003). Iron is one of the ions that is maintained carefully in this organelle in preventing oxidative damage. Some studies have found iron transporters in inner mitochondrial membrane; however, the pathways that use iron in the outer mitochondrial membrane are still not elucidated (Paradkar et al., 2009). Mitoferrin (Mtf) is a transmembrane protein residing in the IMM that functions as a transporter importing iron into mitochondria (particularly the matrix) (Shaw et al., 2006).

Abnormal iron accumulation in mitochondria have many effects and can cause a decrease in mitochondrial membrane potential ($\Delta\psi m$). Membrane potential is the force driving protons into the mitochondria (Perry et al., 2011). Complexes I and III are fundamental for the maintenance of this membrane potential, as Complex I substrates such as pyruvate and malate can maintain the health or compensate the health of mitochondrial membrane potential, this particular complex requires to be maintained. The imbalance of Complex I activity may result in depletion of glutathione and increased lipid peroxidation (Abeti et al., 2016). Beside changes in morphology, alteration of membrane integrity, activation of caspase, drop in mitochondrial membrane potential is one of factors contributed in apoptosis.

The decrease or loss of mitochondrial membrane potential might be an early event in the apoptotic process. However, this condition could be the contrary in which this loss could be the consequence of the apoptotic-signalling pathway (Ly et al., 2003). Mitochondrial membrane potential is crucial to understand, as it is important for maintaining the physiological function of the respiratory chain, resulting in ATP production. The collapse of the mitochondrial membrane potential is initiated by the opening of one of mitochondrial channels such as mitochondrial permeability transition pore (mPTP). This opening trigger the release of apoptogenic factors such as cytochrome c into the cytosol, which in turn triggers other downstream events in the apoptotic cascade.

Activation of mitochondrial apoptotic pathway and generation of excesses mitochondrial reactive oxygen species may advance further damage to the cells and even result in cellular damage. Oxidative stress occurs by an imbalance between

antioxidant defense and pro-oxidant load. Maintaining the structural and functional integrity of this organelle is crucial as its roles involved in energy metabolism, cellular redox state and regulating apoptosis. Peroxidation of lipid is also one of the results of the accumulation of ROS. Mitochondrial membranes and mitochondrial DNA are prone to undergo oxidative damage due to their close proximity to the site of ROS production. Moreover, other factors that cause these sites of mitochondria to be susceptible are high content of PUFA of mitochondrial membranes and lack of mitochondrial DNA histones (Kim & Kim, 2018). Under pathologic condition, mitochondrial fission is increased with swelling and fragmentation.

Many techniques have been developed to analyse functional changes that occur in cellular compartments during apoptosis. Quantification of cells undergoing programmed cell death in mitochondria is crucial as this organelle represents a key organelle for the cell survival. Alteration of mitochondria during apoptosis has been widely described, such as release of cytochrome c, caspase activation, decrease of mitochondrial membrane potential, etc.

1.4 Aims & Objectives

Aims: Clarify the role of excessive iron on β-cell function – insulin synthesis and secretion. (Chapter 3).

Objectives:

- Clarify the role of excessive iron on the level of β-cell iron status by ferritin immunoassay.
- Clarify the role of excessive iron on β-cell insulin secretion and content by insulin immunoassay.
- Identify whether the excessive iron may have an effect on β-cell viability by conducting cytotoxicity assays.
- Identify whether the excessive iron may have an effect on the intracellular iron transporter 1 (DMT1) protein expression by immunoblotting.
- Identify whether the excessive iron may have an effect on SNAP-25 protein expression by immunoblotting.
- Optimise diferric-Tf as a model on the iron delivery into the β-cell.

Aims: Correlate excessive iron mediated ROS generation to β-cell dysfunction and identify whether specific organelles such as the mitochondria are more sensitive to ROS damage. (Chapter 4).

Objectives:

- Clarify the role of excessive iron related to the level of malondialdehyde (MDA) as a result of lipid peroxidation by thiobarbituric acid reactive substances (TBARS) assay.
- Clarify the role of excessive iron on β-cell cytotoxicity through formation of carbonyl group on protein side chains as a form of cellular oxidative damage by immunoblotting.
- Optimise the visualisation of any formation resulted by cellular oxidative damage using confocal microscopy.
- Identify whether excessive iron may have an effect on mitochondrial membrane potential by flow cytometry.

- Assess the effect of excessive iron on mitochondrial oxygen consumption by Agilent Seahorse XF metabolic analyser.

Aims: Identify the role of antioxidant-nanoformulations on small intestine function using caco-2 cell – model for antioxidant-nanoformulations strategy in excess iron. (Chapter 5).

Objectives:

- Identify various iron treatment formulations using potato dextrin and modified citrus peel dextrin with and without the presence of iron inhibitor (EGCG).
- Identify the activity of antioxidants (hesperetin)-related nanoformulations using ferric reducing antioxidant power (FRAP) analysis.
- Identify the activity of cellular antioxidants-related nanoformulations using cellular antioxidant activity (CAA) analysis.

Based on the above assessments, this study will test the hypothesis that iron accumulation in the β-cell may lead to the generation of ROS and promote cellular dysfunction and defects in insulin secretory function. Thus, identifying whether specific organelle such as mitochondria are more sensitive to ROS damage may lead us to a clearer understanding on the mechanism of iron mediated oxidative stress and β-cell dysfunction.

CHAPTER 2
MATERIALS & METHODS

2. Materials & Methods

All chemicals were a cell culture grade and purchased from Sigma-Aldrich (Dorset, UK) unless otherwise stated. MIN6 cells were a kindly gift from Dr. Bo Liu (Division of Diabetes & Nutritional Sciences, King's College London, UK) at passage 34 (originally from Dr. Miyazaki (Miyazaki et al., 1990). Ferritin ELISA kit (product code S-22) from ATI Atlas (Chichester, UK). TBARS Parameter kit (product code KGE013) from R&D Systems (Abington, UK). Pierce LDH Cytotoxicity Assay kit (product no. 88954) was from Thermo Scientific (Illinois, USA). The radioimmunoprecipitation assay (RIPA) was purchased from Thermo Scientific with a product code 10017003 (Thermo Scientific™ Pierce™ RIPA Buffer). Protease Inhibitor Cocktail (PIC, catalogue no. P8340) was from Sigma-Aldrich (Dorset, UK).

Dulbecco's modified Eagle's medium (DMEM), Minimum Essential Medium (MEM), fetal bovine serum (FBS), and reagents were obtained from Invitrogen (Loughborough, UK) and Lonza (Slough, UK). Potassium Chloride (Catalogue no. BP366-500) was from Fisher Scientific (New Jersey, US). The 12-well cell culture dishes, 96-well microtiter plates, and flasks were from Nunc (Roskilde, Denmark). Experimental reagents were prepared using ultrapure water (resistivity of 18.2 MΩ cm). Pipettes, micropipettes, and Eppendorf tubes were purchased from Corning (Amsterdam, The Netherlands). BioRad mini trans-blot® electrophoretic transfer cell was obtained from Bio-Rad (Bio-Rad, UK). Rabbit anti-human NRAMP2 (with- IRE) igG was purchased from Alpha Diagnostic Intl Inc. (Cat.no. NRAMP22-A, San Antonio, USA). Goat anti-rabbit IgG H&L (HRP) (Cat. No. ab205718) and anti- β- tubulin antibody (Cat.no. ab6046) were purchased from Abcam biotechnology company (Abcam, UK). All chemicals in immunoblotting purpose were obtained from Sigma-Aldrich (UK) and Thermo Scientific (UK).

2.1 Cell culture

2.1.1 Caco-2 cell culture

Prior to study the effect of excess iron on the β-cells, these current studies were also investigating the pathways of iron entry into the body. This investigation was carried using Caco-2 cells as the human intestinal cells, in which iron is absorbed. Caco-2

cells were obtained at passage 47 and employed for experimental use at passages 48 and 49. Stock cultures of Caco-2 cell lines were maintained in 75 cm^2 tissue culture flasks in complete medium (Dulbecco's Modified Eagle Medium (DMEM) - Gibco™ GlutaMAX™, Ph 7.4. Media was supplemented with 50 ml Foetal Bovine Serum (FBS), 5 ml antibiotic/antimycotic solution, 5 ml L-Glutamine) for consistency and control of the mammalian cell culture. The cells cultures were incubated at 37°C in an atmosphere of air (95%) and CO_2 (5%) at constant humidity. The culture medium was replaced routinely every other day. Caco-2 cells were trypsinised upon reaching 70% confluence and were seeded onto 8 x 6-well plates at a seeding density of 30,000 cells/cm^2 at passage 48. Replicate 8 x 6-well plates were also seeded similarly at a seeding density of 30,000 cells/cm^2 for optimisation of the initial uptake experiment. At day 14-15 post seeding, the Caco-2 cells differentiated, forming a fully matured gastrointestinal (GI) tract phenotype, and the iron uptake experiments were initiated.

2.1.2 Nanocarrier iron formulation

Nanocarrier systems encapsulating iron were formulated at a collaborator lab (UCL School of Pharmacy). Protein polysaccharide formulations comprised of Potato Dextrin (NF1) and Modified-Citrus Peel Dextrin (NF2) were prepared using 1% (w/v) potato protein solution and 0.1% (w/v) iron as a basis, followed by 0.1% of each polysaccharide to yield the novelty behind NF1 and NF2. The mixture was then combined through a heating process at 60**°**C for 15 min. The volume was altered to 10 ml using de-ionised water and in doing so, an unfolded form of the protein was produced during its cooling period allowing for interaction with different components. Malvern Zetasizer Nano was utilised to conduct a size analysis on potato particles and the results concluded all nanocarriers to be <500 nm.

2.1.3 Iron free feeding in caco-2 cells

On day 13 post-seeding, DMEM was aspirated from the 8x6-well plates and washed with DPBS (Dulbecco's Phosphate- Buffered Saline – pH 7) and cultured in MEM (Minimum Essential Medium – pH 7.4). Medium was supplemented with 5 ml antibiotic/antimycotic, 5 ml L- Glutamine, 1.5 ml Phenol Red solution. Plates were incubated for a 24-hour period.

2.1.4 Caco-2 iron uptake

The pH of the MEM was adjusted to 5.8 to mimic the physiological pH in the duodenum, by titrating MEM with 10 mM HCl stock and 2-(N-morpholino) ethanesulfonic acid (MES) as required. The altered MEM was then sterile filtered using a 0.22 µm sterile membrane filter. Various stock solutions ($FeSO_4$, EGCG) were prepared before preparing treatment media. Two novel nano-formulated forms of iron were provided by UCL School of Pharmacy; Novel Iron 1 and Novel Iron 2.

Table 2.1.4: Composition of various iron treatment formulations, both alone and in the presence of potent iron inhibitor, EGCG

Treatment	Iron Concentration (µM)	EGCG Concentration (µM)
Control	0	0
$FeSO_4$	20	0
$FeSO_4$ + EGCG	20	100
Potato Dextrin (NF1)	20	0
Potato Dextrin (NF1) + EGCG)	20	100
Modified Citrus Peel dextrin (NF2)	20	0
Modified Citrus Peel dextrin (NF2) + EGCG	20	100

Treatments were prepared by aliquoting 14 ml of pH 5.8 MEM into falcon tubes, each with different volumes and concentrations; 20 µM of Ferrous Sulphate, 20 µM NF1 and 20 µM NF2 – alone, and also in the presence of 100 µM EGCG. Ferrous Sulphate was used as a source of free elemental iron to simulate the conditions β-cells might be exposed to in the presence of excessive circulating serum iron. Once the treatments were prepared, the 6-well plates containing media were aspirated and washed with DPBS and the treatments were added (2 ml per well- 3 wells per condition) and incubated for 2 hours at 37°C in a rotatory shaker at 30 RPM. Treatment

was aspirated following on from incubation and cells were washed again with DPBS. Caco-2 cells were fed with fresh MEM with 2 ml per well and incubated for a further 22 hours (37°C in an atmosphere of air (95%) and CO_2 (5%) at constant humidity).

2.1.5 Cell cryopreservation and reconstitution

Most of the cell cultures can be stored at cryogenic temperatures (-196°C), minimizing deterioration of biological material over a time scale of indefinite years. Under cryogenic storage, many advantages can be obtained due to a liquid-nitrogen freezer that maintains these cells at the temperature below -130°C. This process can be applied by many different types of cells, which these cells more likely do not undergo detectable alterations such as genetic change, providing viable results even after thawing. Concomitantly, cross contamination by other cell lines may be suppressed. After undergoing cells trypsinization, in which cells are dissociated using trypsin, cryoprotectant is added to the freezing medium to protect the cells of forming intracellular ice crystal during the process of slow freezing. Dimethylsulphoxide (DMSO) is considered as one of the common cryoprotectants that has been utilised widely. However, this preservative agent has a toxic effect on cell cultures, thereby suitable concentrations required to be considered before diluted with cell suspensions in culture medium.

The appropriate concentration ranges from 5% to 15%, with 10% corresponds to this particular experiment. Gentle handling of cells prior to storing in nitrogen liquid needs to be taken into consideration, thereby reconstitute the cells also requires appropriate steps. Due to toxicity of cryoprotectant, removal of this agent is crucial, minimizing damage to cells. Firstly, the cryogenic vials contain MIN6 cells are removed from their storage and placed in Mr. Frosty (with regards to distance). These cells then removed from Mr. Frosty and placed them in incubator with an atmosphere of 95% air and 5% CO_2 for roughly 10 min to ensure that the cells become semiliquid, and subsequently transferred to a 15 ml centrifuge tube into which 5 ml of fresh growth medium was added. The cell suspension underwent centrifugation at 5000 RPM for 5 min, then the pellet was resuspended in T-75 tissue culture flask containing 10 ml of fresh growth medium.

2.2 Exposure of iron and glucose on MIN6 cells

Table 2.2: List of treatments consist of both glucose and iron on MIN6 cell line

Name of Condition	Treatment	Glucose Concentration (mM)	Iron Concentration (μM)
Ctrl	Basal glu	1.1	0
C1	Glu	5.5	0
C2	Glu	11	0
C3	Fe	0	20
C4	Fe	0	100
C5	Glu + Fe	5.5	20
C6	Glu + Fe	11	100
C7	Glu + Fe	5.5	20
C8	Glu + Fe	11	100

Glucose and iron exposure experiment was carried using serum-free MEM with 5.5 mM glucose. This media was supplemented with 2 mM L-glutamine, 1% antibiotic/antimycotic, 0.1% BSA and 25 mM Hepes, pH 7.4. Cells were seeded at 25 x 10^4 cells/cm^2. The cells were iron starved with serum-free media treatment and incubated overnight prior to the experiment at 37°C with 5% CO_2. Media was then discarded, and cells washed twice with DPBS. MIN6 cells were preincubated for 2 hours in Krebs-Ringer Bicarbonate (KRB) buffer [119 mM NaCl, 4.74 mM KCl, 2.54 mM $CaCl.6H_2O$, 1.19 mM KH_2PO_4, 1.19 mM $MgSO_4.7H_2O$, 25 mM $NaHCO_3$, 10 mM Hepes, pH 7.4, and 0.05% BSA] containing 1.1 mM glucose before the glucose and iron stimulation. MIN6 cells were washed with DPBS and placed in KRB buffer containing varying concentration of glucose (5.5 mM and 11 mM), concentration of iron (20 μM and 100 μM), combination of both glucose and iron concentration, and an addition of tolbutamide concentration (100 μM) as a drug to stimulate insulin secretion.

Preincubation was carried at different time courses at 3 and 24 hours. Cells then were lysed with 500 µL of stock solution (50 mM NaOH, pH 7.4) and the addition of protein inhibitor cocktail (PIC) in the buffer. Cells could either be stored at -20°C or utilised for particular analysis immediately (PrestoBlue®, Ferrozine, Ferritin ELISA & BCA, insulin secretion, and lipid peroxidation assay).

2.2.1 MIN6 cell culture

MIN6 cell line was derived from a mouse insulinoma that has been used extensively in biochemical and molecular research area (Cheng et al., 2012). These cells were prepared and maintained previously. MIN6 cells were obtained at passage 34 in a complete Dulbecco's modified Eagle's medium (DMEM) - GlutaMax®, pH 7.4 supplemented with 10% foetal bovine serum (FBS), 1% antibiotic/antimycotic solution and 25 mM HEPES. The cells were incubated in an atmosphere of 95% air and 5% CO_2 at constant humidity. Stock cultures were grown at 37°C in 75 cm_2 T-flasks, replacing the medium every two days. Cells were seeded in 12-well plates with density of 50 x 10_4 cells/cm_2 for all experimental cultures. MIN6 cells reached confluence within day 3-5 post-seeding in which phenotype of small clusters of cells to be formed (Johnson et al., 2007).

2.2.2 Cell harvesting in MIN6 cell line

50 mM NaOH stock was prepared from the 1 M NaOH stock and Milli-Q. The cell lysis buffer was prepared by adding 140 µl PIC (Protease Inhibitor Cocktail) and 14 ml of 50 mM NaOH stock solution. The 6-well plates were then placed on an ice try where the media was aspirated and washed with DPBS. The MIN6 cells were harvested by adding 350 µl of lysis buffer to each well. Upon completion, the cells were incubated whilst in the ice tray, on a plate rocker (10 RPM) for 20 min. The resulting cell lysates were collected using a sterile cell scraper and collected into individual 0.5 ml micro-centrifuge tubes. Using a 1 ml syringe with 25-gauge needles, each lysate sample was passed six times, re-suspending the lysates to reduce viscosity. The samples were immediately placed in the fridge (4°C) for 24 hours for further analysis.

2.3 Measurement of cellular cytotoxicity

PrestoBlue® cell viability reagent was used to measure the cytotoxicity of cells. Unlike other experiments explained above, this particular experiment was using live cells growing in culture. This reagent contains a cell-permeant compound that was not performed fluorescent in solution though possessed blue colour. This assay was very simple and fast due to a rapid change of colour and a quick uptake by the cells when reagent was added to media. Viable cells that contain the reducing environment then converted PrestoBlue® reagent to an intensively red-fluorescent dye. The protocol was obtained and adapted directly from the kit. Absorbance was then measured at 560-590 nm using a microplate reader (BMG LABTECH, Germany).

2.4 Intracellular total iron quantification

Ferrozine assay was used to quantify the release of iron. The standards were prepared by a serial dilution of a 500 µM iron standard using 10 mM of HCl as diluent into eight different concentrations of iron (0 µM, 10 µM, 20 µM, 30 µM, 40 µM, 60 µM, 80 µM, 120 µM). The cell lysates were aliquoted to each Eppendorf tube containing 200 µl of sample and mixed with 200 µl of 0.1 HCl. Sodium hydroxide (200 µl) with the concentration of 50 mM was added to each of the standard, with separate blank of 400 µl. The samples were added to 200 µl of freshly prepared iron-releasing reagent consisting of equal volumes of 1.4 M HCl and 4.5% (w/v) potassium permanganate in water. Each Eppendorf tube containing both samples and standards were incubated for 2 hours in a 60ºC water bath within a fume hood, due to chlorine gas that is yielded during the reaction. Pre-treatment of a mixed solution of HCl/$KMnO_4$ is crucial due to its ability to release iron quantitatively from proteins including ferritin (Panter, 1994).

Each Eppendorf tube was transferred to a rack and cooled to room temperature for five to ten minutes. After reaching the room temperature, 60 µl of the iron detection reagent was added into each tube, which contained 6.5 mM ferrozine, 6.5 mM neocuproine, 2.5 M ammonium acetate, and 1 M ascorbic acid dissolved in water. Since ferrozine is light sensitive, solution preparation should be carried out limiting exposure to light (Riemer et al., 2004). These tubes underwent incubation for 30 min before the absorbance was measured at 550 nm using a microplate reader. After 30 min, colour development is observed and 280 µl from both standard and sample tubes

is added in duplicate into wells of a 96-well plate. The intracellular iron concentration was determined from the standard curve performed by BCA assay.

2.5 Intracellular ferritin quantification by immunoassay

A spectrophotometric ELISA kit assay was used to measure the total protein concentration of the supernatant. Manufacturer's protocol was followed with minor variations. Three different calibrators (0, 20, 60, 200 ng standard/ml) were chosen to generate a standard curve. Standards and samples (30 µl) were pipetted onto a 96-well plate in duplicate followed by the incubation step as described in the protocol. The absorbance was measured at 490 and 630 nm using a microplate reader. This experiment was followed by measuring the total protein content of MIN6 cells using Pierce BCA kit. The bovine serum albumin (BSA) was used as a stock (2 mg/ml) provided in the kit was used to prepare standards by serial dilutions. Samples were loaded in duplicate onto a 96-well plate (25 µl). Absorbance was determined at 562 nm using above microplate reader (Section 4.3). The ferritin concentration was standardised against the total protein concentration.

2.6 Intracellular insulin quantification by immunoassay

Measurements of insulin are pivotal for the investigation of β-cells function. To determine insulin secretory response in the presence of tolbutamide, MIN6 cells need to be incubated in presence of KRBB for a specific duration of time after which the media is collected and proceeded with extracellular insulin concentration quantification. Unlike standards used in Ferritin ELISA, this particular experiment performed the calibration curve applied four highest calibrators with concentrations 0.2, 0.5, & 1.5 ug/L respectively (Mercodia Mouse Insulin ELISA). Appropriate number of standards and samples (10µl) were transferred onto a 96-well plate in duplicate followed by the incubation step as described in the protocol. The absorbance was measured at 450 nm using a microplate reader.

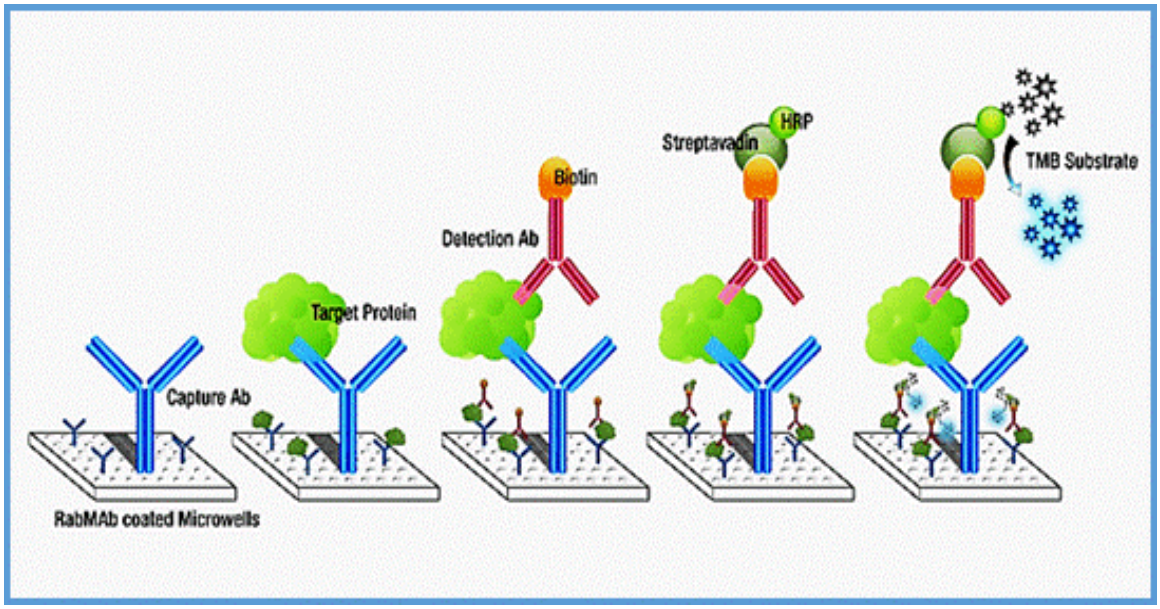

Fig. 2.6. Schematic diagram of sandwich ELISA (image available online intranet.tdmu.edu.ua).

2.7 Lipid peroxidation assessment

Sample supernatants from the static incubation experiments stored at -20°C, were assessed for lipid peroxidation using a Thiobarbituric Acid Reactive Substances (TBARS) (R&D Assay Kit). The procedures were as follows. A stock solution of 167 µM was prepared by combination of 100 µl TBARS Standard and 200 µl TBARS Acid Reagent. This solution was kept at room temperature for 30 min with gentle agitation at 30 RPM. Prior to experiment, all reagents and supernatants should be kept at room temperature for 30 min and water bath should be preheated to reach 80°C.

After 30 min, stock solution was diluted to produce seven different concentrations of standards; 16.7 µM, 8.35 µM, 4.18 µM, 2.09 µM, 1.04 µM, 0.52 µM, and 0.26 µM. Each standard was transferred to a new labelled tube contained 150 µl its standard and 75 µl of TBA reagent. Transferred 105 µl of supernatant to each designated tube (in duplicate). This was followed by the addition of 105 µl TBARS Acid and 105 µl TBA Reagent. Each sample and standard were transferred back to designated tubes and placed in a water bath at 80°C for 1.5 hours. To determine the final reading, a 96-well plate was used to determine the optical density of each well and was measured using a microplate reader set to 532 nm. The data was then determined by subtracting pre-reading from the final reading.

2.8 Ferric reducing antioxidant power (FRAP) assay

ROS and RNS are by-products of normal cellular metabolism that play a dual role as both deleterious and beneficial species. At low or moderate concentrations, these species involve in many physiological roles such as cellular responses to noxia and induction of mitogenic response. However, an overproduction of ROS/RNS and concomitantly deficiency of enzymatic and non-enzymatic antioxidants results in oxidative/nitrosative stress, respectively. Thus, measuring antioxidant activity via ferric reducing antioxidant power (FRAP) assay may contribute some beneficial information relate to this area.

2.8.1 Methodology

This assay applies the reduction of ferric tripyridyl triazine (Fe III TPTZ) complex to ferrous and at the low pH, intense blue colour is formed, in which can be measured in absorption at 593 nm. Prior to starting this experiment, FRAP reagents needs to be made by three different components, which are 300 mM of acetate buffer (pH 3.6), 10 mM TPTZ in 40 mM HCl, and 20 mM Iron (III) Chloride Hexahydrate ($FeCl_3$.6H2O). Trolox, a water-soluble analogue of vitamin E and Epigallocatechin (EGCG), an antioxidant isolated from green tea are antioxidants used as references in this experiment. Moreover, hesperetin is an antioxidant with 97% purity (ShenZhen Dieckmann, China) is used to further being encapsulated with 100% shell protein with polysaccharide made of potato protein to modified citrus pectin (NF1) or potato dextrin (NF2). Methanol, DMSO, and distilled water are used as diluents.

As the FRAP reagents are prepared freshly, 5 ml of acetate buffer, 5 ml of TPTZ solution and 50 ml of the $FeCl_3$.6H2O are added to this reagent. 100 µl of the standards (EGCG and Trolox) is then prepared at different concentrations for the calibration curve (400 – 300 – 200 – 100 – 50 µM) in Eppendorf tubes. Thereafter, 30 µl of nanoencapsulated samples, standards (Trolox and EGCG), pure hesperetin and blank control (DMSO, distilled water or methanol) are added to 900 µl of FRAP reagent, which is incubated for 30 min at RT. Subsequently, the samples are centrifuged at 10,000 g for 6 min at 25ºC and followed by removing 300 µl of the supernatant to be placed in a 96-well plate for further analysis. Absorbance readings are taken using a visible UV microplate reader set at 593 nm.

2.9 Cytotoxicity studies with MTT assay

This is a colorimetric assay that measures the reduction of yellow 3- (4,5-dimethylthiazol-2-yl) -2,5-diphenyl tetrazolium bromide (MTT) by mitochondrial succinate dehydrogenase. The MTT in yellow enters the cells and passes into the mitochondria where it is reduced to formazan product, which gives a dark purple colour. Reduction of MTT can only occur in metabolically active cells. That is the reason why the quantity of formazan product is proportional to the quantity of viable cells.

2.9.1 Methodology

Prior to the day of experiment, four different samples were assembled with concentrations ranges from 20-100 μM. The media was aspirated from each well comprising in three of 96-well plates (clear-black bottom), which was replaced by the addition of test media on the cells. The treatment was performed in six replicate wells. DMEM is considered as the positive control, whereas dH_2O is the negative control. Thereafter, each plate was incubated in an incubator (95% air, 5% CO_2) for period of 24, 48, or 72 h. As elucidated previously in section *2.1.1*, 30, 000 cells/cm_2 was applied as a seeding density with passage 45**.**

Table 2.9.1: List of various concentrations of nanoformulations in presence or absence of hesperetin

Formulation	Indication	Concentration (μM)
NF1	Modified citrus pectin + Hesp	20, 50, 100
NF2	Potato dextrin + potato pectin + Hesp	20, 50, 100
NF3	NF1 (no Hesp)	20, 50, 100
NF4	NF2 (no Hesp)	20, 50, 100

In the following day, 5 mg/ml MTT reagent was prepared freshly in sterile DPBS just before the end of the incubation time. These components are mixed by vortexing until dissolved. Prior to a 24 h incubation period, 20 µl of the MTT reagent was added into each well and subsequently incubated the cells for 4 h at 37ºC. The media was

removed carefully avoiding pipetting adherent cells and followed by inserting of 100 µl of DMSO in each well before mixing the reagent well. The plate is covered with foil to avoid light exposure and is incubated in an orbital shaker for 15 min at 75 RPM. The plate is further analysed, measuring the absorbance at 570 nm in a spectrophotometer. These steps were repeated onto remaining two plates for 48 and 72 h incubation, respectively.

2.10 Cellular antioxidant activity (CAA) assay

The cellular antioxidant activity (CAA) assay measures antioxidant activity of a molecule in a cell culture. The sample treatments enter the cells, the 2′,7′-Dichlorofluorescin diacetate treatment (DCFHDA) is added. It is a cell permeable non-fluorescent probe, which indicates the intracellular level of ROS. DCFH-DA is then deacetylated by cellular esterases and form 2′,7′-Dichlorofluorescin (DCFH) which turns fluorescent upon oxidation. ABAP or 2,2′-azobis (2-amidinopropane) dihydrochloride is added to create oxidative stress in the cells. It enables DCFH to be oxidized in the fluorescent DCF. The ultimate goal of this experiment is to show that the antioxidant properties of nanoencapsulated hesperetin have a cellular impact when cells endure oxidative stress. The antioxidant activity of nanoencapsulated hesperetin prevents the oxidation of DCFH and reduces the formation of DCF, indicating less fluorescence to be found corresponds to the less oxidation in the samples. Pure hesperetin samples should have a lower value of fluorescence since it is an antioxidant, however due to the absence of encapsulation, their antioxidant properties would be decreased on exposure to the environment.

2.10.1 Methodology

Similar to FRAP assay, this experiment applied three of 96-well plates (clear-black bottom) with treatment media composed of HBSS and 10% FBS. The samples are elucidated on Table 2. This analysis is performed using Sessa and adapted from Wolfe's article. In initiating the experiment, a 200 mM stock solution of ABAP (200 mM) is prepared in distilled water and followed by a stock solution of DCFH-DA (20 mM) diluted in methanol, covered with aluminium foil and stored at 4°C. The growth medium is removed from each well and cells are washed with 100 µl of treatment media.

This treatment media is then aspirated and replaced with 200 µl of the various concentrations of NFs applied on the cells. Each condition is twelve times replicated. 200 µl of treatment media is considered as a blank and control. Each microplate is incubated for an hour at 37°C in the cell culture incubator. During incubation time, each of 100 µM DFCH-DA solution and the 600 µM ABAP solution was prepared in treatment medium. After the incubation, media is removed, and cells were washed with 100 µl of treatment medium.

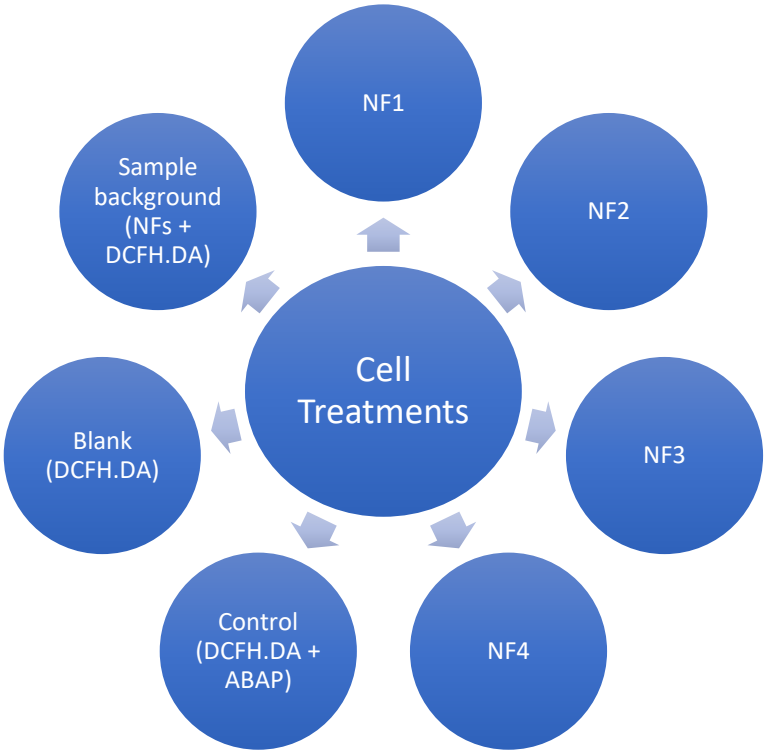

Fig. 2.10.1. A proposed nanoformulations and reagents required to demonstrating CAA assay on caco-2 cells.

Then the cells are treated with 200 µl of DCFH-DA solution (100 µM) and incubated for 30 min at 37°C. Afterwards, cells are washed and 100 µl of ABAP solution (600 µM) is applied in each well except for blank and sample background wells where only contain 100 µl of treatment medium. Place the 96-well plate in a fluorescent microplate reader (FLUOstar OPTIMA, BGM Labtech) at 37°C with emission is measured at 528 nm and excitation at 485 nm for an hour period.

2.11 Immunoblot analysis

2.11.1 Cell lysate preparation

Many analyses can be applied prior to treatment exposure towards cells. Cell lysate was prepared to determine protein content, which would be used as standards amount of proteins using BCA assay as mentioned above. A careful act is required in handling these proteins, as it is their nature to be degraded. Lysis buffer is essential in avoiding protein degradation and enables efficient cell lysis and protein solubilisation. RIPA is a commercially used lysis buffer that has the ability to extract proteins from the cells, including plated cells and pelleted suspension cells. This buffer is supplemented with a known protease inhibitor called PIC to avoid protein degradation. This effective inhibitor is composed of 25 mM Tris-HCl (pH 7.6), 150 mM NaCl, 1% NP-40, 1% sodium deoxycholate, 0.1% SDS.

Loading buffer is essential prior to sample loading into gel cassette. A bromophenol blue dye was added to the protein solution to track the progress of the protein solution through the gel during the electrophoretic run (Boster Biological Technology, 1993). Samples were diluted 1:4 dilution and heated at 95°C for 5 min. This buffer (2X) consists of 50 mM Tris-HCl (pH 6.8), 23% w/v sucrose, 4% w/v SDS, 0.02% bromophenol blue dye, and 100 mM DTT.

2.11.2 Gel casting

Two gel solutions were prepared in a process of gel making, which are resolving and stacking gel solutions. Resolving gel solution is prepared firstly to fill a gel cassette and allow the gel to polymerize for roughly 5-10 min followed by stacking gel solution. A comb is placed into the assembled gel sandwich as the port to load ready samples. This gel can then store at 2-8°C for further application. Prior to SDS-PAGE, remove the comb by pulling it straight up slowly and gently.

Table 2.11.2: Volume of resolving and stacking gel solutions required to fill a gel cassette

Reagents	Resolving gel (10%)	Stacking gel (4%)
30% acrylamide/bisacrylamide	2.25 ml	0.375 ml
Stacking gel buffer (0.5 M Tris-HCl pH 6.8)		0.465 ml
Resolving gel buffer (1 M Tris-HCl pH 8.8)	1.95 ml	
dH_2O	3.75 ml	2.7 ml
10% SDS	75 µl	37.5 µl
15% w/v ammonium persulphate (APS)	75 µl	37.5 µl
TEMED (N,N,N',N', Tetramethylethylenediamine)	15 µl	7.5 µl

2.11.3 Sodium dodecyl sulphate polyacrylamide gel electrophoresis (SDS-PAGE) analysis

Electrophoresis is a technique that has been used widely to separate the charged particles under the influence of electric field. The separation of proteins is based on the electrophoretic mobility of these proteins, which depends on their charge, molecule size, and structure of the proteins. Polyacrylamide gel (PAG) is a versatile supporting matrix due to its character, which possesses a neutral charge produces electroosmosis effect and little adsorption.

The application of SDS as an anionic detergent that mainly functions to break hydrogen bond within and between molecules. Moreover, this detergent could also unfold proteins and work similar to a strong reducing agent such as dithiothreitol (DTT) to break up secondary and tertiary structures. DTT and another reducing agent such as mercaptoethanol also have a major role in disrupting disulfide linkages between cysteine residues. The nature of these chemicals is suitable to employ as the buffer for gel running purpose. SDS-PAGE buffer composition is shown below.
10X running buffer:

250 mM Tris-Base pH 8.3
1.92 M Glycine
1% w/v SDS

The samples were then ready to be loaded into the port of gels. Electrophoresis was performed using the Bio-Rad mini-protean II electrophoresis system at 200 volts (V) for 45 min (Bio-Rad, UK).

2.11.4 Methodology

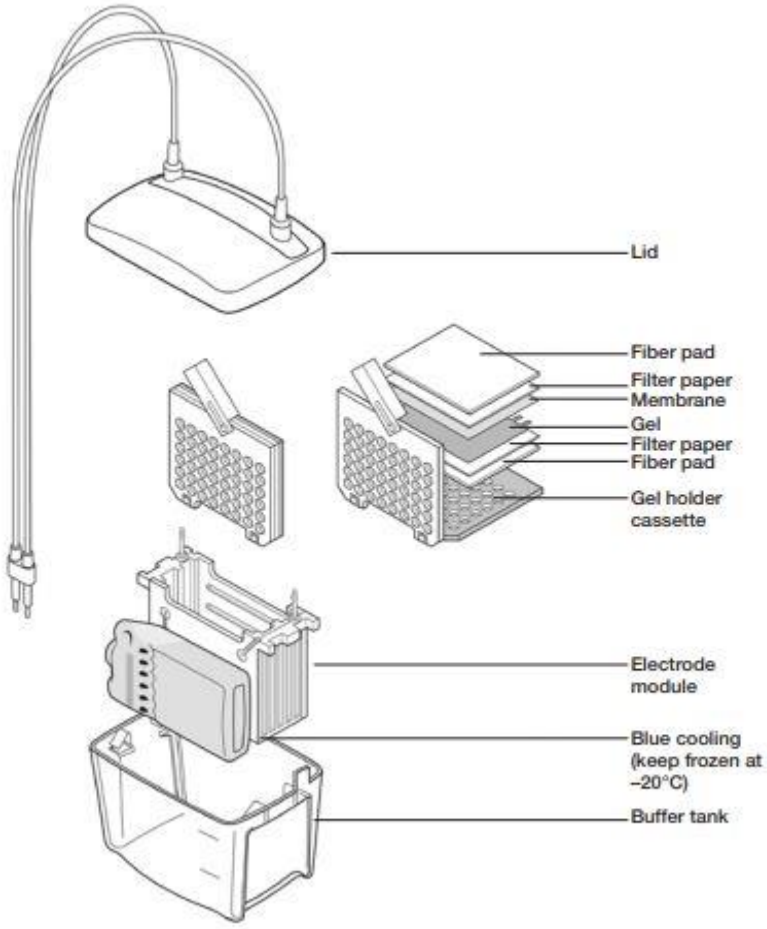

Fig.2.11.4. **BioRad Mini Trans-Blot® electrophoretic transfer cell**. Assembly includes cassettes for holding the gels and membranes; a cooling unit to absorb heat during transfer; and an electrode module that holds the cassettes. The cables attached to the lid are connected to a power supply (image available online www.bio-rad.com).

Different total proteins (15 µg and 10 µg) were loaded in each well. Protein samples were separated by electrophoresis on a 10% SDS-PAGE gel prior to transferring samples into nitrocellulose membrane. After seventy minutes transfer in its buffer at 4°C, nitrocellulose membranes were blocking with 3% BSA at the room temperature. The membranes were incubated with rabbit-anti-rat DMT1 antibodies (Alpha Diagnostic International, USA) (1:1000) for overnight on the rocking platform with faster setting in the cold room. Blots were then probed with anti-β-tubulin polyclonal antibody (Abcam, UK) at 1:500 dilution as a loading control. The membrane was then visualized using ECL Western Blotting detection reagent. Goat anti-rabbit secondary antibody conjugated to horseradish peroxidase (Abcam, UK) was used at 1:2000 and

was analysed by scanning densitometry using a Tanon Image System (Tanon, Shanghai, China).

2.12 Expression of protein carbonyl in MIN6 cells

The formation of carbonyl groups on the side chains of proteins was determined using an OxyBlot™ Protein Oxidation Kit (S7150, Merck Millipore). Cells were lysed using RIPA buffer and the protein concentrations were subsequently determined by performing BCA assays. A weight of 15 µg of protein was selected and used for either direct Western blot analysis or derivatization with the OxyBlot kit by following the manufacturer's instructions, except as noted herein. The protein lysates were derivatized using 2,4-dinitrophenylhydrazine (DNPH), yielding dinitrophenyl (DNP) hydrazone products, which were detected using the SuperSignal™ West Femto substrate (Thermo Fisher Scientific) and analysed by scanning densitometry using a Tanon Image System (Tanon, Shanghai, China). Furthermore, all the DNP bands in each lane were quantified using the ImageJ Software (version 1.52) and analysed in duplicate.

2.13 Estimation of OCR

Oxygen consumption rates were measured in accordance with the manufacturer's instructions (Seahorse Bioscience). Based on the methods elucidated in Section 2.11, all the indications remained the same, except the concentration of oligomycin and FCCP. OCR measurements were made more than five times repeatedly. It was appealing to find that iron and glucose applied distinct concentrations of these agents. The saturating concentration of oligomycin in the presence of iron was 1 µg/ml. On the other hand, cells with glucose content required 2.5 µg/ml. Although these two nutrients employed two separate complex IV inhibitors, there was no distinct concentration of this uncoupler agent, suggesting that 5 µgmol/L was the constant concentration of FCCP. Several analyses resulted from using this particular method, including the ability to estimate the basal respiration, ATP-linked respiration, proton leak, maximal respiration, reserve/spare respiratory capacity, and non-mitochondrial respiration.

2.14 Mitochondrial membrane potential (Δψm) assessment

After appropriate treatment with a suitable culture medium, the medium was replaced with a prewarmed staining solution containing a MitoTracker probe (M7512, Invitrogen). The desired staining concentration was 0.5 μM and the incubation was conducted overnight at 37ºC. The cells were then rinsed three times with DPBS and fixed in a solution of 4% PFA in a complete growth medium at 37ºC for 15 min. Thereafter, the cells were washed once in DPBS and permeabilized with 0.2% (v/v) Triton X-100 for 15 min under the same conditions stated earlier. The cells were scraped, placed in designated flow cytometry tubes, and further analysed using CyAn™ ADP with Summit™ software. Prior to the analysis, the cells were vortexed to avoid any aggregation which might give incorrect results. The cells were analysed at 579 and 599 nm as the excitation and emission wavelengths appropriate for fluorescein, respectively.

2.15 Imaging of live MIN6 cells influenced by Δψm changes

Samples were treated using the methods described in Section 2.2.8. However, instead of scraping cells from the plates, they were stored at 2-8ºC and used at a particular point. Prior to the day of the experiment, the supernatant was discarded and replaced with PBS. The live cells were then imaged using a confocal microscope (Leica Confocal Software, Leica Microsystems Heidelberg GmbH, Germany) with a 63x/0.9 wet objective. We subjected Texas Red to 543-nm helium/neon laser excitation and the emission was recorded through a band-pass 543- to 650-nm filter.

2.16 Expression of SNAP-25–mediated insulin exocytosis

The expression of SNAP-25 protein was quantified using the immunoblotting technique elucidated in Section 2.12, unless stated otherwise. The membranes were incubated with rabbit-anti-rat SNAP-25 antibodies (ab5666 - Abcam, UK) with a concentration of 1 μg/ml. This protein weighs approximately 25 kDa, which allows the detection of its bands at this similar weight. Goat anti-rabbit secondary antibody conjugated to horseradish peroxidase (Abcam, UK) at a ratio of 1:2000 was used. The blots were then probed with goat polyclonal anti β-actin (ab8229 - Abcam, UK) at 1:500 dilution as a loading control.

2.17 Cell Culture with transferrin treatments

Cells were treated with human transferrin (Sigma Aldrich, UK) (0.005, 0.05, 0.5, 2, and 5 g/L) for 24 h and supplemented with tolbutamide as an insulin secretagogue. Altogether, this protein was exposed towards the cells with other experimental agents such as iron and glucose that were added as demonstrated previously in Section 2.2.

2.18 Statistical analysis

All the experiments were performed three-time independently, with each treatment condition applied in triplicate. The data is presented as the mean ± SEM and the differences between the samples were analysed with the Student's *t-test*, using the GraphPad Prism software (Version 7.0). The results were considered significantly different if *P* was less than *0.05*.

CHAPTER 3
RESULTS

3. Results

3.1 Introduction

Aim: To clarify the role of excessive iron on β-cell function – insulin synthesis and secretion.

Objectives:

- Clarify the role of excessive iron on the level of β-cell iron status by ferritin immunoassay.
- Clarify the role of excessive iron on β-cell insulin secretion and content by insulin immunoassay.
- Identify whether the excessive iron may have an effect on β-cell viability by conducting cytotoxicity assays.
- Identify whether the excessive iron may have an effect on the intracellular iron transporter 1 (DMT1) protein expression by immunoblotting.
- Identify whether the excessive iron may have an effect on SNAP-25 protein expression by immunoblotting.
- Optimise diferric-Tf as a model on the iron delivery into the β-cell.

Failure of pancreatic β-cell has been found to be involved in the pathogenesis of T2D. Conventionally, it is believed to be caused by disruption of insulin action and its secretion, leading to relative insulin deficiency (Kahn, et al., 2014). T2D can later be developed only when the compensatory mechanisms such as nutrient excess, β-cell hypertrophy and hyperplasia, recruitment of β-cell mass, or even exocrine acinar tissue fail (Backe et al., 2016). Iron is crucially required for normal β-cell function. This micronutrient is involved in mitochondrial Fe-S clusters, which are important proteins that contribute to the production of ATP. Exocytosis of insulin and its further secretion can take place in the presence of an increased level of ATP/ADP ratio. However, under the conditions that affect the levels of intracellular iron, it can potentially cause diseases. Since β-cell majorly lacks enzymatic antioxidants, they are particularly vulnerable to oxidative stress (Wang & Wang, 2017). The levels of this micronutrient need to be maintained tightly within the body in preventing unwanted outcomes.

This chapter utilises pancreatic β-cell line, MIN6 cells as a model to perform the particular experiments due several notable characteristics being demonstrated. MIN6 cells form physiologically relevant clusters of islets (Fig. 3.1A-B) (pseudoislets) and express key proteins involved in glucose uptake such as GLUT-2 and glucose metabolism (glucokinase) (Skelin et al., 2010). Furthermore, this cell displays the structural and functional characteristics of mature β-cell - the ability for GSIS. Oftentimes, MIN6 cells experienced a sudden loss of glucose-induced insulin secretion, which is a minor disadvantage that could be supplemented with insulin secretagogues. These characteristics indicate that this cell line is an appropriate model for studying the mechanism of excessive iron accumulation mediated oxidative stress and β-cell dysfunction via the perturbations of insulin secretion.

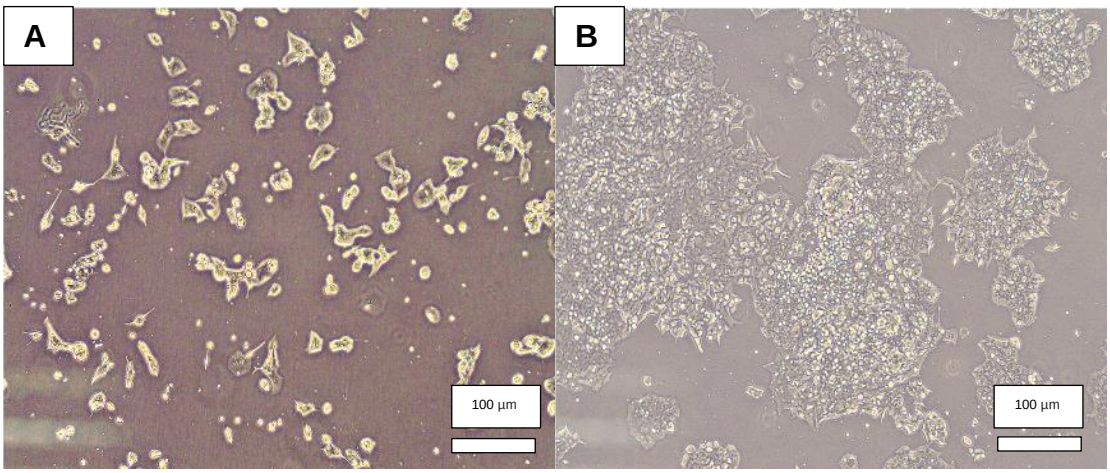

Fig. 3.1A-B MIN6 cells were grown on a tissue culture T-75 flask and photographed through a microscope (x10) with a passage number of 37. A: Morphology of MIN6 cells on day-3; B: Morphology of MIN6 cells on day-6.

Protein-related iron uptake in pancreatic β-cell such as transferrin is worth examined. Moreover, proteins that are involved in homeostasis such as DMT1 and ferritin were also identified. As previously mentioned, iron exhibits a critical role in insulin secretion, insulin exocytosis machineries such as SNAP-25 as one of core components of SNARE complex proteins are also demonstrated. Lastly, the effect of excessive iron in conducting pancreatic β-cell toxicity was also identified.

MIN6 cells are a pancreatic β-cell line, which has been used in this project to assess the effect of various compounds loaded in four different time courses (Table 3.1). Various analyses (Fig. 3.1C) below were performed to observe the effects of iron and glucose on cells as an *in vitro* model to mimic physiological conditions *in vivo*. Moreover, apo-Tf as an iron-bound protein is also added to the cells to mimic human physiological conditions. The passage number of the cells is within the range of 11-18 and 37-40 for each of the analyses below.

Table 3.1 Various experimental conditions of iron and glucose with four incubation times on MIN6 cells

	Experimental Conditions								
	Ctrl	C1	C2	C3	C4	C5	C6	C7	C8
Glu (mM)	1.1	5.5	11	-	-	5.5	5.5	11	11
Fe µM	-	-	-	20	100	20	100	20	100
3 h	✅	✅	✅	✅	✅	✅	✅	✅	✅
24 h	✅	✅	✅	✅	✅	✅	✅	✅	✅
48 h	✅	✅	✅	✅	✅	-	-	-	-
72 h	✅	✅	✅	✅	✅	-	-	-	-

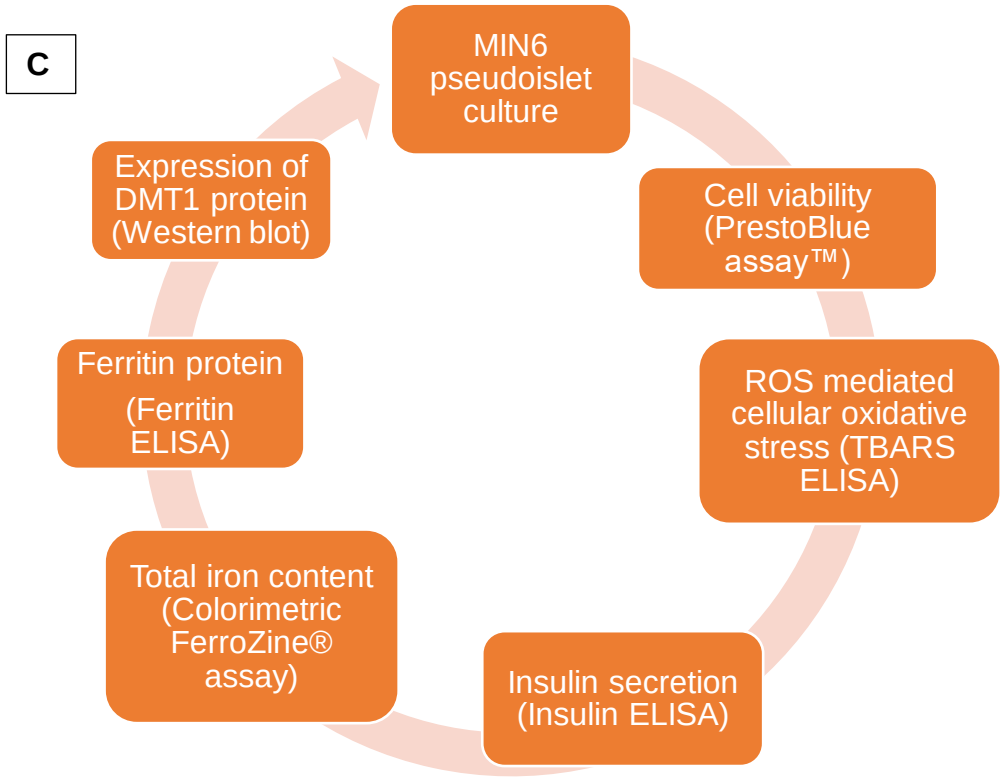

Fig. 3.1.C A diagram of different analyses performance using pancreatic β-cells MIN6, both in cell lysate and live cells.

3.1.1 Examination of DMT1 as the iron transporter

It has been known that DMT1 is involved in iron metabolism, which plays a crucial role in transporting ferrous iron. This protein has been found in every cell type as every cell requires iron to perform variety of biological processes. The expression of DMT1 was evaluated on MIN6 cells in 3 and 24 h incubation. Addition of two concentrations of iron (20 µM & 100 µM) were loaded to examine their effect on DMT1 detection. This experiment applied β-Tubulin as a loading control to ensure a consistent protein loading across the gel. Moreover, addition of this control is essential for proper interpretation in regard to obtaining the data. As shown in figure 3.1.1, normal and high iron concentrations exhibited no effect on intracellular DMT1 levels compared to control (*P>0.05*), although two concentrations of iron showed slight decrease in DMT1 levels (3 h).

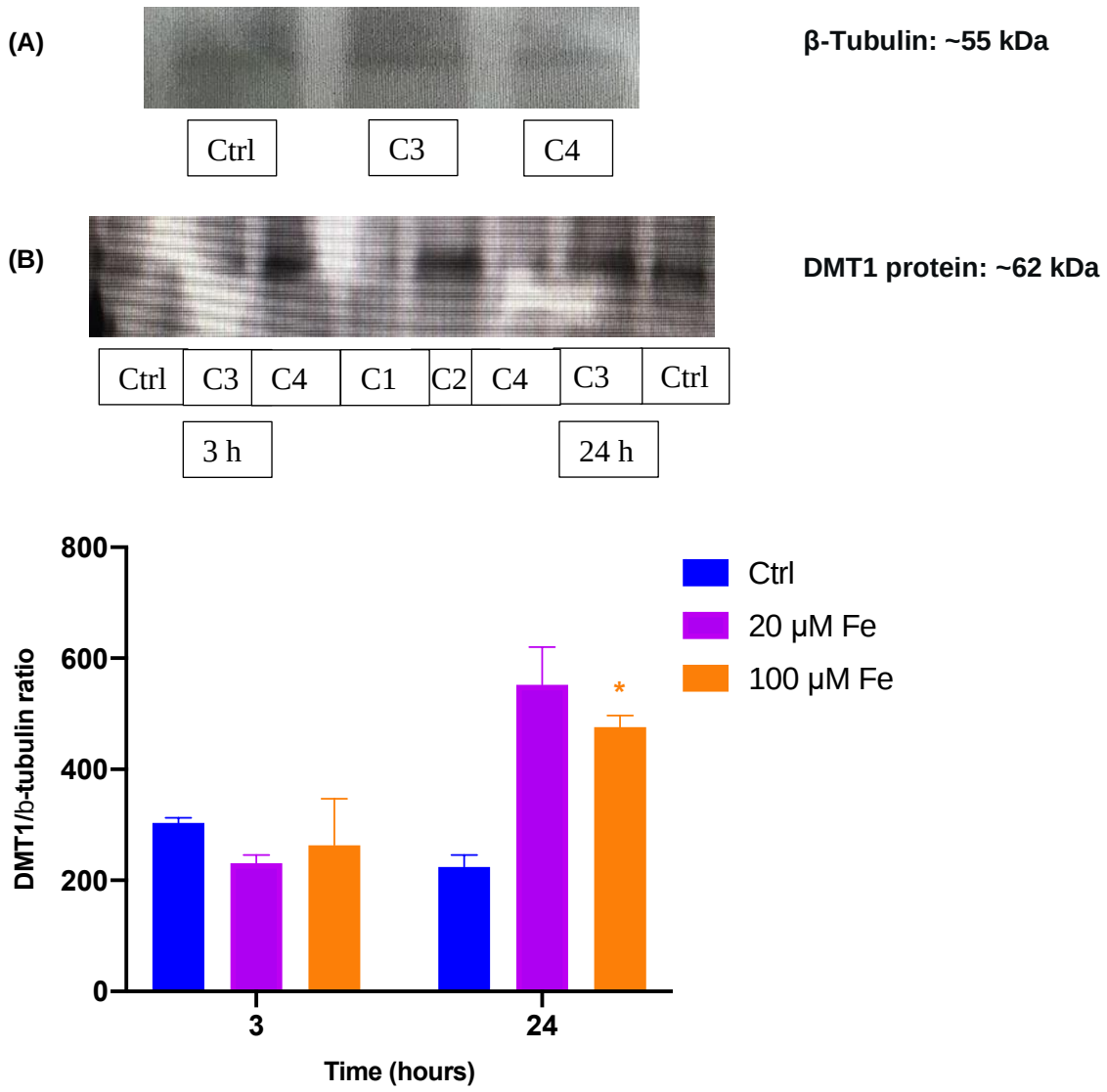

Fig. 3.1.1. DMT1 detection performed by western blotting in 3 h and 24 h incubation. To normalise the levels of protein detected, β-Tubulin was utilised. The protein was extracted and run through a 10% agarose gel. The results above are: (A) Different bands obtained by western blot, consisting of β-Tubulin (control) and DMT1 (protein interest). (B) The expression of DMT1 protein in 3 h and 24 h incubation. Gel loading was as follows (from the left): lane 1 – ctrl (3 h), lane 2 - normal iron (C3 – 3 h), lane 3 - high iron (C4 – 3 h), lane 6 - high iron (C4 – 24 h), lane 7 - normal iron (C3 – 24 h), lane 8 - ctrl (24 h). Data represent mean ± SEM. *P<0.0325. n=3.

On the other hand, both normal and high iron concentrations demonstrated higher levels of DMT1 with high iron twice as high than the control (52.9%) at 24 h. Moreover, although normal iron should noticeably demonstrate significant DMT1 levels compared to control, no significant difference was observed (*P>0.05*). This led to a further analysis of a range of iron concentrations and additional of experimental periods to acquire more information and understanding on the effect of iron on DMT1 protein at larger scales.

3.1.2 Assessment of circulating transferrin-bound protein

As elucidated earlier, circulating iron has to bind to a particular protein, Tf, which represents the normal form of circulating iron. MIN6 cells were exposed to various concentrations (0.005, 0.05, 0.5, 2, & 5 g/L) of Tf. These concentrations of Tf were expected to bind to iron within the circulation. Ferrozine assay was used to assess intracellular total iron content related to iron-bound protein and circulating iron-bound Tf. Fig. 3.1.2A showed that the highest Tf concentration was obtained from 5 g/L compared to 0.005 g/L (32.4 ng/mg protein vs 28.4 ng/mg protein). This result was followed by 0.005 g/L (28.4 ng/mg protein) and 0.05 g/L (27.5 ng/mg protein) as the second and the third highest Tf concentrations, respectively. Surprisingly, 0.5 g/L was considered as the normal Tf level physiologically, exhibiting the lowest Tf concentration (24.1 ng/mg protein).

Fig. 3.1.2B-E demonstrated a range of concentrations of Tf with the addition of two designated iron concentrations towards the level of total iron content. The data shows that normal iron exhibited insignificant decreased iron content in most of the designated Tf concentrations loaded. However, high iron demonstrated higher total iron content throughout all conditions. Figure 3.1.2E, represented the highest Tf concentration (5 g/L) with the addition of high iron, depicted to significantly increase 70.9% iron content compared to normal iron control (*P<0.05*). Iron content levels were progressively decreased in concomitant with decrement of Tf concentrations. Tf concentration of 2 g/L showed the second highest total iron content (63.8%) followed by 0.5 g/L (57.1%) and 0.05 g/L (55.0%), respectively. Therefore, it is proposed that the addition of increased Tf into the cells elevates total iron content levels.

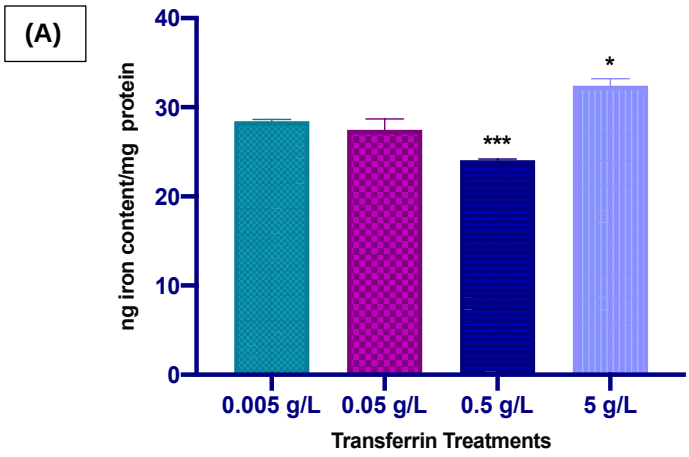

Fig. 3.1.2A. These data illustrated a range concentration of Tf loaded into MIN6 cells, followed by addition of iron concentrations for 24 h. The above experiments are as follows: (A) The effect of MIN6 cells on the exposure of distinct concentrations of Tf. The data represent mean ± SEM. ***P<0.0002, *P<0.039. n=3.

Other analyses such as ferritin and MDA levels should be observed as well to identify the effect of Tf towards MIN6 cells. The addition of this protein was to find out whether all the above analyses would demonstrate different effects towards MIN6 cells. Surprisingly, similar effects were observed at 48 and 72 h in quantifying total iron content levels in the absence of Tf. The only difference was that the level of total iron content increased significantly in the presence of Tf, particularly at 100 µM iron. Thus, it is suggested that a range of iron concentrations exposed to cells have no different effects compared to cells with the absence of Tf. Furthermore, the additional concentrations of glucose and the number of analyses is required to applied in order to obtain valid information that could strengthen the current data.

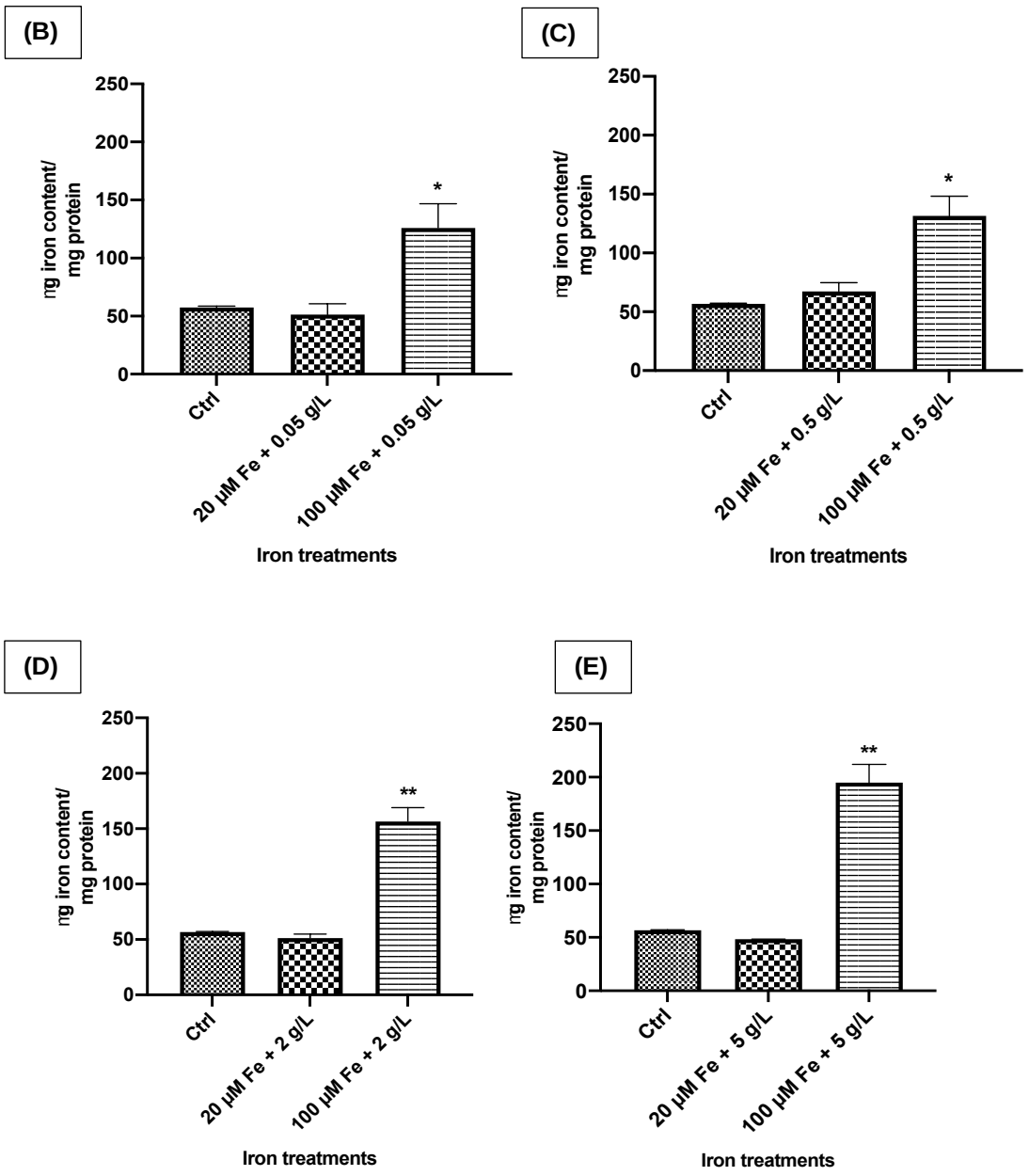

Fig. 3.1.2B-E. These data illustrated a range concentration of Tf loaded into MIN6 cells, followed by addition of iron concentrations for 24 h. The above experiments are as follows: (B) Concentration of iron content in presence of 0.05 g/L Tf with addition of iron concentrations. (C) 0.5 g/L Tf with addition of iron concentrations. (D) 2 g/L Tf with addition of iron concentrations. (E) 5 g/L Tf with addition of iron concentrations. The data represent mean ± SEM. *P<0.0138 (0.5), *P<0.048, **P<0.0031 (5), **P<0.0036 (2). n=3.

3.1.3 Estimation of total iron content

Estimating iron content is fundamental to advance further analyses as it can provide the quantity of intracellular iron and whether iron accumulates in cultured cells. MIN6

cells were incubated in the presence of various range of iron (20 μM & 100 μM) glucose (5.5 mM & 11 mM), combinations of iron and glucose (Table 3.1), and all with the addition of tolbutamide in 3, 24, 48, and 72 h. As shown in figure 3.1.3, iron and glucose demonstrated no change on intracellular iron content compared to its control (3 h). However, iron concentrations alone and conditions containing combinations of iron and glucose exhibited a significant increase of iron content compared to control at 24 h incubation ($P<0.05$). In addition, although glucose concentrations alone demonstrated higher iron content, the levels were insignificant compared to control ($P>0.05$). The highest level of iron content exhibited by a condition containing high iron and normal glucose resulted in a 41% increase compared to control (24 h).

Furthermore, the level of iron content was significantly increased at 48 and 72 h in iron and glucose concentrations compared to control ($P<0.05$). However, normal glucose demonstrated insignificant higher level ($P>0.05$) compared to control. High iron exhibited a 34.4% increase of iron content compared to all conditions (48 h incubation). Similar to 48 h incubation, iron and glucose concentrations alone demonstrated significant changes with high iron exhibiting twice as much as control (76.2 nmol/mg protein vs 34.8 nmol/mg protein) (72 h).

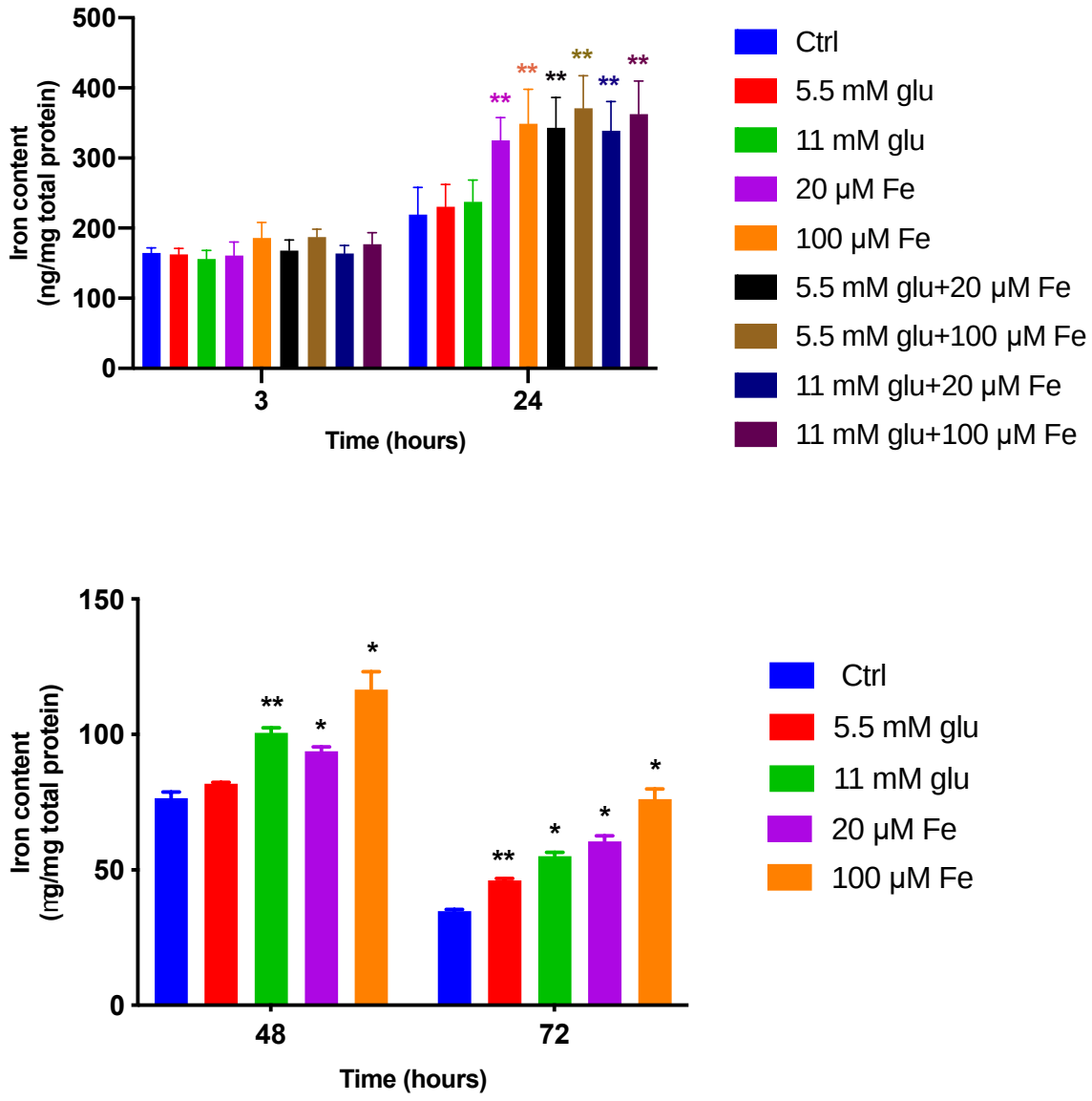

Fig. 3.1.3. To determine the quantification of iron intracellularly, MIN6 cells were exposed to different concentrations of iron and glucose, and all with the addition of tolbutamide. These cells were incubated in 3, 24, 48 and 72 h. These effects were performed with ferrozine-based colorimetric assay. The data represent mean ± SEM. **P<0.003 (C3 – 24 h), **P<0.0077 (C4 – 24 h), **P<0.0025 (C5 – 24 h), **P<0.0026 (C6, C7 – 24 h), **P<0.0062 (C8 – 24 h); **P<0.0059 (C2 – 48 h), *P<0.0156 (C3 – 48 h), *P<0.049 (C4 – 48 h), **P<0.007 (C1 – 72 h), *P<0.017 (C2 – 72 h), *P<0.0266 (C3 – 72 h), *P<0.035 (C4 – 72 h). n=4.

This phenomenon suggested that excess iron and glucose might have an effect on iron metabolism starting at 24 h incubation onwards.

3.1.4 Estimation of cellular ferritin content

It is crucial to quantify intracellular ferritin content as this protein has been considered as iron storage protein, which has been found in many different human tissues. Since

iron overload has led to many different diseases, the amount of storage iron, which is correlated to this protein has to be considered. As shown in figure 3.1.4, iron and glucose demonstrated no effects on ferritin levels at 3 h incubation. In addition, conditions containing iron and glucose also exhibited no changes on ferritin levels. Glucose concentrations seemed to slightly increased ferritin level and iron slightly reduced it at 3 h. Similar effects remained observable
at 24 h in which iron, glucose, and combinations of iron and glucose demonstrated no effects on iron storage.

Unexpectedly, iron and glucose conditions led to significant changes in ferritin levels at 48 h. High iron exhibited fifteen times higher of ferritin levels than its control (270.5 ng/mg protein vs 17.8 ng/mg protein), which was followed by normal iron with five times increase (173.0 ng/mg protein vs 17.8 ng/mg protein). Moreover, high glucose demonstrated ferritin levels almost twice as high as its control (47.7%). In contrast, glucose showed no effect on ferritin levels compared to control at 72 h incubation. An opposite effect was observed by high iron in which ferritin levels was significantly increased, four times higher (76.1%) than its control ($P<0.05$). Thus, it is suggested that high iron concentration exposure upon MIN6 cells resulted in high ferritin concentrations in both 48 h and 72 h.

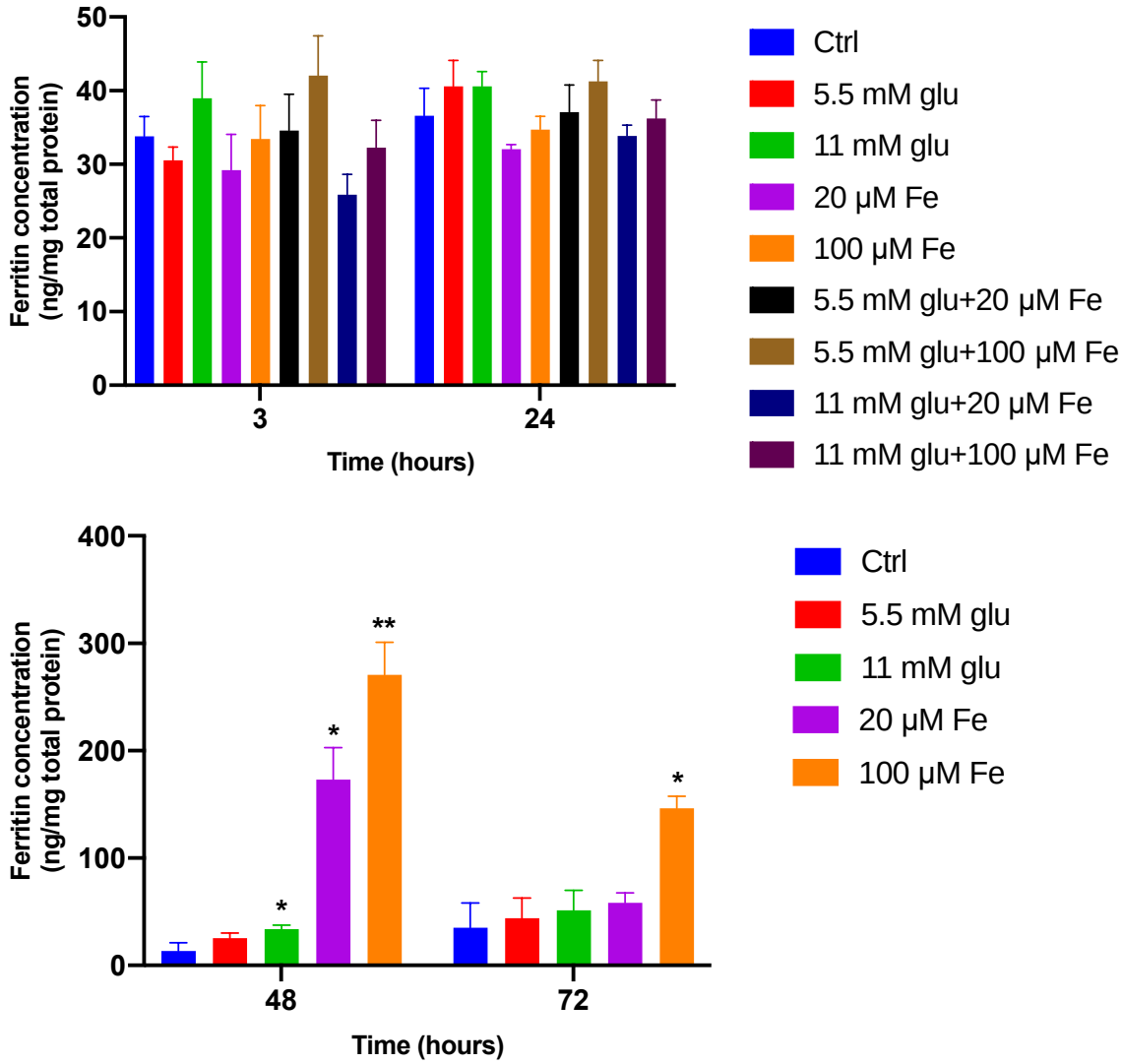

Fig. 3.1.4. The effect of iron, glucose, combinations of iron and glucose at a variety of concentrations, all with the addition of tolbutamide on MIN6 cells. This assessment was performed at four different time points indicating short-term (3 h), mid-term (24 & 48 h), and long-term (72 h) exposure. The data represent mean ± SEM. *P<0.028 (C2 – 48 h), *P<0.023 (C3 – 48 h), **P<0.006 (C4 – 48 h); *P<0.025 (C4 – 72 h). n=4.

3.1.5 Assessment of cellular viability

Many techniques have been developed in assessing the cytotoxicity of the cells. However, PrestoBlue® is a new, simple, and extremely fast live assay to estimate the viability of the cells and their cytotoxicity. The results obtained below demonstrated the effects of MIN6 cells towards various concentrations of iron, glucose, and combinations of iron and glucose in which tolbutamide was added at 3, 24, 48 and 72 h.

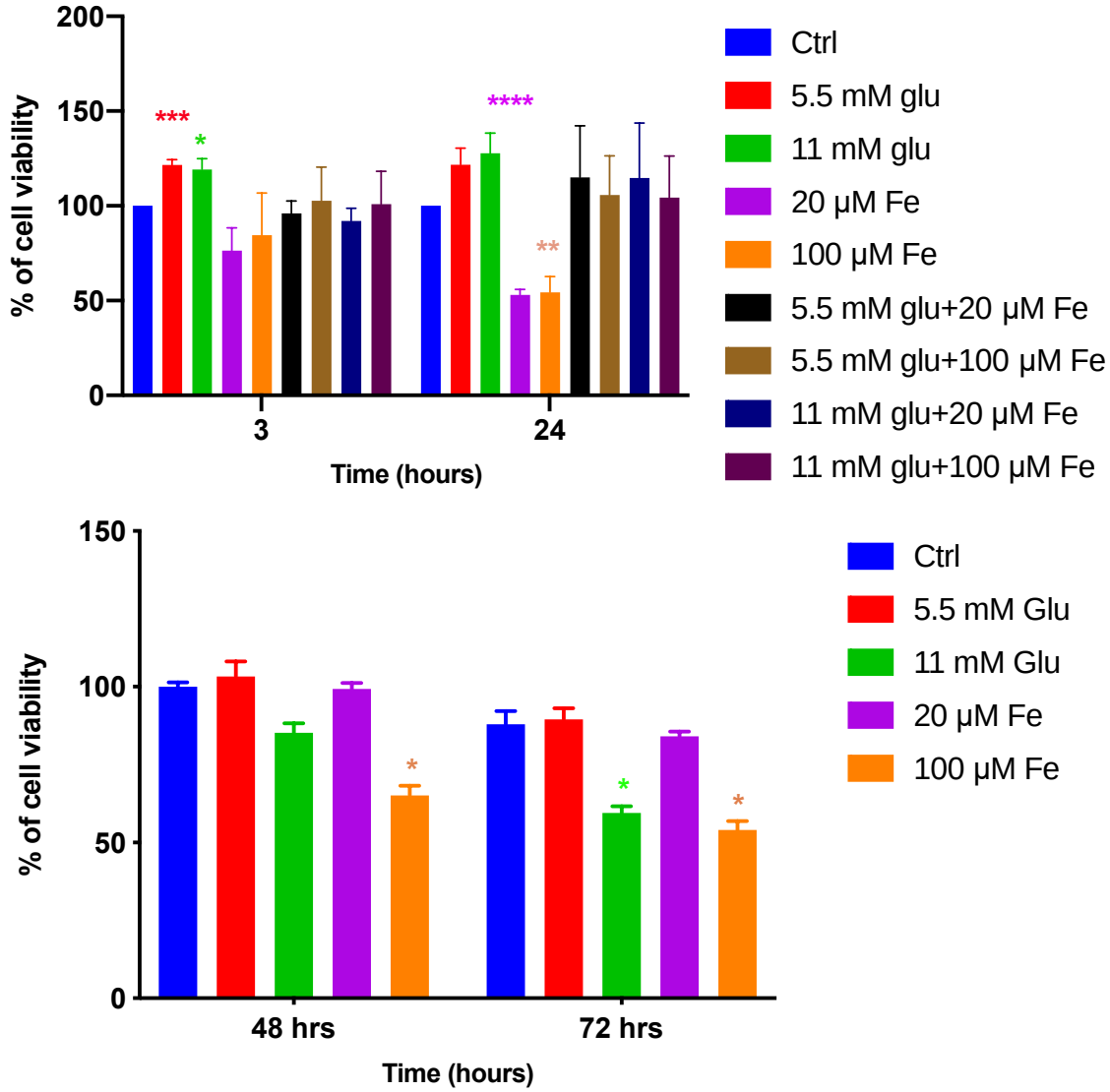

Fig. 3.1.5. The estimation of cell viability and cytotoxicity was performed by PrestoBlue® assay in four incubation times (3, 24, 48 and 72 h). MIN6 cells were exposed to various concentrations of iron, glucose, combinations of iron and glucose in which tolbutamide was added. The data represent mean ± SEM. ***P<0.0003 (C1 – 3 h), *P<0.0147 (C2 – 3 h); ****P<0.0001 (C3 – 24 h), **P<0.0055 (C4 – 24 h); *P<0.021 (C4 – 48 h), *P<0.033 (C2 – 72 h), *P<0.019 (C4 – 72 h). n=4.

Cell viability assessment can be used to support the analysis of MDA levels (Chapter 4). As shown in figure 3.1.5, iron and glucose demonstrated changes on the viability of cells (at all given conditions). Normal and high glucose concentrations exhibited significantly increased cell viability, 21.6% and 19.2% higher than the control, respectively (3 h incubation). On the other hand, although iron concentrations

demonstrated decreased percentage of cell viability, the levels were insignificant (*P>0.05*). At 24 h incubation, similar effects were observed both in iron and glucose concentrations in which glucose concentrations increased cell viability, but iron concentrations decreased it. However, glucose concentrations depicted an insignificant result compared to control, whereas both normal and high iron demonstrated significant reduction almost twice as much as the control (47% and 46%, respectively).

At 48 h incubation, glucose concentrations demonstrated slight changes in which normal glucose demonstrated an insignificant increase of cell viability, but high glucose depicted an opposite effect (*P>0.05*). In contrast, high iron concentration significantly reduced the percentage of cell viability with 35% reduction compared to control. Similar effects were also observed at 72 h in which high iron exhibited 46% reduction of cell viability, followed by high glucose with 40.5% reduction of cell viability. This result provided consistent data obtained in previous analyses, suggesting that high iron and high glucose generated impairment on cellular function, which involved in myriad diseases include T2DM.

3.1.6 Assessment of insulin content

Measurement of insulin is essential as β-cell function is being investigated. Intracellular insulin content was quantified to determine the balance between insulin synthesis and secretion. As shown in figure 3.1.6, iron and glucose slightly altered the level of intracellular insulin content in which the values were increased insignificantly compared to control in 1 h incubation (*P>0.05*). In addition, the combinations of iron and glucose concentrations demonstrated no changes on insulin content.

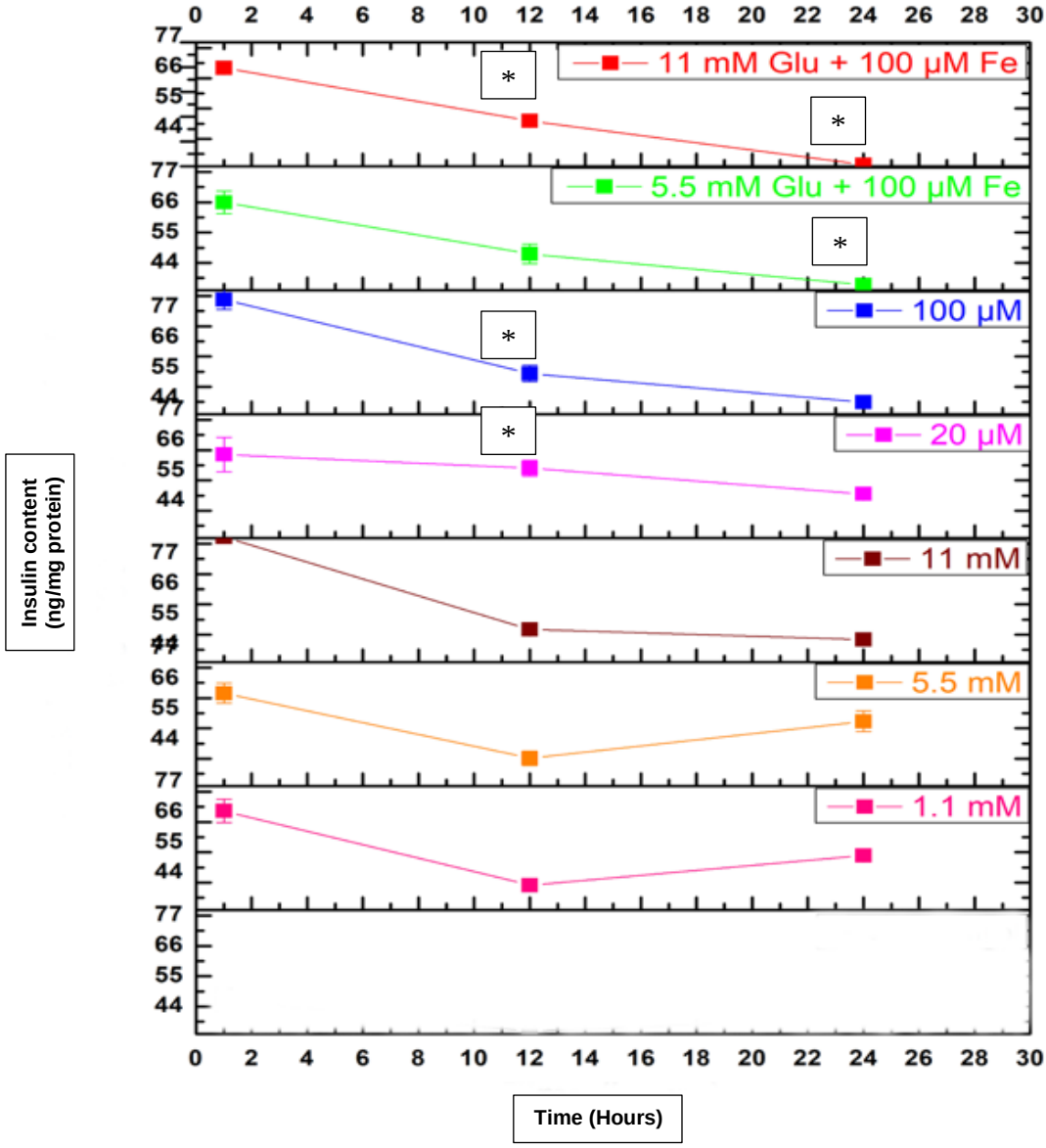

Fig. 3.1.6. Intracellular insulin content was performed using insulin ELISA in cultured cells. MIN6 cells were exposed to various concentrations of iron, glucose, and combinations of iron and glucose, all with the addition of tolbutamide at designated incubation times. The data represent mean ± SEM. *P<0.0193 (C3-12 h), *P<0.022 (C4-12 h), *P<0.0148 (C6-12 h); *P<0.0229 (C6-24h), *P<0.011 (C8-24h). n=3

In contrast, only iron (53.01 µg/mg protein vs 38.13 µg/mg protein) exhibited a significant increase of insulin content at 12 h incubation compared to control. Moreover, although glucose demonstrated higher insulin content, the value was insignificant (*P>0.*05). At 24 h incubation, iron reduced insulin content insignificantly (20 µM Fe: 12.3%; 100 µM Fe: 10.2%), whereas glucose increased its value insignificantly (5.5 mM Glu: 4%). Thus, it is suggested that iron and glucose have no change on insulin content at 1 h. Iron started to undergo an increase at 12 h significantly. However, at 24 h, iron and glucose demonstrated an opposite effect in which iron reduced insulin content and glucose increased it.

3.1.7 Assessment of insulin secretion

The data in figure 3.1.7 showed insulin secretion levels in various conditions of iron, glucose, and combinations of iron and glucose at 5, 10, 30, 60, 180, & 144 minutes. The results below comprise of different insulin secretion levels as an effect of glucose against control (Fig.3.1.7A), iron against control (Fig.3.1.7B), combinations of iron and glucose against control (Fig.3.1.7C), and direct measurements of iron, glucose, and combinations of iron and glucose at 5, 10, 30, and 60 min (short term) (Fig.3.1.7D), which was also applied at 24 h incubation (long term) (Fig.3.1.7E).

As shown in figure 3.1.7A-C, glucose concentrations (5.5 mM Glu: 10.5 µg/mg protein vs 9.02 µg/mg protein; 11 mM: 9.7 µg/mg protein vs 9.02 µg/mg protein) slightly increased insulin secretion both at 3 and 24 h (Fig. 3.1.7A). On the other hand, normal iron had no effect on insulin secretion (8.7 µg/mg protein vs 8.7 µg/mg protein), but high iron slightly increased insulin secretion (9.3 µg/mg protein vs 8.7 µg/mg protein) compared to control (3 h) (Fig. 3.1.7B). This was also observed at 24 h incubation. Furthermore, insulin secretion was slightly increased in all conditions containing iron and glucose combinations compared to control. However, a condition containing normal iron and normal glucose combinations exhibited the highest insulin secretion at both 3 and 24 h incubation (10.2 µg/mg protein vs 8.3 µg/mg protein; 33 µg/mg protein vs 17.7 µg/mg protein, respectively) (Fig. 3.1.7C).

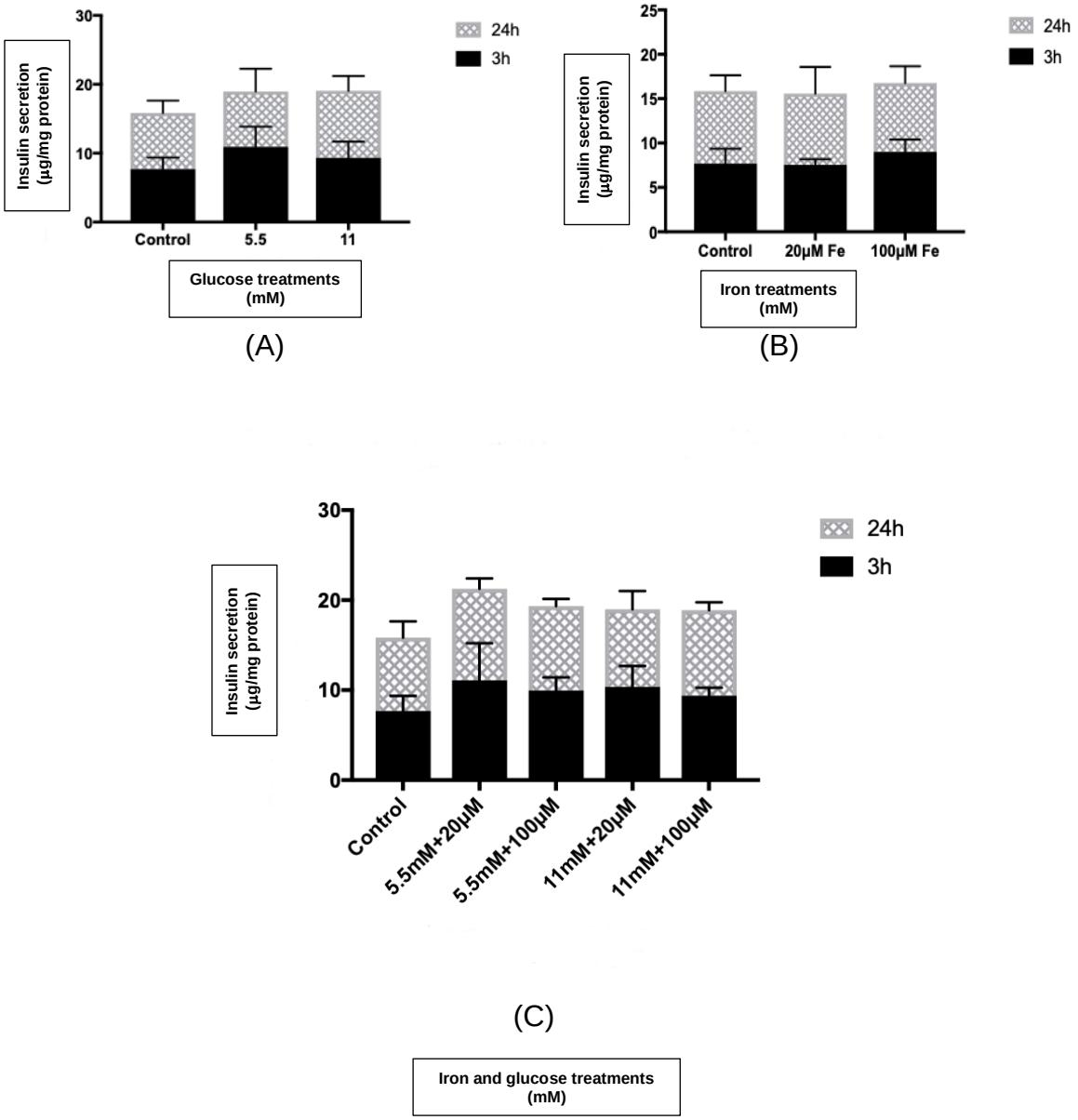

Fig. 3.1.7A-C. To determine insulin secretion due to the effects of different concentrations of iron, glucose, and combinations of iron and glucose, all with the addition of tolbutamide on MIN6 cells. A range of incubation times were applied: (a,b,c) Insulin secretion concentrations in 3 & 24 h. The data represent mean ± SEM. n=3

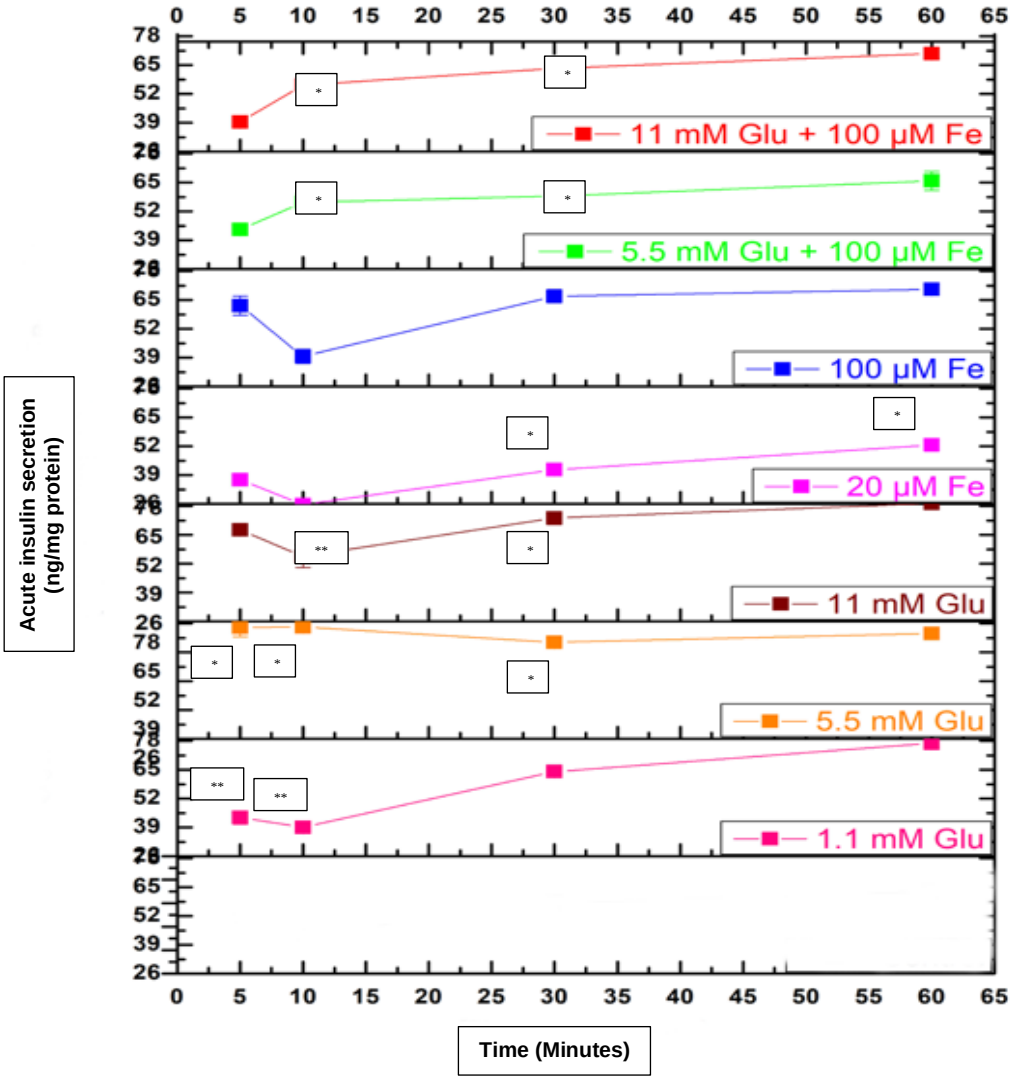

(D)

Fig. 3.1.7D. To determine insulin secretion due to the effects of different concentrations of iron, glucose, and combinations of iron and glucose, all with the addition of tolbutamide on MIN6 cells. A range of incubation times were applied: Insulin secretion concentrations acutely (5, 10, 30, 60 min). The data represent mean ± SEM. **P<0.004 (C1-5min), *P<0.02 (C2-5min); **P<0.0036 (C1-10min), *P<0.037 (C2-10min), **P<0.005 (C3-10min), *P<0.026 (C6-10min), *P<0.01 (C8-10min); *P<0.05 (C1-30min), *P<0.033 (C2-30min), *P<0.016 (C3-30min), *P<0.026 (C6-30min), *P<0.01 (C8-30min); *P<0.013 (C3-60min); n=3

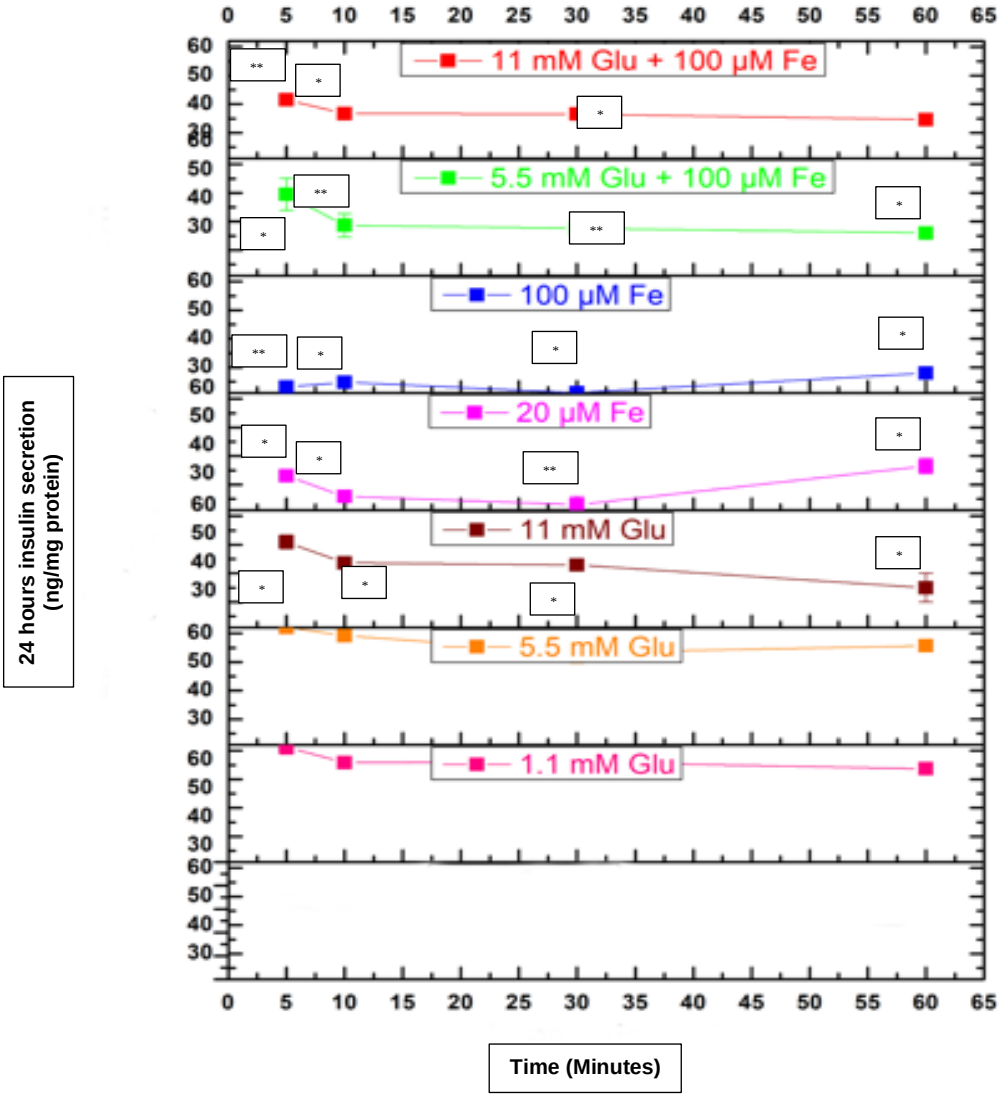

(E)

Fig. 3.1.7E. To determine insulin secretion due to the effects of different concentrations of iron, glucose, and combinations of iron and glucose, all with the addition of tolbutamide on MIN6 cells. A range of incubation times were applied: Insulin secretion concentrations at 24 h (5, 10, 30, 60 min). The data represent mean ± SEM. *P<0.049 [C2-24h (5min)], *P<0.022 [C3-24h(5min], **P<0.004 [C4-24(5min], *P<0.013 [C6-24h(5min)], **p<0.003 [C8-24h(5min)]; *P<0.034 [C2-24h(10min)], *P<0.022 [C3-24h(10min)], *P<0.02 (C4-24h(10min)], **P<0.005 [C6-24h(10min)], *P<0.027 [C8-24h(10min)]; *P<0.015 [C2-24(30min)], **P<0.004 [C3-24h(30min)], *P<0.016 [C4-24h(30min)], **P<0.005 [C6-24h(30min)], *P<0.018 [C8-24h(30min)]; *P<0.044 [C2-24h(60min)], *P<0.034 (C3,C4,C6-24h(60min)]. n=3

Short term incubations were taken simultaneously on MIN6 cells and depicted fluctuations among all conditions at several incubations. At 5 min incubation, iron and glucose exhibited higher insulin secretion with 33% and 26.2% compared to control,

respectively. In addition, the combinations of iron and glucose reduced insulin secretion insignificantly compared to control (*P>0.05*). However, normal iron reduced 33.3% of insulin secretion, but high iron depicted no change compared to control (10 min incubation). An opposite effect was observed in glucose concentrations in which insulin secretion (5.5 mM: 9.6% and 11 mM: 14%) was increased insignificantly (*P>0.05*). At 30 min incubation, iron and glucose increased insulin secretion insignificantly. In contrast, normal iron reduced 13.3% of insulin secretion, but increased 18.8% secretion at high iron concentration along with high glucose depicting the highest insulin secretion (23.1% compared to control) (60 min incubation) (Fig. 3.1.7D).

After a long-term incubation (24 h), several time courses (5, 10, 30, & 60 min) were applied and insulin secretion was measured. Persistent results were observed in which high iron and high glucose demonstrated significant reductions in levels of insulin secretion (63.5%, 56.1%, 74.5, 47.2% & 31.7%, 35.1%, 34.5%, 43.4%, respectively) across various time courses compared to control (*P<0.05*) (Fig. 3.1.7E). This consistency was also shown by conditions containing iron and glucose combinations. Thus, it is suggested that various fluctuations have been observed among these time courses, but consistency was demonstrated by long term incubation, showing that high iron and high glucose exhibited significant reductions of insulin secretion across four different short-term periods within 24 h incubation.

3.1.8 Expression of SNAP-25–mediated insulin exocytosis

Identifying the effect of iron and glucose on SNAP-25 is pivotal as this protein is involved in regulating the exocytosis of insulin. MIN6 cells were exposed to selected concentrations of iron and glucose for 24 and 48 h. β-actin was used as the housekeeping gene in this particular experiment owing to its molecular weight and a lack of cross-effect towards the protein of interest. Figure 3.1.8 depicts the

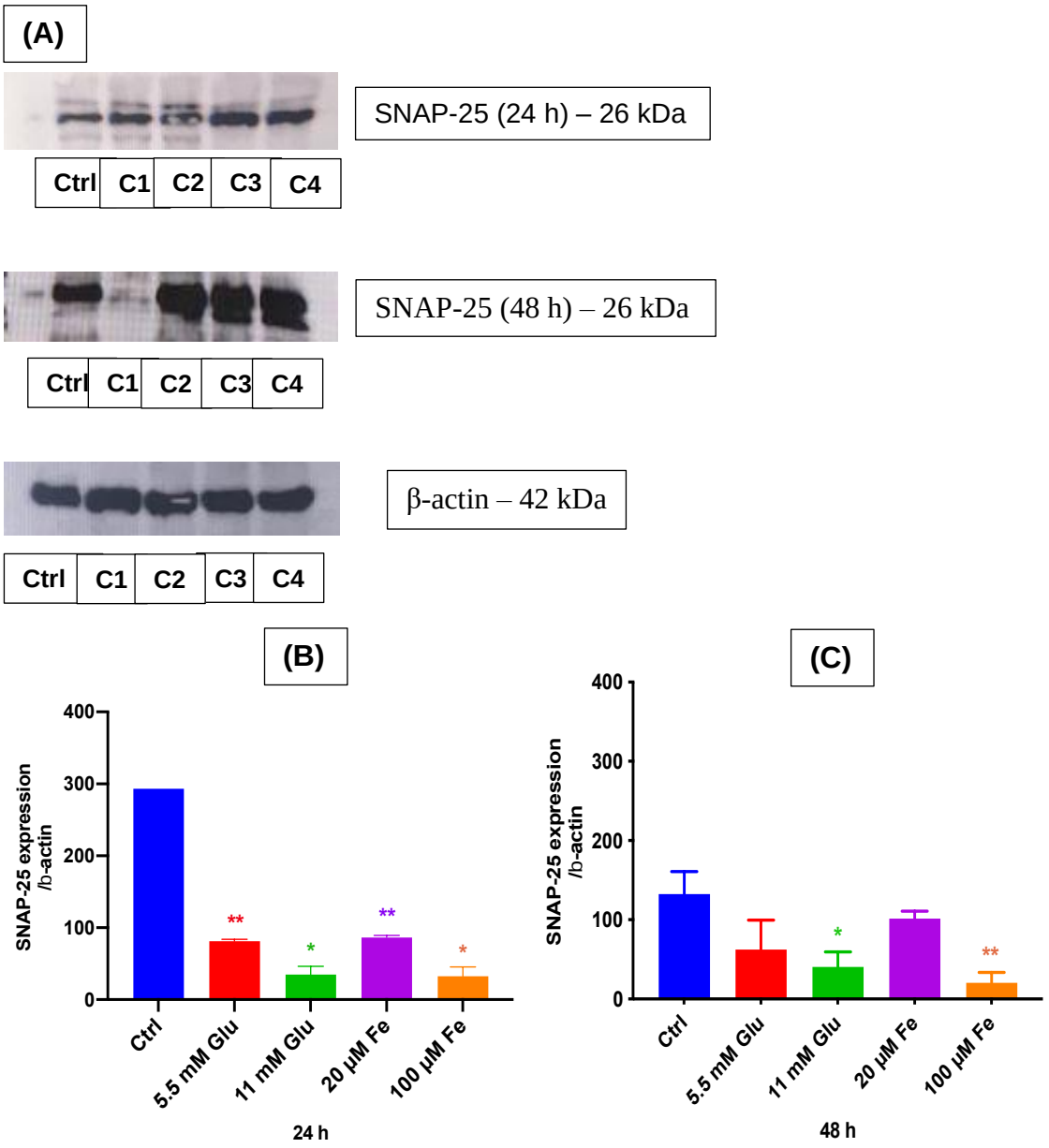

Fig. 3.1.8. SNAP-25 protein expressions in pancreatic β-cell (MIN6) within two distinct timelines, 24 and 48 h, in the presence of iron and glucose. Protein expression was identified using western blotting. (A) Distinctive bands of SNAP-25 (24 and 48 h) and β-actin. (B) Expression of SNAP-25 in 24 h determined as an area under the curve (AUC). (C) Expression of SNAP-25 in 48 h. Gel loading was as follows (from top left): lane 1 - ctrl, lane 2 - normal glucose (C1), lane 3 - high glucose (C2), lane 4 - normal iron (C3), lane 5 - high iron (C4). (from middle right): lane 1 - ctrl, lane 2 – C1, lane 3 – C2, lane 4 – C3, lane 5 – C4. The data represent mean ± SEM; n=4. **P<0.0086 (5.5 mM Glu – 24 h), *P<0.028 (11 mM Glu – 24 h), **P<0.0082 (20 μM Fe – 24 h), *P<0.032 (100 μM Fe – 24 h), *P<0.02 (48 h), **P<0.0076 (48 h).

measurements of protein oxidation expression using OxyBlot. The high iron and glucose concentrations decreased the SNAP-25 expression levels at both time points,

compared to that in the control. The high iron concentration produced the lowest expression of this particular protein in comparison to that under all the other conditions both at 24 and 48 h.

A significant reduction in MIN6 β-cell SNAP-25 protein expression was evident at 24 h upon exposure to 100 μM iron (65 vs 293) and 11 mM glucose (34.7 vs 293). A similar expression of SNAP-25 was also noticed after 48 h of incubation, in which the high iron and glucose concentrations induced significant reductions compared to that in the control (48.4 vs 132.5 and 43.1 vs 132.5, respectively). Moreover, the normal iron and glucose concentrations did not significantly decrease the SNAP-25 levels compared to that in the control (62.6 vs 132.5 and 101.5 vs 132.5, respectively) after 48 h of incubation. However, after 24 h of incubation, they decreased the SNAP-25 levels significantly compared to that in the control (86.6 vs 293 and 81.1 vs 293). These results suggest that high iron and glucose concentrations significantly reduce the levels of SNAP-25 in MIN6 cells even in the short-term (24 h).

3.2 Discussion

Diabetes mellitus is a complex disease with multiple complications affecting people of all ages. Myriad research worldwide has explored this area to find the cure of this disease, and yet it remains a mystery. However, the findings of these research contribute valuable knowledge in understanding some mechanisms involved in diabetes mellitus. Iron is an intriguing nutrient that has been identified as one of the factors contributes to the progression of T2DM. Iron participates in many biological processes in the human body, include playing an essential role in the production of ATP and metabolic processes such as DNA repair and replication, regulation of gene expression (Lasocki et al., 2014). Unfortunately, many researchers have found that the breakdown of metal homeostasis appear to cause a plethora of diseases. Higher levels of intracellular iron can be involved in the regulation of cell proliferation by regulating transcription factors, controlling cell cycle progression and apoptosis (Evan & Vousden, 2001).

Iron metabolism, which involves its uptake, distribution, storage, and secretion, has been well established. Understanding these particular mechanisms are important as

they contribute to iron homeostasis. Since disposal of excess iron is usually a slow process in humans, this metal has to be tightly regulated, particularly iron uptake from the intestine. DMT1 is an integral membrane-bound transport protein composed of 12 predicted transmembrane domains and several N-linked glycosylation sites (Fleming, 1997). DMT1 (also called Nramp2) has a crucial role both in intestinal iron absorption and iron transport across the membrane-acidified endosomes (Canonne-Hergaux et al., 2001). The function of this protein is to transport several, not all divalent metal, which located on the apical membrane of enterocyte and endosome associated membrane.

Results depicted in figure 3.1.1 proposed that high iron (100 μM) increased the expression of DMT1. This can be seen in 24 h incubation, in which DMT1 expression was twice increased with high iron concentrations compared to the control. However, DMT1 was downregulated demonstrated by high iron, though its decrease was insignificant (*P>0.05*) (at 3 h). This data is in conformity with the data elucidated by Koch and his colleagues in 2003. Their paper emphasized that high amounts of DMT1 were found in islet cells of the pancreas (Koch et al., 2003). They suggested that this protein might render a genetic disease so-called hereditary hemochromatosis, leading to the development of diabetes mellitus (Sheth & Brittenham, 2000). In addition, Hansen and colleagues showed in their studies that iron mediated oxidative stress can increase expression of DMT1 (Hansen et al., 2011), which was speculated in contributing subsequent damage to the cell type (Ramos, 1992). This is supported by our data which demonstrate that high iron exhibited almost twice (46%) as high cytotoxicity values in 24 h incubation (Fig. 3.1.6).

As previously described, ferric iron is traditionally bound to apotransferrin forming a diferric-Tf, with the purpose of distributing iron into the cells. Figure 3.1.2 demonstrated that though the addition of this protein bound to iron resulted in significant outcomes of total iron content intracellularly (*P<0.05*), the same effects remained with its absence. Once iron is distributed into the cells, it can be transported into mitochondria or stored in an iron-storage protein, ferritin. Ferritin is considered a major store of intracellular iron, with storage being a key component of iron metabolism. This protein is a fundamental in controlling the amount of iron available to the body. It has the ability to store and release iron in a controlled fashion, which helps to prevent iron disorders

like iron overload, anaemia, and other iron-related diseases. The results illustrated in figure 3.1.4, show ferritin levels increased in an iron-dependent manner, when incubated at 48 h (fifteen times higher) and 72 h (four times higher) with excess iron. This data corresponds to total iron content (Fig. 3.1.3) performed by colorimetric Ferrozine assay exhibited by the treatment condition containing high iron concentrations. Serum ferritin is crucial to analyse as this protein is an indicator of tissue iron status.

Ford & Cogswell (1999) elucidated that an increase of these 24-peptide subunits has been positively correlated with the risk of developing T2DM (Ford & Cogswell, 1999). In addition, this study is also confirmed by Aregbesola and colleagues, who suggested that ferritin levels above normal was related to an increased risk of diabetes mellitus (Aregbesola et al., 2013). The potential reason for the increased ferritin in the β-cell is that ferritin exhibits antioxidant properties as it acts as a molecule against iron toxicity by neutralising unused free iron (Juckett et al., 1995). Moreover, β-cell is particularly sensitive to oxygen radicals due to lack of intracellular antioxidants. This high amount of ferritin can explain why iron is preferentially retained in the β-cell. Relationships between serum ferritin levels with diabetes mellitus are likely to be conflicted. However, iron can be released from ferritin, converting Fe^{3+} into Fe^{2+} by the action of a reducing agent, in which its release is accelerated in comparison with decreased antioxidant concentration (Hallowell, 1993). Under this condition, elevated levels of free iron is released from ferritin, implying that this protein may act as an undesirable molecule.

Interestingly, this phenomenon has also been observed in pre-diabetes, where there is in concomitant low transferrin saturation as an iron-bound protein systematically (Cheung et al., 2013). The link between increased serum ferritin levels with the risk of diabetes mellitus has come to the attention of many researchers, though its mechanism remains to be fully understood. It is suggested that however that the link between these two is via oxidative stress initiated by iron as a catalyst for ROS, such as hydroxyl radical. This oxidative stress mediates the apoptosis of pancreatic islets, decreasing their capacity to secrete necessary insulin (Cooksey et al., 2004).

Iron has been considered to be involved in insulin secretory mechanism. High iron can generate free radical production and formation of ROS. Figure 3.1.8 showed that excess iron progressively decreased secretion of insulin after a long-term incubation (24 h). This condition could be caused by impairment of insulin secretion and insulin resistance because of an elevated and continuous exposure of intracellular ROS (Kasuga, 2006). Similar effects are also observed with the data obtained for insulin content (Fig. 3.1.7). T2DM is a complex disease that is rendered by numerous factors, both inside and outside of the body. Impairment of insulin secretion and its resistance can lead to hyperglycaemia, which is a determined characteristic of T2DM. A study performed by Shaaban and colleagues (2006) concluded that excess iron negatively impacted insulin action in healthy people. Furthermore, a considerable body of evidence indicates that excess iron increases risk for insulin resistance in diabetes mellitus, as well as other diseases such as cardiovascular diseases both in nondiabetic and diabetic individuals (Shaaban et al., 2006).

The ultimate effect of chronic impairment of insulin secretion due to excess iron and glucose is oxidative stress in the mitochondria, and finally apoptosis. Multiple studies encompassing various proteins have been designed to identify the factors involved in this complex condition. It has been found that SNARE core complexes, which are proteins involved in insulin exocytosis, are likely to be sensitive towards oxidative stress. It has been stated that SNAP-25 is the most sensitive protein towards oxidative stress amongst two membrane-anchored SNAREs (Giniatullin et al., 2006). In addition, Giniatullin et al. have illustrated that H_2O_2 exhibits the strongest inhibitory effect on SNAP-25 compared to that of either syntaxin or synaptobrevin (Giniatullin et al., 2006); they concluded that SNAP-25 was the most sensitive to modification by ROS. Regrettably, the reason for its vulnerability towards oxidative stress is not yet fully understood. Some possibilities include its distinctive structure, which is unable to anchor into a membrane due to the absence of a transmembrane segment (Jahn & Scheller, 2006).

Despite this drawback, SNAP-25 has another way of attaching to the membrane via lipid modifications such as palmitoylation (Jahn & Scheller, 2006). Figure 4.3.5 shows that SNAP-25 expression diminishes in MIN6 cells in the presence of high iron and glucose concentrations for 24 and 48 h, compared to that in the control. A significant

shift is obvious even at 24 h. These data are in accordance with earlier data collected in this study, which indicate that high iron and glucose concentrations significantly decrease insulin secretion (24 h) (*P<0.05*) (Fig. 3.1.7d). A study performed by Nagamatsu et al. showed that the syntaxin 1 and SNAP-25 levels in GK rat islets decreased by approximately 60% compared to those in the control. The decrease altered the process of insulin secretion; this was further proven by a restoration in insulin secretion following the overexpression of syntaxin 1A and SNAP-25 by approximately 135% and 200%, respectively (Nagamatsu et al., 1999). The alteration of this protein may cause insulin secretion perturbations associated with the regulation of Ca^{2+} dynamics and membrane potential in the β-cells.

When β-cells sense the presence of glucose, the cytosolic levels of Ca^{2+} increase owing to molecular processes. This increase stimulates and activates the SNARE machinery, which mediates insulin granule fusion with the plasma membrane. The first phase of insulin release depends on the local influx of Ca^{2+} originating from the ER, whereas the sustained long-lasting second phase involves more complex intracellular signalling such as ATP levels, phosphoinositides, and the release of Ca^{2+} from intracellular stores (Barker & Berggren, 2013; Lees et al., 2017). Exocytosis of insulin is regulated by the cytosolic ATP levels and is followed by Ca^{2+}-dependent steps. The role of ATP in insulin exocytosis is to phosphorylate phosphatidylinositol groups through phosphatidylinositol kinases located within the plasma membranes (Keating, 2008). Compared with other types of cells in the body, pancreatic β-cells experience difficulty in switching to anaerobic respiration; such high oxygen-dependence requires the availability of glucose. In other cell types, however, respiration is under the control of the cell itself. Therefore, mitochondria have to function effectively to mediate the exocytosis of insulin secreted in response to a rise in blood glucose levels.

The study of SNAP-25 is crucial because it has been shown to modulate several processes, including the activity of potassium voltage gated channels (MacDonald et al., 2002). Similar to other proteins involved in the core complex of SNARE, SNAP-25 also contains amino and carboxy terminals that bind to different proteins; this is a prerequisite for the formation of four-helix bundles. Its amino and carboxy terminals bind to syntaxin 1 and VAMP2, respectively. This moves secretory granules such that

they are in close contact with the plasma membrane, leading to membrane fusion. Evidence has shown that enhancing the level of exocytosis proteins can improve the longevity of cells and reduce the occurrence of diseases such as cancer, diabetes mellitus, and neurodegenerative disorders.

As mentioned previously, iron has a dual role - it is essential notably in both cellular metabolism and aerobic respiration. However, the involvement of this metal leads to formation of free radicals that can cause cellular cytotoxicity and oxidative damage on the cellular components. The effect of excess iron and glucose on the viability of the cells was confirmed by PrestoBlue® (Fig. 3.1.6). in line with the previous results, toxicity caused by excess iron exhibited significant reduction of cell viability percentage compared to control both at 48 and 72 h ($P<0.05$). This toxicity characterises an initial stage of defective insulin gene expression. If β-cell was exposed to these concentrations for a prolonged period and happened repeatedly, it may undergo exhaustion, promoting the inhibition of insulin secretion.

When cells undergo this condition, cells can be fully recovered since it has no defects in insulin synthesis. This condition may be different once cells are damaged by toxicity, which may cause irreversible damage to the component of cells, interfering with insulin content and insulin secretion. This ultimately encounters impairment of secretion and action of insulin and other metabolic processes. Furthermore, due to tight involvement of iron in mitochondria, it is prone for iron to contribute in the formation of free radicals.

This damage alters the function of mitochondria by being a catalyst of ROS production, which is considered to have a deleterious effect on cell structures, consequently leading to ageing and various disease states. Since pancreatic β-cells are particularly susceptible to ROS due to less intracellular antioxidants content, numerous diseases could occur, particularly the deadly and epidemic disease – diabetes mellitus. Thus, further experiments are required to investigate the mechanism of mitochondrial dysfunction in high iron conditions.

CHAPTER 4
RESULTS

4.1 Introduction

Aims: To correlate excessive iron mediated ROS generation to β-cell dysfunction and to identify whether specific organelles such as the mitochondria are more sensitive to ROS damage.

Objectives:

- Clarify the role of excessive iron related to the level of malondialdehyde (MDA) as a result of lipid peroxidation by thiobarbituric acid reactive substances (TBARS) assay.
- Clarify the role of excessive iron on β-cell cytotoxicity through formation of carbonyl group on protein side chains as a form of cellular oxidative damage by immunoblotting.
- Optimise the visualisation of any formation resulted by cellular oxidative damage using confocal microscopy.
- Identify whether excessive iron may have an effect on mitochondrial membrane potential by flow cytometry.
- Assess the effect of excessive iron on mitochondrial oxygen consumption by Agilent Seahorse XF metabolic analyser.

Mitochondria have been discovered to be linked to myriad metabolic diseases such as cardiovascular diseases and diabetes mellitus. These cellular powerhouses are crucial because they manufacture ATP and other metabolites used by cells. They have been studied together with a variety of proteins that originate from these distinct organelles (5% of DNA codes) and others that are imported from the cytosol (Pfanner & Geissler, 2001). ATP is produced from oxidizable substrates such as glucose, amino acids, and fatty acids, which undergo several transformations that generate electrons. These electrons are transported via a series of reactions called the ETC, which eventually reduces oxygen to water. This transfer of electrons from one protein to other releases protons from the matrix into the intermembrane space, producing a protonmotive force (Δp). This force can regulate the movement of protons downhill across the inner mitochondrial membrane (Divakaruni et al., 2014).

The generation of ATP is less efficient in the absence of oxygen, which is hence pivotal in cell respiration. Oxygen is required for ATP generation in the ETC, producing an

eighteen-fold higher yield than that in anaerobic respiration. Respiration is measured to assess the relationship between ATP synthesis and the oxygen consumption rate during oxidative phosphorylation - a crucial part of energy metabolism (Divakaruni et al., 2014). The rate of oxygen uptake in cells is related to the functioning of mitochondria and has been implicated in the progression of disease (Fink & Cookson, 2005; Wu et al., 2007). The ability to predict certain pathways indicating the diseased state of a cell can provide significant insight for preventing multiple diseases.

In this study, several factors that control the rate of oxygen consumption were measured. Each of these factors is valuable in interpreting the possible state of mitochondria. These factors include basal respiration, ATP-linked respiration, proton leak, maximal respiration, reserve/spare respiratory capacity, and non-mitochondrial respiration. In addition to identifying the oxidative reactions driven by ROS, non-enzymatic reactions of proteins were also observed. The results led to the identification of MDA as a result of lipid peroxidation.

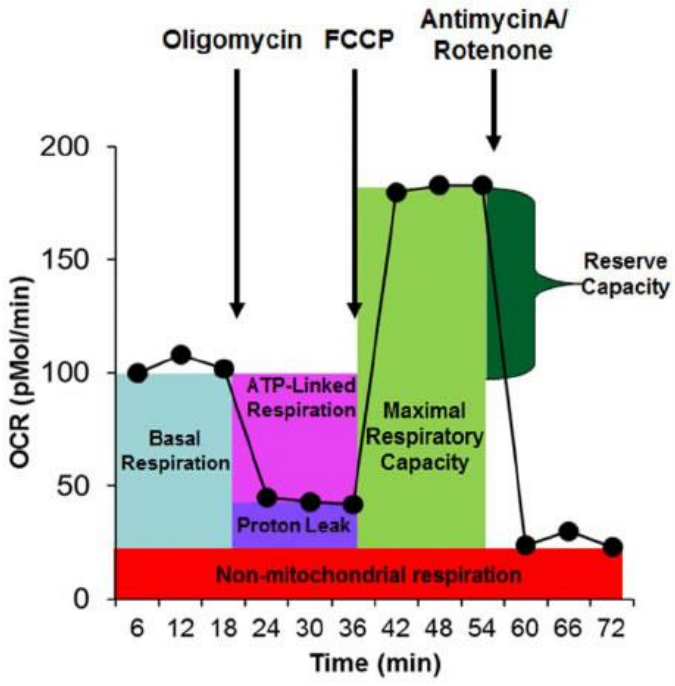

Fig. 4.1. Mito stress test profile of Seahorse XF cell, depicting the key parameters of mitochondrial function. (Rose et al., 2014).

4.1.1 Factors in OCR characterisation

4.1.1.1 Basal respiration

Basal respiration can be defined as an endogenous process that drives the synthesis of ATP and it can be derived by deducting non-mitochondrial respiration (Rose et al., 2014). It can be estimated by adding oligomycin to inhibit ATP synthase (see Fig. 4.1).

4.1.1.2 ATP-linked respiration

ATP-linked respiration is controlled by three different processes: ATP utilisation, ATP synthesis, and substrate supply and oxidation. The rate of ATP-linked respiration depends on the demand for cellular ATP. The energy produced increases proportionally based on the motility of the cells as well as the activity of some processes in which energy is required. These processes include biosynthesis of macromolecules, proteasome activity, and membrane repolarization (Divakaruni et al., 2014). Furthermore, an alteration in ATP-linked respiration is also associated with an alteration in the consumption of membrane potential, which reflects changes in ATP synthesis. ATP synthase is an enzyme that mediates the transfer of protons from the IMM back into the matrix to power the synthesis of the energy carrier molecule, ATP. A perturbation of this enzyme may result in a less effective ATP synthesis rate. ATP-linked respiration can be improved by the supply and oxidation of respiratory substrates such as fats, carbohydrates, and proteins. Therefore, maintaining and supplying enough substrates can stabilise ATP generation and contribute to the healthy development of cells.

4.1.1.3 Proton leak–linked respiration

Proton leak activity can be detected in mitochondria as well as intact cells and is considered as the major contributor to the standard metabolic rate (Rolfe & Brand, 1997). An increase in proton leak–associated respiration can reflect either mitochondrial damage (Dranka et al., 2011) or the normal physiological response (Divakaruni & Brand, 2011). The migration of the so-called proton leak into the matrix consumes mitochondrial membrane potential without producing ATP. This results in mechanisms of incomplete coupling of substrate oxygen consumption with the generation of ATP. In addition, the electron slippage within the IMM could also lead to

such incomplete coupling because no protons are transferred across the IMM into the IMS, leading to an increase in oxygen consumption at high protonmotive forces (Kadenbach, 2003).

4.1.1.4 Maximal respiration

It is very crucial to estimate the maximal respiration via substrate oxidation as this could reveal how pharmacologic compounds or genetic modifications can affect cellular metabolism. Uncoupling agents such as FCCP, DNP, and Bam 15 cause protons to move across the inner membrane, resulting in maximal activity of the ETC (Nicholls, 2008). These agents are also known as ‘uncouplers’ because the activity of the respiratory chain is uncoupled from ATP synthesis.

4.1.1.5 Reserve capacity/spare respiratory capacity

The function of reserve capacity is to help cells respond appropriately towards an increase in ATP demand and maintain the cell activity in periods of stress. It is the difference between the basal and maximal respiration. The measurement of this metric depends on multiple parameters and is very useful in modelling particular systems that exhibit oxidative stress (Dranka et al., 2011; Dranka et al., 2010) or ion homeostasis (Choi et al., 2009). However, it is less likely to be useful in identifying the molecular mechanisms of action (Divakaruni et al., 2014). Hence, the capacity of reserve bioenergetics is a context-dependent parameter associated with the health or steady state of mitochondrial functions.

4.1.1.6 Non-mitochondrial respiration

Non-mitochondrial respiration can be estimated by adding electron transport inhibitors such as rotenone (complex I inhibitor) and antimycin A (complex III inhibitor). This parameter denotes processes of oxygen consumption outside mitochondria or those that are non-mitochondrial (Chacko et al., 2014). For instance, non-mitochondrial OCR in leukocytes can include that of NADPH oxidases, cyclooxygenases, and lipoxygenases that are associated with enzyme-related inflammation (Chacko et al., 2014). For certain types of cells, including leukocytes and monocytes, the function of this measurement is to provide a significant overall rate (Kramer et al., 2014).

Generally, the rate of this parameter is assumed to be constant in most cells; it is very low but not insignificant (Divakaruni et al., 2014).

4.1.2 Protein oxidation as a major target of oxidative stress

Mounting evidence suggests that multiple human pathologies are associated with the oxidation of proteins. As mentioned previously, each cell exhibits a different level of defence and certain cells generate more intracellular antioxidants than others. It is well established that oxygen is crucial to our body and is involved in numerous biochemical processes. Unfortunately, a wide range of radicals are inevitably formed as part of normal aerobic metabolism. Two radicals that are widely produced in the presence of oxygen are peroxyl radicals and peroxides. These products, particularly protein peroxides, then continue to oxidize other proteins and targets. More free radicals and chain reactions are induced, leading to the production of mainly aldehyde and ketone groups (referred to as carbonyl derivatives), which are widely regarded as protein damage markers (Dalle-Donne. et al., 2004). These forms of protein oxidation include nitrotyrosination, carbonylation, and methionine and sulfhydryl oxidation (Stadtman et al., 2003; Stadtman, 1990). Furthermore, our bodies are also constantly being exposed to endogenous and exogenous oxidants, increasing stress to cells that are susceptible due to a lack of antioxidants.

Despite many other targets for oxidation, such as lipids, carbohydrates, and nucleic acids, proteins exhibit a wide range of factors that cause their extensive damage. Due to their critical abundance and high rate constants for reactions, they surpass all other biological molecules and become the major targets for oxidation. In addition, several factors such as the formation of chain reactions and the relative location of the target to oxidants can also be associated with further damage. Modification of oxidised proteins can produce some physical and chemical property alterations, including protein unfolding, aggregation, backbone fragmentation, and subunit dissociation (Davies, et al., 1997). In addition to direct oxidative modification of proteins by ROS, well-established secondary products are also formed via lipid peroxidation (MDA and 4-HNE) and are sugar-bound via glycation.

ROS can modify both amino acid side chains and protein backbones. All amino acids can be modified but cysteine and methionine are particularly sensitive to oxidative modifications (Cabreiro et al., 2006). These two amino acids can even be oxidised into their reduced forms, which are disulfides and sulfoxides, respectively, under mild conditions (Cabreiro et al., 2006). Protein side chains, including prolines, arginines, lysines, and threonine, are also vulnerable to these oxidative modifications (Dalle-Donne et al., 2003; Liebler, 2007). As mentioned earlier, there are multiple low-molecular-weight free-radical scavengers (ascorbic acids, tocopherols, carotenoids, polyphenols, flavonoids, etc.). SOD (an antioxidant enzyme) readily converts superoxide anions into hydrogen peroxide (Levine et al., 1999). CAT and GPx can eliminate H_2O_2 by converting it into the most reactive ROS species, •OH. However, when the level of oxidative stress in the body is high, the expression of these enzyme antioxidants increases; if the level of OS persistently increases, then their levels decrease. The reduction of these antioxidants could occur either directly through oxidative damage or OS-induced inhibition of gene expression, resulting in a decrease in their activity or concentration.

4.1.2.1 Mechanisms of protein removal

It has been well established that there are major enzymes responsible for protein degradation in mammalian cells, including cytosolic calpains, lysosomes, and proteasomes. However, only lysosomes and proteasomes have been demonstrated to be involved in this process. Lysosomes are membrane-bound organelles found in cells, and their function is to digest various molecules through autophagy (Takenouchi et al., 2015). The specific enzyme found in this organelle is known as acid hydrolase, which comprises hydrolytic enzymes that play a role in recycling proteins intracellularly (Braulke & Bonifacino, 2009). This enzyme has been so named because it requires an acidic environment to function efficiently. In addition, lysosomes are equipped with membrane-bound proton pumps which can maintain their pH levels between 4.5 and 5.5 (Dunlop et al., 2009).

In addition to lysosomes, proteasomes are also representative proteolytic machinery involved in protein degradation in the ubiquitin–proteasome system (UPS) (Wang & Robbins, 2014). Proteasomes exist in several isoforms and exhibit a multi-catalytic

effect, with each isoform possessing a 20S subunit also known as a catalytic core (Wang & Robbins, 2014). A proteasome in a 26S form comprises two 19S regulatory particles and a 20S core particle (which consists of two outer alpha and two inner β-rings). Out of the seven subunits of the β ring, only three β-subunits can carry the active sites or exhibit proteolytic activity (B1, B2, and B5 subunits) (Wang & Robbins, 2014). Before the target protein is recognised and degraded by a proteasome, it must be ubiquitinated by a protein called ubiquitin in a process called ubiquitination. Ubiquitin is a 76-amino-acid protein that can be considered as a marker for a particular damaged protein within cells (Guerra & Callis, 2012). Ubiquitination is catalysed sequentially by three enzymes: Ub activating enzyme (E1), Ub conjugating enzyme (E2), and Ub protein ligase (E3) (Wang & Robbins, 2014). Each enzyme plays a different role in integrating active ubiquitin into a target protein, which is eventually recognised by the proteasome. The protein is degraded into its individual amino acids, which could be used for other purposes within the cells. These two processes of autophagy and UPS by lysosomes and proteasomes, respectively, are necessary to maintain the quality of proteins and other molecules in cells (Willis & Patterson, 2013).

4.2 Results

4.2.1 Expression of protein carbonyl in MIN6 cells

Proteins are vital to our body as they are involved in most intracellular reactions. Their post-translational modifications may include peroxidation, which needs a proper review. Figure 4.2.1A depicts several unstained wells that contain negative controls of the designated iron and glucose and compares their iron and glucose concentrations. The function of a negative control is to show whether proteins have undergone oxidative modifications (Stankowski et al., 2011). Surprisingly, negative controls appeared in the bands of the 48-h incubation sample, which may have been due to the spilling over of excess protein solution into the neighbouring well.

The results of the 48-h sample (Fig. 4.2.1C) show that high iron content increases protein modifications by 78%, indicating a higher AUC than that of the control ($P<0.05$). It has been shown that excess iron is associated with ROS-mediated

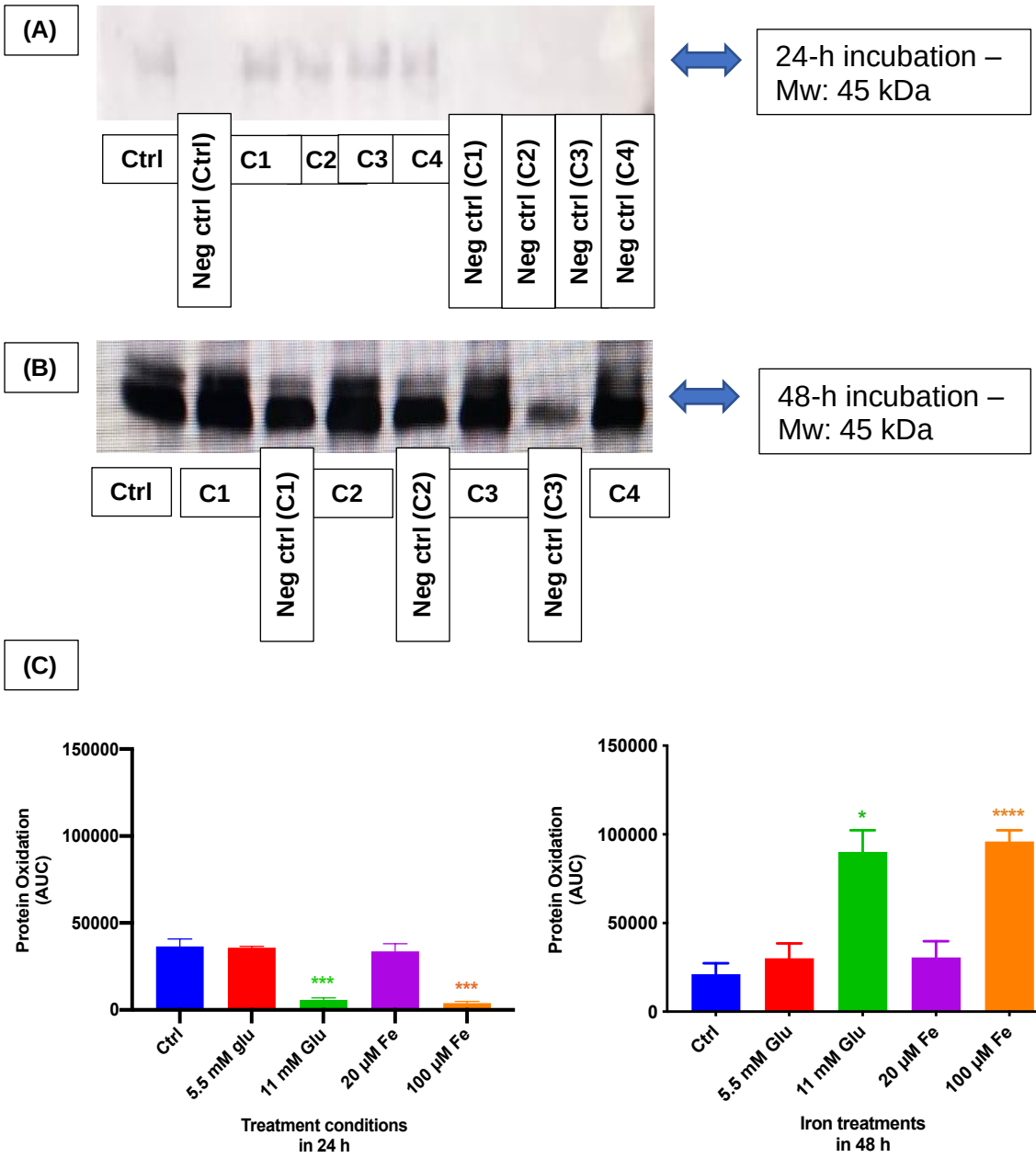

Fig. 4.2.1. The estimation of carbonyl groups on the side chains of proteins was performed using OxyBlot™ Protein Oxidation kits in both 24- and 48-h periods. The protein was extracted and subjected to the western immunoblot technique using 10% agarose gel. The results shown above are: Different bands of protein expression in western blot after (A) 24- and (B) 48-h incubations. (C) Expression of protein oxidation in 24- and 48-h incubation times, demonstrated by the area under the curve (AUC). Gel loading was as follows (from top left): lane 1 - ctrl, lane 2 - negative ctrl of ctrl, lane 3 – normal glucose (C1), lane 4 - high glucose (C2), lane 5 - normal iron (C3), lane 6 - high iron (C4), lane 7 – neg ctrl of C1, lane 8 – neg ctrl of C2, lane 9 – neg ctrl of C3, lane 10 – neg ctrl of C4. (From bottom left): lane 1 - ctrl, lane 2 – C1, lane 3 - neg ctrl of C1, lane 4 – C2, lane 5 - neg ctrl of C2, lane 6 – C3, lane 7 - neg ctrl of C3, lane 8 – C4. The data represent mean ± SEM; n=3. *P<0.015 (11 mM Glu), ***P<0.0002 (11 mM Glu, 100 µM Fe), ****P<0.0001.

oxidative stress (Ito et al., 2017). A similar effect was also demonstrated by a high glucose concentration, owing to which the AUC value increased by 76.5% compared

to that of the control. Although protein oxidation increased under normal iron and glucose conditions, compared to that under control conditions, the results were insignificant (*P>0.05*). Unexpectedly, opposite effects were observed after 24 h of incubation, which demonstrated that protein oxidation significantly decreased under both high iron (89.1% reduction) and glucose (84% reduction) concentrations compared to that of the control (*P<0.05*). In addition, both normal iron and glucose conditions resulted in a slight increase compared to that in the control (*P>0.05*).

These results suggest that high iron and glucose concentrations initially decrease protein oxidation (short-term) but then induce an increase in the long-term. This might be due to a direct rescue addressed by the pancreatic β-cell defence system via the activation of endogenous antioxidants, in which cells are protected more efficiently in the short-term. However, under a continuous stress condition, protein modifications are compromised.

4.2.2 Estimation of OCR

Figure 4.3.2 displays the oxygen consumption rate profiles of pancreatic β-cells (MIN6 cell line), i.e. the control and with various concentrations of both iron and glucose. As shown below, glucose and iron induced significant changes in the OCR during a short-term exposure (24 h). Samples with glucose concentrations displayed higher OCRs than those with iron and the control (Figs. 4.2.2A&B), which was confirmed by every factor contributing to the state of mitochondrial health (Figs. 4.2.2C-H). As depicted in Fig. 4.2.2C, the basal respiration levels varied with the glucose concentration. The normal glucose concentration slightly decreased basal respiration (39.8 pmol/O_2/protein vs 43.6 pmol/O_2/protein) whereas high glucose concentrations (11 mM – 51.6 pmol/O_2/protein & 25 mM – 64.5 pmol/O_2/protein) increased it, with only 25 mM glucose exhibiting a significance (*P<0.05*). Unexpectedly, both normal and high iron concentrations significantly reduced basal respiration compared to that in the control (75.8% & 78.9% reductions, respectively) (*P<0.05*).

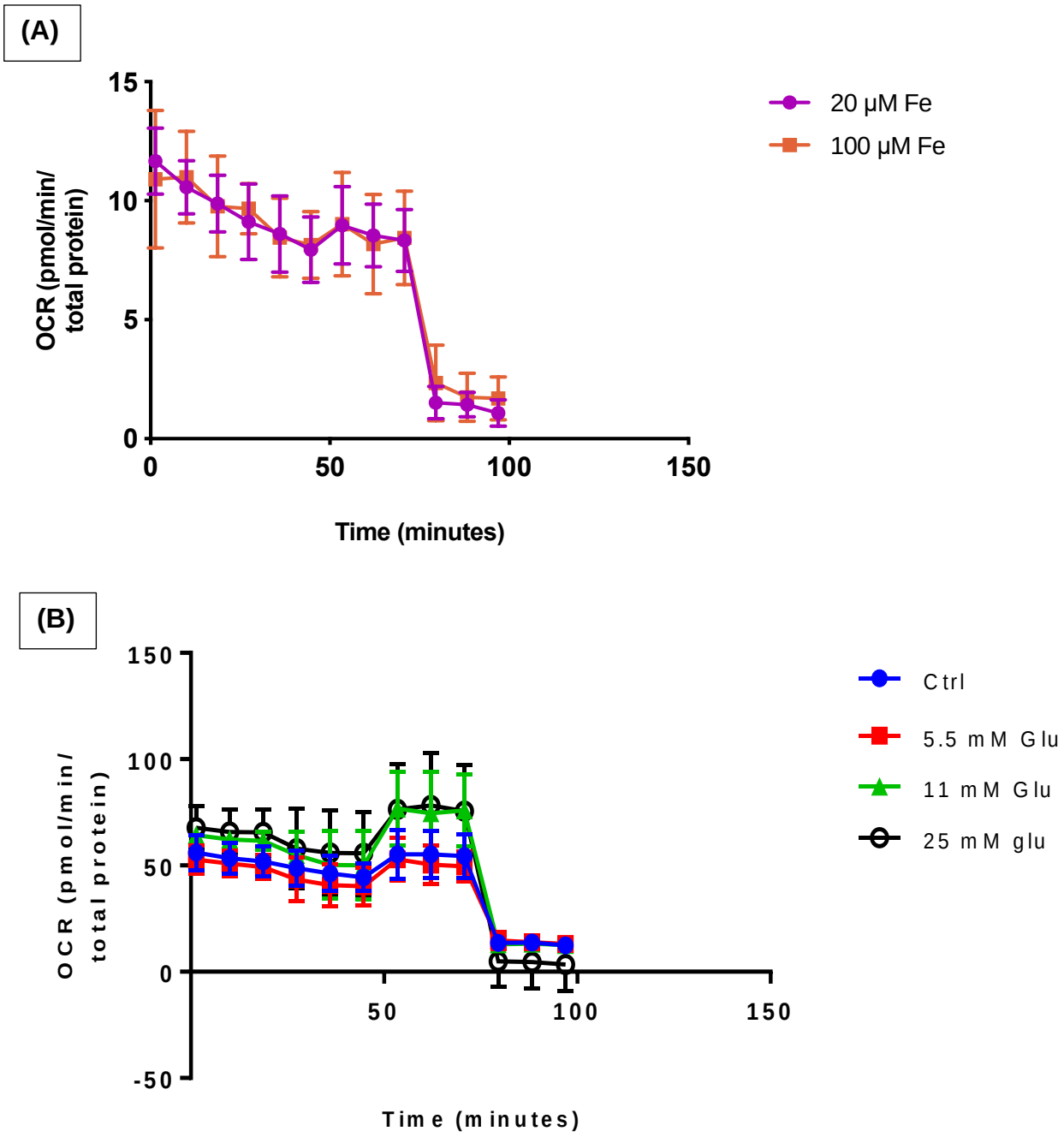

Fig. 4.2.2A-B. Oxygen consumption profiles of pancreatic β-cells (MIN6) within a 24-h period in the presence of iron and glucose. Cells were plated at 50 x 10_4 cells/well in XF24 plates. The Seahorse experimental method was used along with the addition of several distinct agents involved in the electron transport chain in mitochondria, including oligomycin, FCCP, antimycin A, and rotenone. (A) OCR in the presence of iron. (B) OCR in the presence of glucose. The data represent mean ± SEM; n=5.

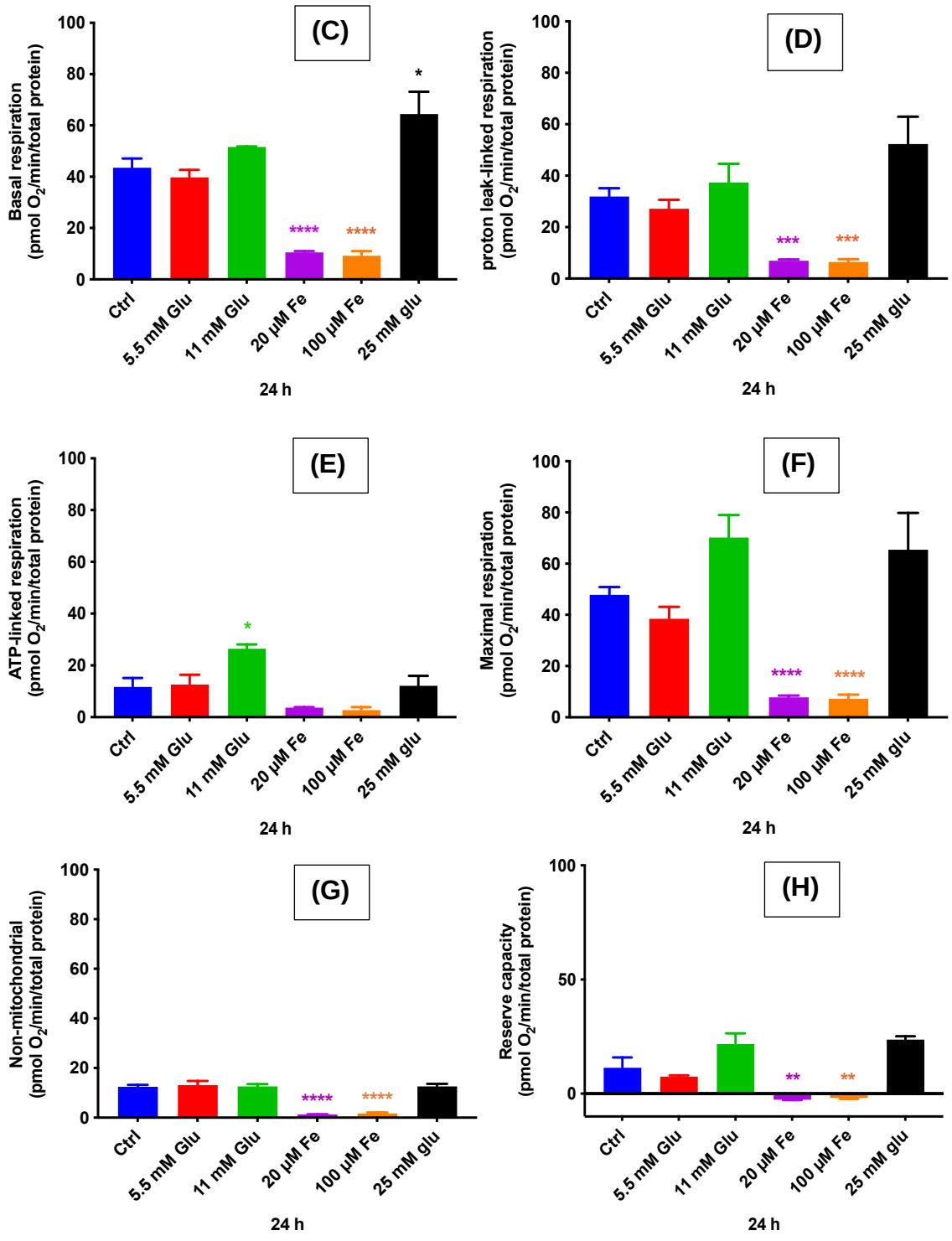

Fig. 4.2.2C-H. Oxygen consumption profiles of pancreatic β-cells (MIN6) within a 24-h period in the presence of iron and glucose. Cells were plated at 50 x 10_4 cells/well in XF24 plates. The Seahorse experimental method was used along with the addition of several distinct agents involved in the electron transport chain in mitochondria, including oligomycin, FCCP, antimycin A, and rotenone. (C) Basal respiration. (D) Proton leak–linked respiration. (E) ATP-linked respiration. (F) Maximal respiration. (G) Non-mitochondrial respiration. (H) Reserve/spare capacity. The data represent mean ± SEM; n=5. ****P<0.0001 (20 & 100 µM Fe – C), *P<0.046 (25 mM Glu – C), ***P<0.0003 (20 & 100 µM Fe – D), *P<0.05 – E). ****P<0.0001 (20 & 100 µM Fe – E), **P<0.007 (20 µM Fe – E), **P<0.009 (100 µM Fe -E).

Persistent effects were observed in the presence of normal and high iron concentrations and were reflected in all the remaining factors associated with the OCR. Normal and high iron concentrations significantly reduced the proton leak–linked respiration, maximal respiration, non-mitochondrial respiration, and reserve capacity (*P<0.05*). However, the decrease in ATP-linked respiration was insignificant, although the values were noticeably higher than that of the control. On the contrary, 11- and 25-mM glucose yielded higher values of all these factors compared to the other conditions. In addition, the normal glucose concentration induced several fluctuations across these factors (increase/decrease) compared to those of the control. However, all the glucose concentrations slightly increased non-mitochondrial respiration compared to that in the control. These results suggest that glucose alters the OCR, elevating the levels of all the parameters involved, whereas iron decreases it, which might be due to the degradation of the mitochondrial proteins involved in transporting iron from the cells into the mitochondria.

4.2.3 Measurement of ∆ψm

Lipid peroxidation estimation is one of the techniques used to determine the apoptosis level intracellularly. Assessing the involvement of ∆ψm may contribute further knowledge to understand the apoptotic pathway. Figure 4.2.3 displays the effects of various concentrations of iron and glucose on MIN6 cells under four different incubation times (1, 2, 5, and 6 days). The control represents the undyed condition. Moreover, normal iron and glucose represent controls for comparing high iron and glucose, respectively. The median intensity was the only measurement taken as it shows the brightness or level of protein expression, which represents the intensity of the dye protein that was inserted. First day indicates the exposure of cells in the short-term, second day is in the intermediate-term, and 5 & 6 days was considered as long-term exposures.

The results demonstrate that high-iron exposure for intermediate and long terms might be responsible for the occurrences of mitochondrial permeability transition (MPT). Each condition produced consistent trends in every timeline, except on the first day, in which the normal iron sample unexpectedly showed the highest protein intensity (950). Subsequently, it was interesting to observe that the high iron concentration

induced changes in ∆ψm even on the first day (41.7% reductions), which potentially caused mitochondrial alterations. However, this change was not as significant as that exhibited after other experimental incubation times. From the second day, the high iron concentration decreased the median intensity significantly, which indicated significant reductions in ∆ψm. It decreased ∆ψm by 49.6% compared to the normal iron concentration starting on the second day, followed by 32.7% and 43.5% reductions on the fifth and sixth days, respectively. Similar effects were demonstrated by the high glucose concentration, compared to the normal iron concentration, which induced lower ∆ψm levels under all the experimental conditions; however, the values were insignificant (*P>0.05*).

Therefore, iron and glucose alter the ∆ψm levels in the short-term, although the changes are insignificant. After intermediate exposure, the high glucose concentration did not significantly affect the ∆ψm levels compared to the normal glucose concentration but iron started decreasing them significantly. Iron concentrations continued to diminish the level of ∆ψm on the day 6 whereas glucose did not induce significant changes.

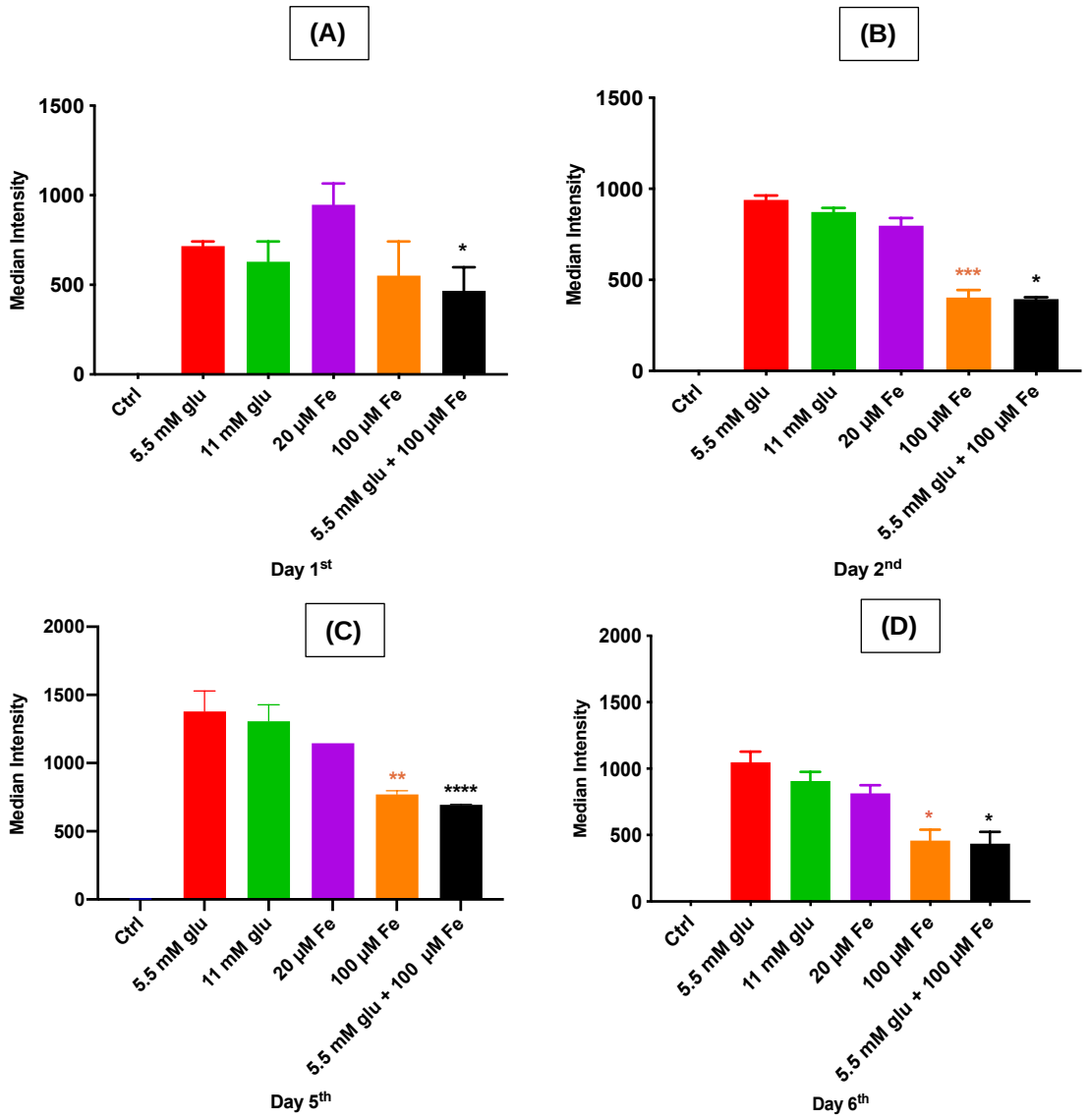

Fig. 4.2.3. Changes in mitochondrial membrane potential determined by flow cytometry in four different periods (1, 2, 5, and 6 days) using a fluorescent dye called Texas Red (excitation ideally suited to the 561- or 594-nm laser lines). MIN6 cells were exposed to both iron and glucose at various concentrations. (A) Flow cytometry analysis of mitochondrial membrane potential level by application of median intensity (charts). (B) Flow cytometry analysis of mitochondrial membrane potential level by application of median intensity (graphs). The data represent mean ± SEM; n=3. *P<0.016 (Day 1), ***P<0.0003 (Day 2), *P<0.03 (Day 2), **P<0.0055 (Day 5), ****P<0.0001 (Day 5), *P<0.039 (Day 6 - 100 µM Fe), *P<0.038 (Day 6 – 5.5 mM Glu + 100 µM Fe).

4.2.4 Imaging of live MIN6 cells influenced by ∆ψm changes

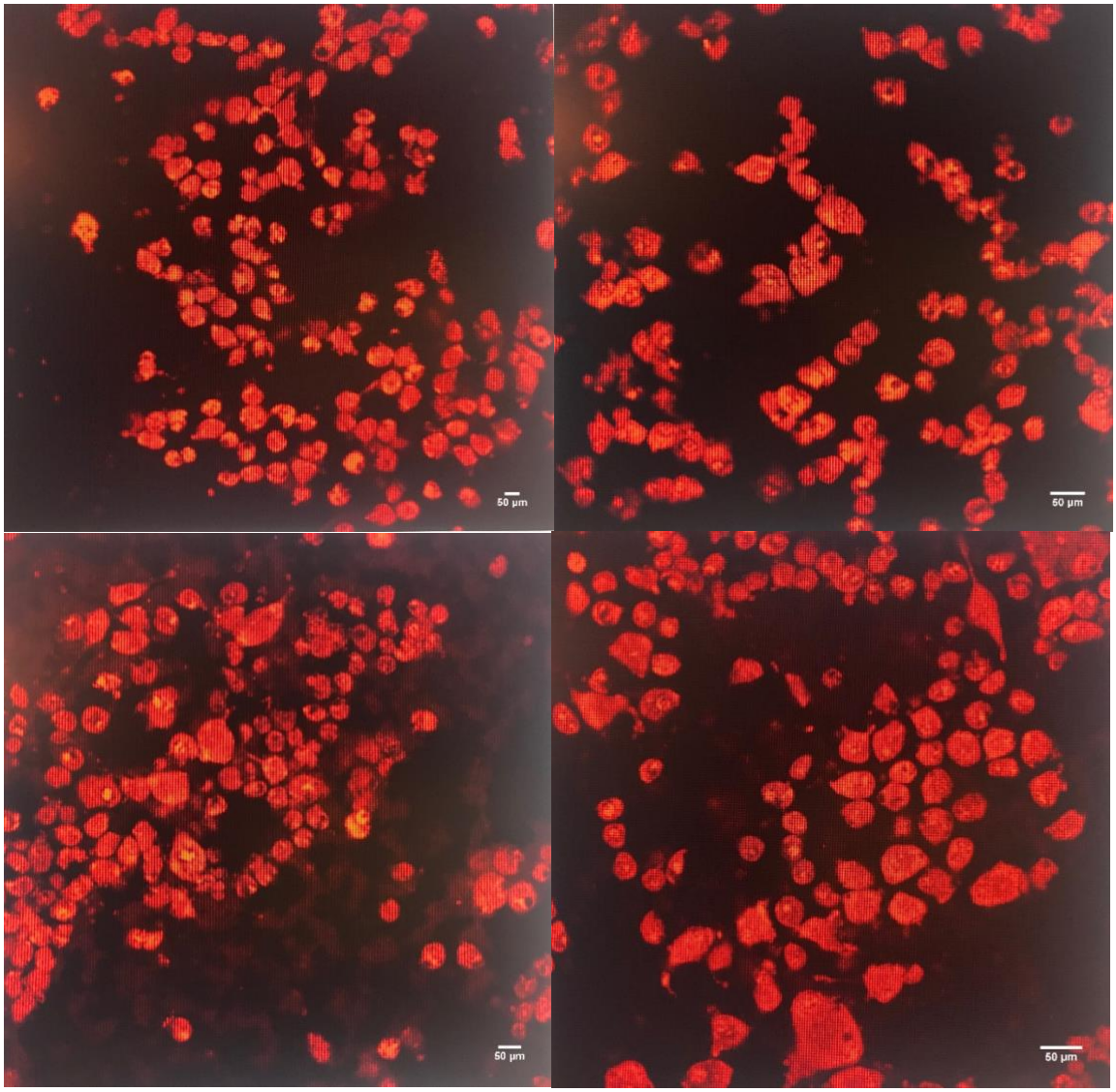

Fig. 4.2.4. Different morphologies of MIN6 cells treated with MitoTracker Red dye, which is concentrated inside the matrix (one of the compartments of a mitochondrion). This assessment was conducted in a 24-h period using confocal microscopy captured by Leica Confocal software. Morphology of cultured MIN6 cells exposed to (A) normal glucose concentration (5.5 mM), (B) high glucose concentration (11 mM), (C) normal iron concentration (20 µM), and (D) high iron concentration (100 µM).

Figure 4.2.4 depicts various morphologies of cells exposed to a range of iron and glucose concentrations. These altered morphologies resulted from changes in ∆ψm of the MIN6 cells in the presence of iron and glucose. Figures 4.2.4A&B display cultured cells treated with normal glucose and iron concentrations, respectively, whereas Figs. 4.2.4C&D display those treated with high glucose and iron concentrations.

As shown, normal glucose and iron concentrations induce a similar round morphology with several irregular shapes of cells. In addition, the cells also have a similar size, although those shown in Fig. 4.2.4B (normal iron) are slightly bigger.

The size of the cells started to change drastically when the cells were treated with the high glucose concentration. Although a majority of the cells remained similar in size to those exposed to the normal glucose concentration, several cells had undergone an alteration, showing larger sizes with elongated shapes. A similar effect was observed in the cells exposed to the high iron concentration. Furthermore, the number of cells with elongated shapes and larger sizes were higher than that under normal iron conditions. These sequential events suggested that MIN6 cells started to undergo morphology changes, including changes in size and shape, in the presence of the normal iron concentration; these changes developed even further in the cells exposed to high glucose and iron concentrations. These alterations were confirmed by the results of flow cytometry, which indicated alterations in the cells exposed to high glucose and iron concentrations in the short-term (24 h) (Fig. 4.2.3A).

4.2.5 Estimation of lipid peroxidation marker

It is known that metal-induced generation of ROS results in an attack of several intracellular compartments, one of these is PUFA residues of phospholipids (Siems et al., 1995). This quantification may provide a valuable knowldege on the level of cell death. As shown in figure 4.2.5, iron and glucose demonstrated no effects on MDA levels both at 3 and 24 h incubation. Although slight changes were observed at glucose concentrations alone and conditions containing iron and glucose, MDA levels were increased insignificantly compared to control ($P>0.05$) (24 h). In contrast, MDA levels were significantly increased in iron and glucose at both 48 and 72 h incubation ($P<0.05$). Iron and glucose concentrations exhibited more than 50% higher MDA levels compared to its control with high iron demonstrating the highest MDA level, 62.7% higher than its control (323.9 nmol/mg protein vs 120.8 nmol/mg protein).

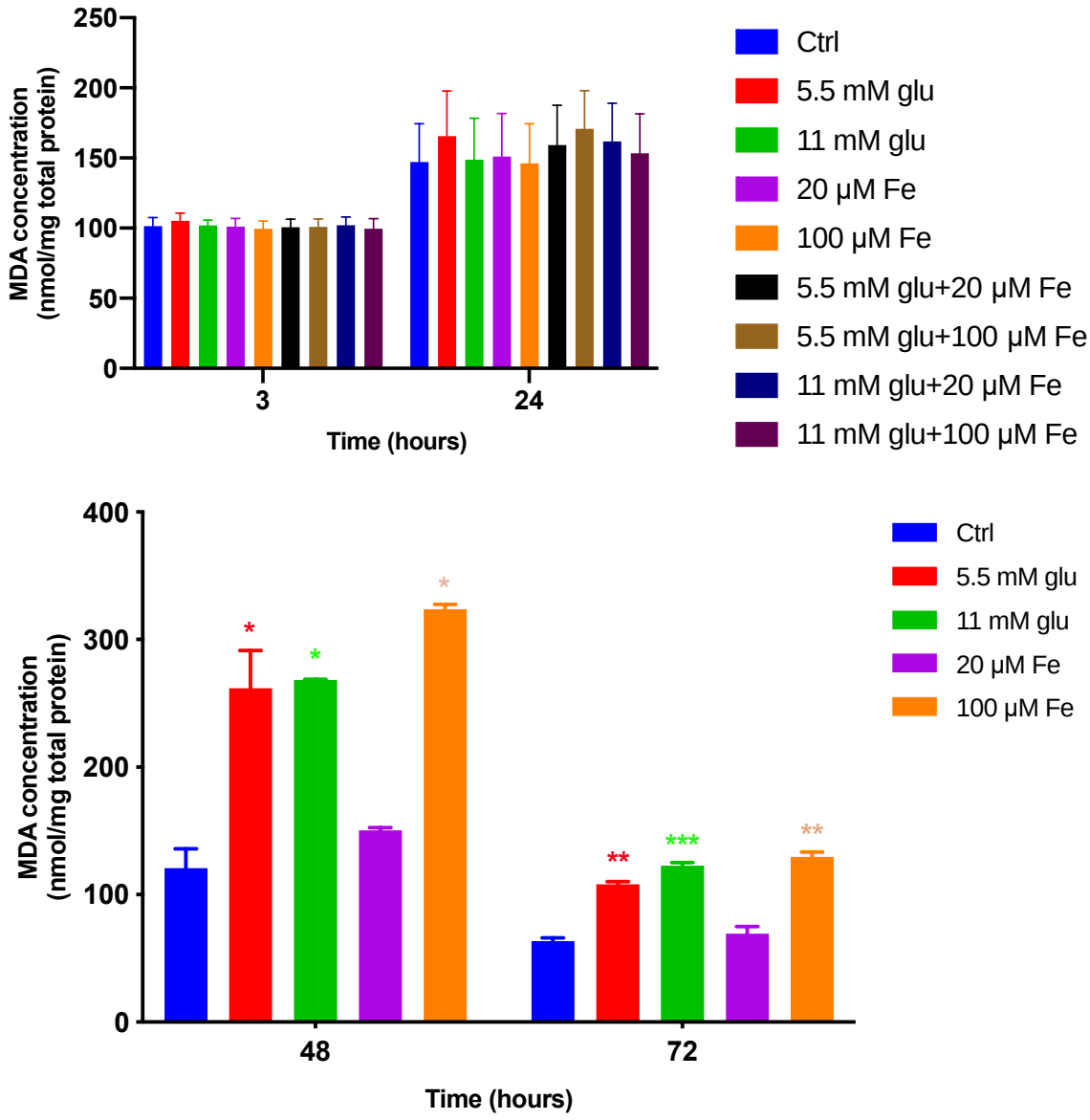

Fig. 4.2.5. The estimation of lipid peroxidation marker performed by TBARS assay in four incubation periods (3, 24, 48 and 72 h). Excessive iron and glucose increased the concentration of MDA compared to the control both the 48 and 72 h time points. The data represent mean ± SEM; *P<0.046 (C1 – 48 h), *P<0.048 (C2 – 48 h), *P<0.0415 (C4 – 48 h); **P<0.002 (C1 – 72 h), **P<0.009 (C2 – 72 h), ***P<0.0005 (C4 – 72 h). n=4.

The effect remained at 72 h incubation in which iron and glucose exhibited significantly increased levels of MDA compared to control (*P<0.05*). Consistent with the result at 48 h, high iron remained the highest MDA level with 51% compared to control (129 nmol/mg protein vs 63.65 nmol/mg protein) followed by high glucose with 48% (122.65 nmol/mg protein vs 63.65 nmol/mg protein). Therefore, the current data proposed that in both 48 and 72 h, MIN6 cells demonstrated higher MDA levels, though its levels

declined drastically at 72 h. It showed that at 48 h incubation, the cells started to undergo stress that may lead to ROS mediated cellular lipid peroxidative effects.

4.3 Discussion

Mitochondria are cellular organelles that are involved in numerous processes within the body and they play an important role in iron metabolism and the production of ATP. It is well acknowledged that mitochondria are linked to numerous diseases, including neurodegenerative (Parkinson's disease, Alzheimer's) and metabolic diseases (diabetes mellitus). Innumerable studies have been conducted to characterise this extremely dynamic organelle, including its structure and functions, and the results indicate that its distortion can contribute to the pathogenesis of a range of chronic diseases. Several methods have been developed to identify the physiological state of this organelle, such as the Seahorse test and Clarke-type electrode technique. The Seahorse test has many benefits and is considered to provide a higher sensitivity (6 x 10_7 vs 10_5) than that of the Clarke-type electrode technique. Moreover, various processes that control the OCR can also be elucidated, providing valuable insights into normal cellular function.

As previously stated, ROS can damage cell membrane lipids, proteins, and DNA. However, proteins have become one of the most susceptible targets of hydroxyl radicals due to their frequent involvement in cellular reaction catalysis (Stankoswki et al., 2011) as well as their abundance (Davies, 2016). The oxidation of proteins can be promoted by ROS via the side chains of susceptible amino acids, including lysine, proline, threonine, and arginine. These reactions yield ketones and aldehydes that subsequently react with DNPH protein products, producing the primary protein carbonyl. Long-term high iron (78%) and high glucose (76.5%) exposure of cells significantly increases the extent ($P<0.05$) of protein oxidation (Fig. 4.2.1) compared to that in the control. The opposite occurs in a short-term condition: high iron and glucose concentrations significantly reduce the levels of protein oxidation (89.1% and 84%, respectively) compared to that in the control. This might be due to a direct rescue addressed by the pancreatic β-cell defence system via the activation of endogenous antioxidants, in which cells are protected more efficiently in the short-term. The

consequent effects enable several alterations on proteins and hence in their conformation, activity, and function.

The identification of these alterations is important because the perturbations caused by protein carbonylation can alter mitochondrial functionality with respect to, for example, energy metabolism or pH regulation. Such protein oxidation can be counteracted by cellular defence mechanisms, i.e. lysosomal and proteasomal pathways. Furthermore, similar to glutathione peroxidases that can catabolise H_2O_2 into water, a variety of enzymes can reverse the effects of protein carbonylation, including aldehyde dehydrogenases, aldo-keto reductase, and alkenal/one oxireductase, by diminishing the reactivity of lipid aldehydes (Frohnert & Bernlohr, 2013). Unfortunately, some materials are poorly degraded and easily accumulated within cells. Moreover, some types of tissues and their defence systems exhibit limited standards towards repairing and maintaining the state of the cells. Pancreatic β-cells are more prone to the resulting perturbations owing to a lack of natural antioxidants. Hence, the identification of oxidative stress due to the role of protein carbonylation may provide valuable insight into preventing carbonyl stress–associated diseases such as diabetes mellitus.

Owing to alterations in intracellular proteins (responsible for structures and functions) as a consequence of oxidative stress, their parent organelles are compromised. As shown in Fig. 4.2.2, the elevation of glucose concentrations (11 and 25 mM) leads to higher basal respiration, proton leak, ATP-linked respiration, reserve capacity, and maximal respiration, which have been shown to cause higher OCR levels. This observation is in accordance with the study performed by Hutton and Malaisse, showing that OCR levels increase in response to an increase in glucose concentrations (Hutton & Malaisse, 1980). Several agents, including oligomycin, FCCP, and a combination of antimycin A and rotenone, have been used to elucidate the function of mitochondria. Oligomycin inhibits ATP synthase by blocking proton channels, thus decreasing the OCR levels necessary for oxidative phosphorylation of ADP to ATP. Conversely, FCCP uncouples the activity of the respiratory chain from ATP synthesis and hence raises the maximal value of the OCR. Lastly, the injection of antimycin A with rotenone targets the ETC, producing a minimal OCR value

(Divakaruni et al., 2014). Each of these agents is used to estimate various parameters affecting the indicators of oxidative phosphorylation.

Contrary to the concentrating effects of glucose, it is intriguing that iron reduces the OCR both within and outside mitochondria. Both normal and high levels of iron have this effect, whereas the effect of glucose is concentration dependent. Conversely, normal and high iron concentrations induce similar rates of oxygen consumption, which are extremely low compared to that in the control and with different concentrations of glucose (Fig. 4.2.2). This observation suggests that iron may not have a short-term effect on the mitochondrial OXPHOS state, which agrees with the results obtained by Cejvanovic in mice biopsies (Cejvanovic, 2016). Furthermore, consistent results demonstrate that all the parameters involved in controlling the OCR show the lowest levels in the presence of both normal and high iron concentrations. The mechanism of the iron-induced effects on OXPHOS has not been fully elucidated. However, they might be due to the degradation of mitochondrial proteins involved in iron transport from the cytoplasm into the mitochondria.

As shown in Fig. 4.2.2D, high glucose concentrations induce higher proton leaks compared to the control, suggesting that this parameter can either reflect the normal physiological response (Divakaruni & Brand, 2011) or damage of mitochondria (Dranka et al., 2011). As previously mentioned, all other bioenergetic parameters that were altered are likely associated with oxidative stress, eventually yielding to organelle dysfunction under long-term conditions. A normal glucose concentration does not induce a significantly higher non-mitochondrial-associated OCR compared to that in the control. Chacko et al. identified that in the presence of stressors such as ROS, non-mitochondrial respiration typically increases (Chacko et al., 2014).

Another disrupted factor that is associated with the state of mitochondrial health is $\Delta\psi m$. Mitochondrial damage can initiate apoptosis. Disruption of the mitochondrial membrane potential is considered the major sign of dysfunction of this organelle. A loss in $\Delta\psi m$ has been observed in cases of impaired mitochondrial ETC, which decreases ATP production (Kim & Kim, 2018). A decrease in $\Delta\psi m$ makes the membrane permeable, triggering the mitochondrial apoptotic pathway.

Cytochrome c is then released into the cytosol via the activation of pro-apoptotic caspases in the mitochondria, which is caused by the opening of the MPTP. This condition may be triggered by many factors, but excess iron is the underlying reason for this damage.

This finding is consistent with the results shown in Fig. 4.2.3, which depicts significant reductions in $\Delta\psi m$ in the presence of excess iron in MIN6 cells. Starting from the second day of incubation, the $\Delta\psi m$ level drastically decreased upon exposure to a high iron concentration (49.6% reduction), compared to that in the control. This effect persisted through the 5^{th} (32.7%) and 6^{th} days (43.5%). In addition, although the $\Delta\psi m$ level was lower than that under normal iron conditions on the first day, the result was insignificant (*P>0.05*), which was in accordance with the results of the OCR (Fig. 4.2.2). These observations suggest that mitochondria may have the capacity to withstand high iron concentrations under short-term conditions. However, short-term exposures to high iron concentrations (as early as the second day) can cause pathological changes in the $\Delta\psi m$. Furthermore, high iron concentrations induce a very low $\Delta\psi m$, which suggests the occurrence of continuous apoptosis and/or a possible increase in the membrane permeability (sixth day incubation). Although the effects of short-term exposure to high iron concentrations on the $\Delta\psi m$ are insignificant, this does not necessarily mean that no alteration occurs.

Unlike iron, glucose concentrations induced consistent effects under both short- and long-term exposures. However, these effects were significantly higher (*P<0.*05, median intensity: ~1400 vs 900) on the fifth and sixth days compared to those under previous conditions. These data correspond to the OCR results, which show that high glucose concentrations induce higher levels of proton leak. A high mitochondrial membrane potential is likely to increase proton leakage, which ultimately leads to higher production of ROS. These results are also supported by the data obtained using confocal microscopy (Fig. 4.2.4). Pancreatic β-cells undergo morphological transitions in response to high iron and glucose concentrations. Picard et al. concluded that the transitions of this organelle were due to cellular stresses induced by MPT and ROS (Picard et al., 2013).

At low concentrations, ROS provides beneficial effects in many metabolic processes. Unfortunately, these powerful agents can be important mediators of damage to cell structures, nucleic acids, lipids, and proteins, associated with some physical changes biochemically (Valko et al., 2006). Lipid peroxidation is one biological process resulting from the attack by metal-induced generation of ROS as lipids are extremely sensitive to oxidation (Siems et al., 1995). MDA is the primary aldehyde product of peroxidation that is mutagenic in bacterial and mammalian cells and is carcinogenic in rats (Valko et al., 2007).

In the present study, the effect of excess iron-generated ROS, lead to increased MDA (measured by TBARS) contributing to apoptosis initiation. Figure 4.2.5 showed that excess iron demonstrated higher MDA levels, which started at 48 h incubation likely as a result of ROS mediated cellular lipid peroxidative effects. Moreover, another major aldehyde product of this cell structure is 4-hydroxy-2-nonenal (HNE), characterised as a major toxic product and yet considered as weakly mutagenic. This weak feature grants MDA as a marker of lipid peroxidation, which is highly evidenced in patients with T2DM. It can be seen that there is an extremely increased level of MDA in a presence of excess iron, which suggests that there is an increased production of free radicals. These free radicals promote lipid peroxidation, resulting in the chain reaction and damage to various molecules, eventually leading to cell damage (Gutteridge, 1995).

Since pancreatic β-cells are particularly susceptible to ROS, owing to less intracellular antioxidant content, numerous diseases of these cells could occur, particularly the deadly and epidemic disease called diabetes mellitus. A number of treatments have been developed for such conditions, including iron chelation and phlebotomy; some medicines, such as SGLT2, in addition to other drugs are still under research and clinical trials. Moreover, nanoformulations containing a variety of antioxidants have been studied because they exhibit characteristics that can be potentially therapeutic and can hence decrease the prevalence of metabolic diseases.

CHAPTER 5
RESULTS

5.1 Introduction

Aim: To identify the role of antioxidant-nanoformulations on small intestine function using caco-2 cell – model for antioxidant-nanoformulations strategy in excess iron.
Objectives:

- Identify various iron treatment formulations using potato dextrin and modified citrus peel dextrin (prepared at UCL as one of the collaborators) with and without the presence of iron inhibitor (EGCG).
- Identify the activity of antioxidants (hesperetin)-related nanoformulations using ferric reducing antioxidant power (FRAP) analysis.
- Identify the activity of cellular antioxidants-related nanoformulations using cellular antioxidant activity (CAA) analysis.

As previously mentioned, iron has been implicated in various metabolic and neurodegenerative diseases owing to its role in generating oxidative stress. Hence, it is necessary to devise a strategy for efficient iron absorption in the small intestine in a controlled fashion so that it can be used for multiple purposes within the cells. Nanoformulations/nanoencapsulations have gained the attention of many researchers and have been developed to promote the complexity of iron metabolism and homeostasis. Nanoencapsulation can be defined as the coating of a particular substance within another material at the nanoscale (Khan et al., 2019). The substance that was coated in this project was an antioxidant. Antioxidants are molecules that possess therapeutic properties which help protect the structure and function of cells from oxidative damages. An antioxidant is a powerful substance, but its properties can be weakened when it is exposed to a specific cell's environment. Hence, the encapsulation method might be a suitable tool for preserving antioxidant properties.

A novel strategy that has been developed to this end is solid lipid nanoparticles (SLNs). It has been used widely owing to several benefits, including its suitability for the environment within the human body. Biocompatibility and biodegradability are two known properties of these substances which make them safe; their composition is similar to that of lipids or antioxidants. SLNs contain iron/antioxidant coated inside a lipid shell. The shell is made up of a potato protein combined with a polysaccharide such as modified citrus pectin (First formulation) or potato dextrin (Second formulation)

with the size range of <500 nm (Fig. 5.1). Each of these shells demonstrates the requisite properties for delivering a particular substance to the target efficiently and effectively.

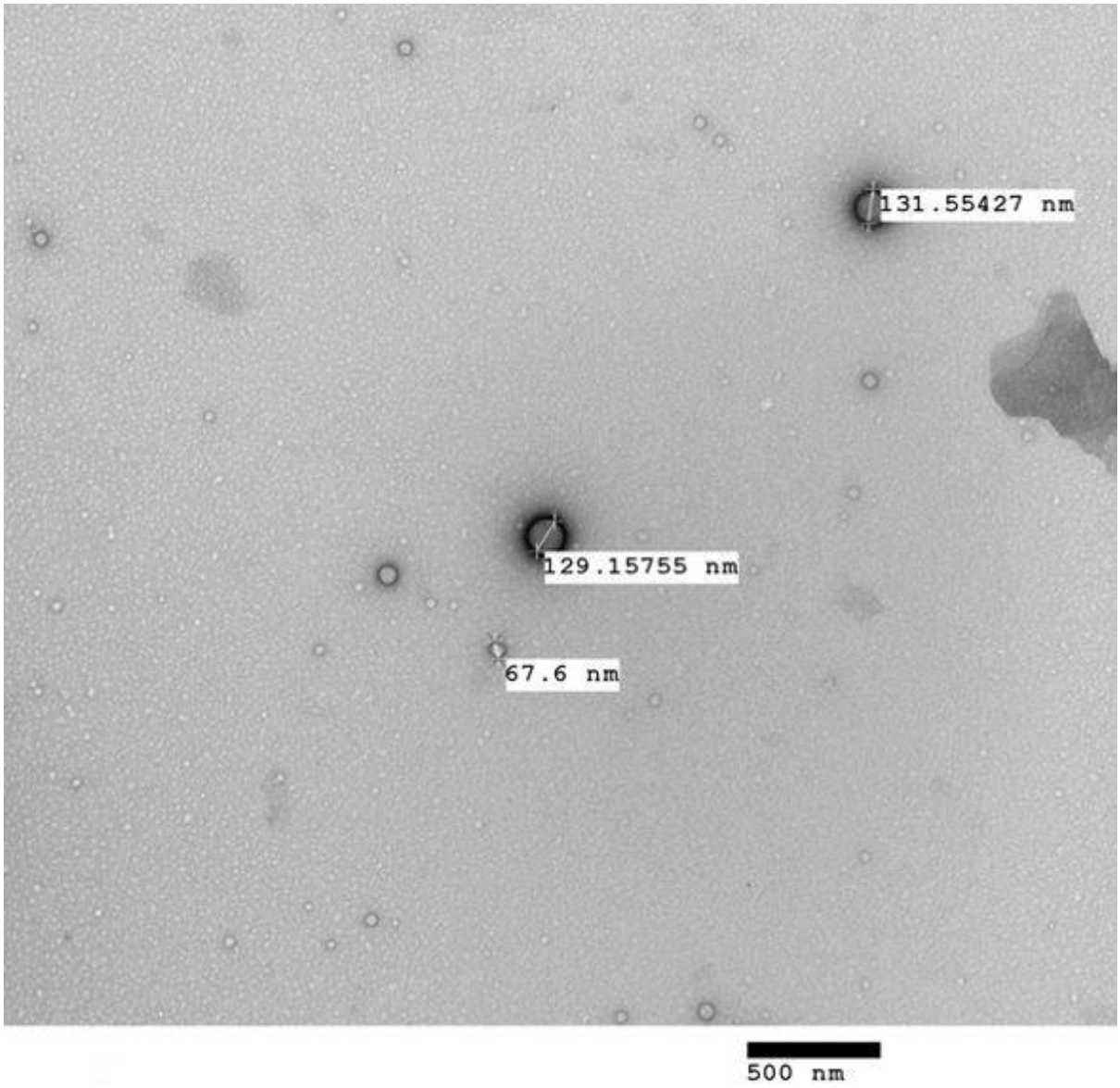

Fig. 5.1. Representative transmission electron microscopy (TEM) image of loaded protein polysaccharide formulations at 135,000x magnification (Philips Biotwin CM120, Philips Co, The Netherlands). All formulations were observed to be <500 nanometre size range.

Prior to testing the activity of antioxidants coated by nanoformulations made of these two types of polysaccharides, another model was developed in order to compare commercial $FeSO_4$ (typical prescribed form of iron supplements) to iron coated with nanoformulations. Moreover, EGCG was added as an iron inhibitor to identify the efficacy and efficiency of the two types of nanoformulations that demonstrated higher absorbance of iron in the intestinal Caco-2 cell line.

Several analyses were performed to identify the antioxidant toxicity-coated nanoformulations. The activity of the antioxidant and its cytotoxicity in Caco-2 cells were measured. Caco-2 cells were applied to mimic the intestinal environment in which iron and other substances are absorbed before entering circulation. Trolox or 6-hydroxy-2,5,7,8-tetramethylchroman-2-carboxylic acid is an analogue of vitamin E that was selected as a reference owing to its ability to provide maximum antioxidant activity. The level of antioxidant activity was observed by the measurement of CAA and FRAP assay. This strategy was expected to decrease the level of oxidative stress within the cells. Thus, cytotoxicity was also measured by MTT to confirm whether nanoformulations coated antioxidants exhibited any toxicity.

5.1.1 Quantification using FRAP assay

Figure 5.1.1 represents the antioxidant activity of three different nanoformulations, measured as per the Trolox equivalency. Two distinct NFs were prepared with the antioxidant, hesperetin. The first NF (Dextrin) was composed of potato protein with potato dextrin and hesperetin, whereas the second NF (Citrus) comprised potato protein with modified citrus pectin and hesperetin. This experiment was performed using an antioxidant activity assay called FRAP assay.

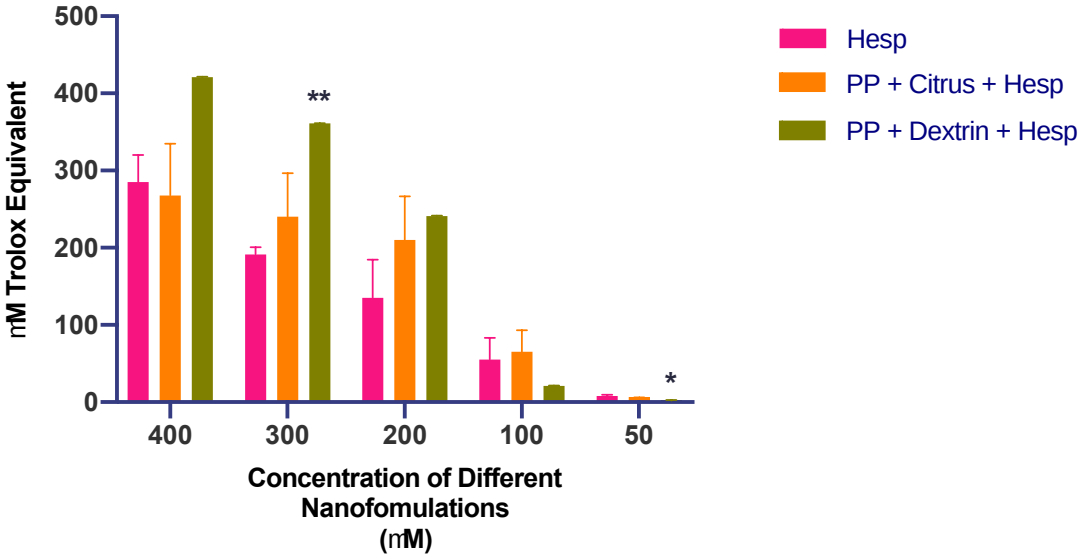

Fig. 5.1.1. Antioxidant activity of nanoformulations composed of hesperetin, determined using FRAP assay. The data represent mean ± SD. Hesp: hesperetin, PP: potato protein. *P<0.0283, **P<0.0015. n=2

As shown in Fig. 5.1.1, the antioxidant activity is proportional to the concentration of added hesperetin, NF1, and NF2. However, NF1 showed 81.2% and 62.3% lower antioxidant activity levels at 50 and 100 µM, respectively.

NF2 also exhibited lower antioxidant levels at 50 and 400 µM, compared to those of hesperetin alone (31.3% & 6.1%, respectively). Nevertheless, NF1 and NF2 showed higher antioxidant activity levels in comparison to hesperetin alone. At 400 µM, the antioxidant levels of NF1 and NF2 were six-fold and three-fold higher than that of hesperetin, respectively. This trend was observed at all concentrations of the formulations, except 50 µM. Moreover, NF1 exhibited a higher antioxidant activity than that of the two other formulations. Therefore, nanoformulations composed of dextrin with hesperetin are likely to be more efficient than those made of modified citrus pectin with hesperetin.

5.1.2 Cytotoxicity studies with MTT assay

The MTT assay has been extensively applied to assess the cytotoxicity of substances towards cell metabolic activity, which manifests as a colour change. This assay was used to observe the effects of the non-encapsulated antioxidant and nanoencapsulated-antioxidant on Caco-2 cells after 24- and 48-h incubations. Two types of NFs were prepared using dextrin and modified citrus pectin (PP+PD & PP+MCP) with and without hesperetin. The two nanoformulations without hesperetin were considered as the control and reference for 100% cell viability. As shown in Fig. 5.1.2, the shells composed of the two modified potato proteins exhibited no toxicity towards the cells. Application of MCP without hesperetin resulted in the highest cell viability at all concentrations.

Unexpectedly, the use of both NF1 and NF2 containing hesperetin led to a lower cell viability than that observed under blank conditions at all concentrations. In addition, non-encapsulated hesperetin generated higher cytotoxic effects than hesperetin encapsulated in the two nanoformulations ($P<0.05$). Similar results were also observed after 48 h of incubation.

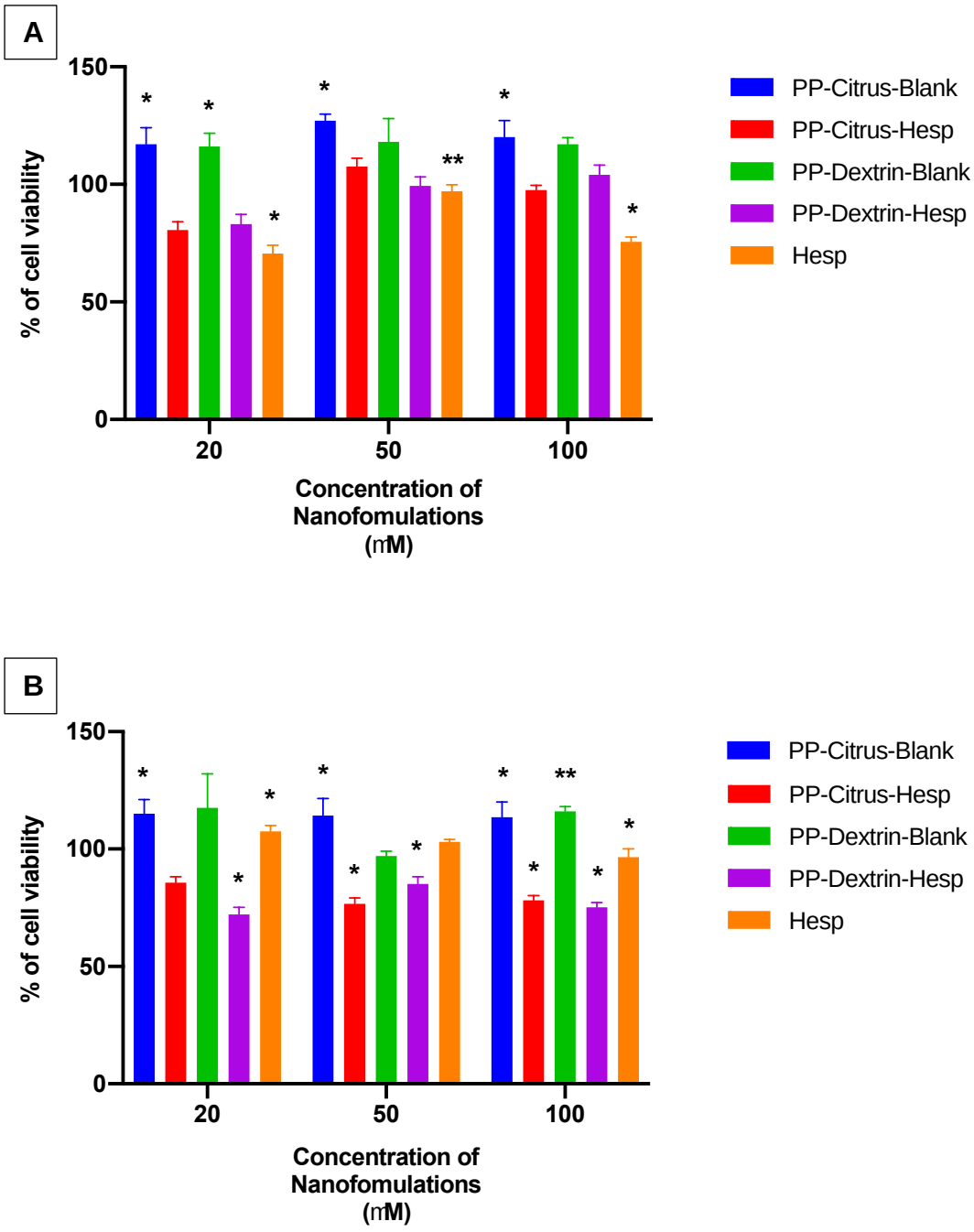

Fig. 5.1.2. Cytotoxicity of pure non-encapsulated hesperetin and nanoformulations of hesperetin towards Caco-2 cells, determined using MTT assay. A). Twenty-four- and B). Forty-eight-hour incubation periods. The data represent mean ± SD. *P<0.023 (NF2 blank vs NF2), *P<0.022 (NF1 blank vs NF1), *P<0.014 (NF2 blank vs Hesp), *P<0.011 (NF1 vs Hesp); *P<0.026 (NF2 blank vs NF2), **P<0.09 (NF2 blank vs Hesp); *P<0.05 (NF2 blank vs NF2), *P<0.022 (NF1 blank vs Hesp); *P<0.045 (NF2 blank vs NF2), *P<0.025 (NF2 vs Hesp), *P<0.012 (NF1 vs Hesp); *P<0.04 (NF2 blank vs NF2), *P<0.01 (NF2 vs Hesp), *P<0.03 (NF1 vs Hesp); *P<0.035 (NF2 blank vs NF2), **P<0.047 (NF1 blank vs NF1), *P<0.044 (NF2 vs Hesp), *P<0.040 (NF1 blank vs Hesp), *P<0.033 (NF1 vs Hesp). n=2.

This suggests that encapsulation shells composed of potato dextrin and modified citrus pectin do not exhibit cytotoxicity towards these cells. In contrast, hesperetin is toxic and can be useful in cancer treatments.

5.1.3 Quantification using CAA assay

Unlike the FRAP assay, the CAA assay measures the activity of an antioxidant within the cells. The formulations and concentrations optimised in the FRAP assay were also used for the CAA assay of the Caco-2 cell culture. As shown in Fig. 5.1.3, both the nanoformulations without hesperetin exhibited a significant increase in cellular antioxidant activity compared to those with hesperetin. However, NF1 exhibited a higher cellular antioxidant activity than NF2 both with and without hesperetin. Unexpectedly, non-encapsulated hesperetin exhibited higher cellular antioxidant activity compared to NF2 with/without hesperetin (at 20 µM). Moreover, similar results were observed at 50 µM (382 vs 190.5); non-encapsulated hesperetin increased cellular antioxidant activity compared to NF2 without hesperetin and decreased it significantly compared to NF2 with hesperetin (169 vs 238) at 100 µM.

Ironically, the antioxidant activity of NF1 under blank conditions progressively decreased as the concentration increased, whereas that of NF2 fluctuated. NF2 increased the CAA value at 50 µM but decreased it at 100 µM (501 vs 169, respectively). On the other hand, NF2 without hesperetin (blank) decreased the activity at 50 µM and increased it at 100 µM (190.5 vs 320.6, respectively). Similar to NF1, uncoated hesperetin progressively decreased the CAA unit as its concentration increased.

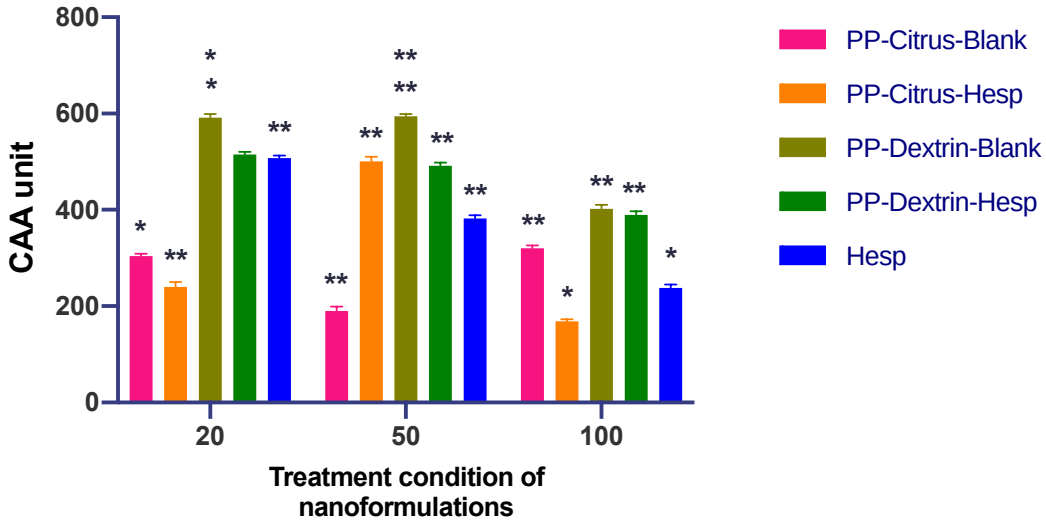

Fig. 5.1.3. Cellular antioxidant activity under different treatment conditions with various concentrations (20 µM - 50 µM - 100 µM). Data represent mean ± SEM. *P<0.028 (NF2 blank vs NF2), *P<0.014 (NF1 blank vs NF1), *P<0.012 (NF1 blank vs Hesp), **P<0.0012 (NF2 blank vs Hesp), **P<0.0018 (NF2 vs Hesp); **P<0.0016 (NF2 blank vs NF2), **P<0.0063 (NF1 blank vs NF1), **P<0.0016 (NF1 blank vs Hesp), **P<0.0075 (NF1 vs Hesp), **P<0.0033 (NF2 blank vs Hesp), **P<0.0091 (NF2 vs Hesp); **P<0.002 (NF2 blank vs NF2), *P<0.011 (NF2 blank vs Hesp), *P<0.013 (NF2 vs Hesp), **P<0.0039 (NF1 blank vs Hesp), **P<0.0046 (NF1 vs Hesp). n=2.

In summary, dextrin-coated hesperetin and its blank demonstrated the highest CAA at all concentrations but the value decreased as the concentration increased, which was similar to the results for non-encapsulated hesperetin. In contrast, the citrus formulation and its blank showed lower CAA at all concentrations but the values fluctuated, eventually leading to a decrease in the CAA at 100 µM.

5.1.4 Iron uptake in Caco-2 cells

Various stock formulations of $FeSO_4$ and novel nano-carrier formulations containing potato protein–derived polysaccharides (Citrus peel pectin and potato dextrin) were prepared and their ferritin concentrations were compared. Minimum Essential Medium (MEM) was used as a control owing to its iron-free nature, with a ferritin concentration of 7.6 ng/mg. Ferritin was used as an indirect marker of iron absorption owing to its robust properties in comparison with total iron. $FeSO_4$ induces a ferritin concentration of 68.0 ng/mg. Two nano-carrier iron formulations, Dextrin (NF1) and Citrus (NF2), were tested against $FeSO_4$, to determine whether they were more efficacious and better tolerated. NF1 presented a ferritin concentration of 121.9 ng/mg, whilst NF2 had a relatively lower concentration of 96.2 ng/mg.

Figure 5.1.4A shows that NF1 is more effective than $FeSO_4$, with a 79.3% increase in iron absorption. NF2, however, is slightly less effective than $FeSO_4$, inducing a 41.5% increase. The difference in efficacy between NF1 and NF2 is 21%. $FeSO_4$, in comparison to NF1, shows a 41.5% greater efficacy.

$FeSO_4$, NF1, and NF2 were also tested in the presence of EGCG, an inhibitor of iron absorption. Once EGCG was added to each formulation, the ferritin concentration decreased significantly, except in the case of NF2, which was not inhibited significantly. $FeSO_4$ treatment in isolation resulted in a high ferritin concentration; however, co-treatment with EGCG produced a significant decrease (by 84%) in ferritin concentration (9.07 ng/mg) owing to EGCG's inhibitory effects. NF1 induced the highest iron concentration; however, EGCG co-treatment led to inhibition and therefore the positive effects detected in isolation were lost.

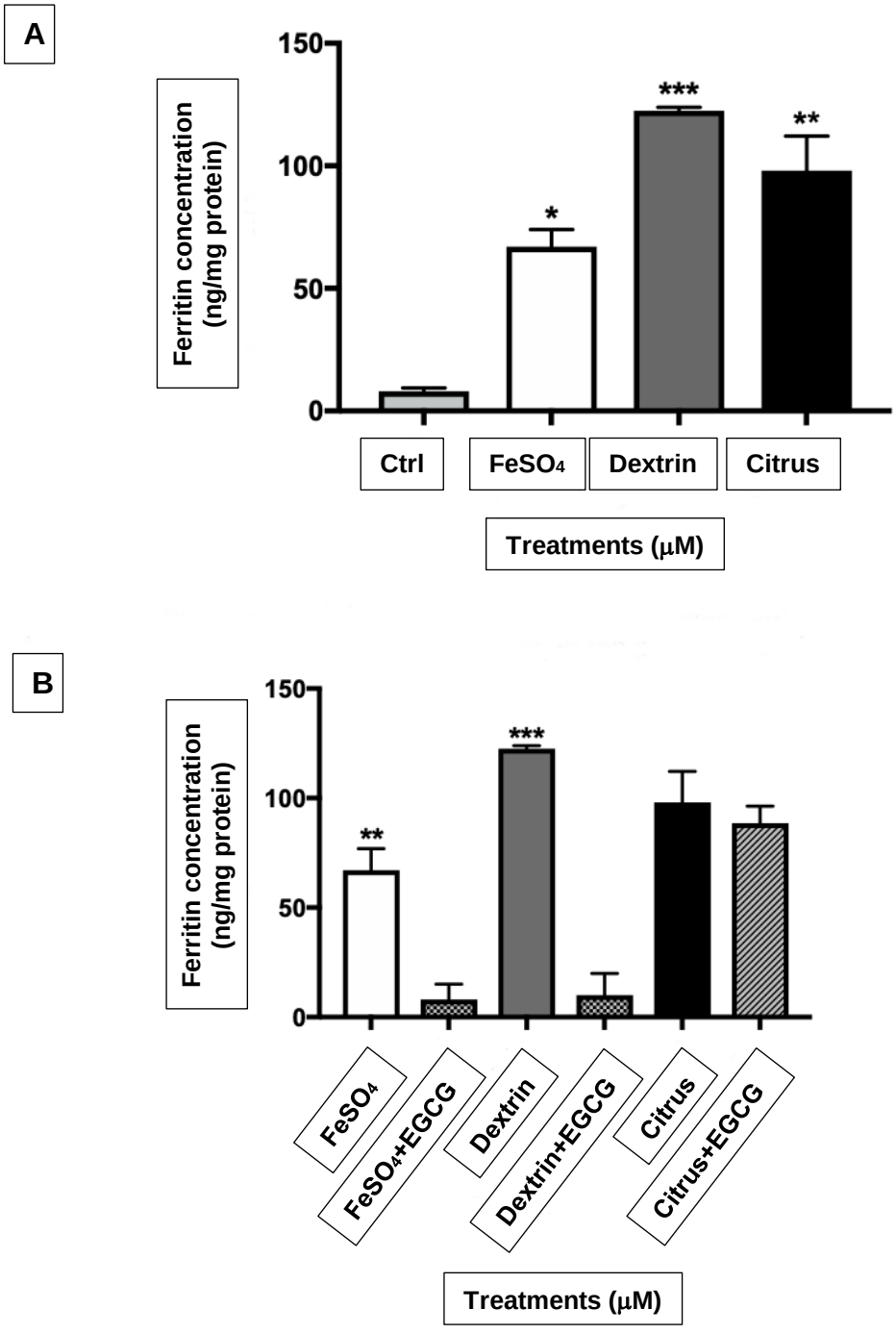

Fig. 5.1.4. Total ferritin concentrations (ng/mg total protein) observed for the most commonly prescribed oral supplement for iron deficiency in the UK ($FeSO_4$) and two nano-carrier iron formulations (Dextrin and Citrus). These treatments were tested using the Caco-2 cell line incubated with 20 μM of iron for each treatment. A). In the absence of 100 uM EGCG. B) In the presence of 100 uM EGCG. Data were generated through ELISA and expressed as mean ± SEM. A) *P< 0.01, **P< 0.003, *** P<0.001; B) **P<0.007, ***P<0.0002, significantly different, as shown. (n=2).

NF1 with EGCG displayed a significant decrease in iron uptake (9.56 ng/mg), similar to $FeSO_4$ with EGCG, with a percentage difference of 5.26%. EGCG inhibits iron uptake from NF1 by a staggering 87% (Fig. 5.1.4B). The ferritin concentration after NF2 treatment was not as significant as that after NF1 treatment. However, the statistics suggest that co-treatment with EGCG inhibited uptake from NF2 by only 10%, with a ferritin concentration of 86.6 ng/mg, which was not much higher than that during co-treatment of EGCG with $FeSO_4$ and NF1; hence, NF2 was more potent. This led to the notion that if NF2 is further developed into a dietary supplement, the consumption of polyphenols such as tea/coffee would not affect the iron concentration to a great extent, unlike in the case of the NF1 formulation.

5.2 Discussion

Overproduction of free radicals causes oxidative stress and may eventually lead to chronic diseases such as cancer, cardiovascular diseases, chronic inflammation, and diabetes mellitus. Public awareness about diabetes mellitus is increasing as this chronic disease, which causes immense complications, has become progressively prevalent both in developed and developing countries. T2DM is the most common form of diabetes and is marked by abnormal carbohydrate, lipid, and protein metabolism associated with impaired insulin secretion and insulin resistance. Iron is the most abundant trace metal that has been linked to human pathophysiology involving the formation of free radicals, ultimately leading to oxidative damage.

Since many chronic diseases are caused by oxidative stress associated with an increase in the formation of ROS, scientists have been developing some strategies to overcome such conditions, with iron gaining attention as of one of the metals that has been constantly researched in cross-studies between nutrition and medicine. Nanoparticles composed of various materials that are primarily characterised as biodegradable have been widely developed. Biodegradable materials are non-toxic, biotolerable, biocompatible, biodegradable, and water-soluble. In preparing these sub-nano particles, natural polysaccharides have been extensively utilised, and their use has significantly increased (Zhang et al., 2011; Yang et al., 2008; Aumelas et al., 2007); Leonard et al., 2003).

Polysaccharides are one of the main structural elements of polymeric carbohydrates formed via glycosidic bonds; they can be obtained from various sources. Polysaccharides can be composed of complex chemicals with varying molecular weight, which exhibit diversity in structure and properties. Modified polysaccharides can form self-assembled nanoparticles comprising a hydrophilic outer layer and a hydrophobic core. Hydrophobic drugs and other materials that possess a low ability to be absorbed can be administered using a variety of delivery methods. Dextran is a modified polysaccharide that can form amphiphilic polymers, making it suitable for encapsulating and releasing a particular drug in a hydrophobic domain. Citrus pectin is also a potential antioxidant which is characterised as an anti-inflammatory or anti-cancer material that blocks galectin-3 activity; galectin-3 has been found to be overexpressed in most types of cancer cells (Nangia-Maker et al., 2002). Moreover, recent research also indicates that citrus pectin chelates heavy metals, which are linked to various diseases (Eliaz et al., 2006).

Antioxidants possess therapeutic properties with some potency to counter diseases; therefore, combinations of antioxidant formulations and delivery systems have been tested in this regard. Hesperetin is an antioxidant that has been reported to exhibit antitumor ability *in vitro* and *in vivo* by inducing apoptosis of cancer cells, without toxicity (Wu et al., 2016). It has also been demonstrated to inhibit significant proliferation and induce apoptosis in hepatocellular carcinoma cells. This study is a cross-examination evaluating the use of two types of polysaccharides as encapsulating agents. Potato dextrin and MCP were used to encapsulate iron and a particular antioxidant; these formulations induced higher values of cell viability (Fig. 5.1.2). This experiment was followed by an investigation into the activity of the antioxidant both in its encapsulated and free states. The potato dextrin–encapsulated antioxidant displayed an elevated intracellular (5.1.3) and non-intracellular (Fig. 5.1.1) antioxidant activity in comparison to MCP.

Higher absorption of the coated agents and stability of the shells composed of dextrin and citrus pectin are two of the many prerequisites of suitable components in developing nanoformulations. In this study, $FeSO_4$ and EGCG were used as the iron source and inhibitor, respectively, and they were coated with these two polysaccharides. It has been known that

iron absorption can be impaired by dietary ingredients such as dairy products, eggs, and caffeinated beverages. Since the interest in dietary polyphenols has increased (tea is the most consumed beverage in the world after water), the effects of ultra-pure EGCG (100 μM) on a human intestinal cell line (Caco-2) were studied. This investigation was conducted to elucidate whether the regular consumption of this polyphenolic compound, which is a potent inhibitor, causes any impairment in the absorption of dietary iron.

The consumption of iron supplements could lead to a high iron content in our body. Since a high concentration of circulating iron might cause β-cell dysfunction, an experiment was designed using the Caco-2 cell line to investigate the combined effects of novel formulations and compare them with those of iron preparations currently in the market. Intracellular ferritin protein formation was considered an indirect marker for measuring iron absorption in the Caco-2 cells, owing to the robust properties of ferritin. The results show that amongst the various treatments, the hydrophilic molecule, $FeSO_4$, induces lower iron absorption levels in comparison to proteinated sources of iron, such as Potato Dextrin and MCPD (Fig. 5.1.4A). Dextrin induces the highest iron absorption, followed by citrus, at 96.2 ng/mg ferritin concentration.

When all the three iron sources were tested in the presence of EGCG (Fig. 5.1.4), there was a distinct decline in ferritin concentration, with $FeSO_4$ and Dextrin both exhibiting similar effects upon EGCG contact. Citrus, however, was not significantly affected by EGCG, thereby illustrating its potential to bypass the effects of inhibitors (Fig. 5.1.4B). The NF1 formulation (Dextrin) may have been less stable and could have possibly degraded over time, thus causing the shell to break open upon EGCG contact, releasing its constituents. Secondly, EGCG's interaction with Dextrin may have yielded an insoluble complex with iron (due to surface interaction), which was too large to enter the cell, thus leading to its excretion rather than generating the inhibitory effects of the receptor.

The formulations (Table 2.1.4) were tested with the purpose of increasing iron absorption through the small intestine, particularly in the duodenum. These strategies may also be applied under conditions of iron overload in studies to treat excess iron–

related diseases, including T2DM. They may be used to facilitate the delivery of a particular antioxidant to target pancreatic β-cells. In addition, the selection of nanoformulations needs to be based on the aforementioned requirements in order to successfully deliver an agent of interest into a specific target. The findings of this study suggest that citrus pectin is a suitable shell component for nanoformulations owing to its higher stability in the presence of EGCG. Therefore, pectin nanoformulations containing a particular antioxidant may exhibit a potent therapeutic effect. Such an approach could decrease the prevalence of chronic diseases and their parent nutritional disorders both in developed and developing countries.

CHAPTER 6

Conclusions and Future Directions

6.1. General Discussion

The incidence of type 2 diabetes is steadily increased over the years all around the world, affecting many lives that are at risk of death (Roglic, 2016). Many strategies have developed with a hope that this disease might come to an end. However, it has been projecting to rise even more than it is expected (Roglic, 2016). This thesis comprises of four major objectives: to clarify the role of excessive iron on β-cell function - insulin synthesis and secretion; to correlate excessive iron mediated ROS generation to β-cell dysfunction; to identify whether specific organelles such as mitochondria are more sensitive to ROS damage; to identify the role of antioxidant-nanoformulations as a strategy to counter ROS damage on pancreatic β-cell.

Identifying the effect of excessive iron on the synthesis and secretion of insulin on β-cell was being observed. Excessive iron and glucose contributed to the decrease of insulin secretion and increased its content chronically. In addition, SNAP-25 as one of the important components of the SNARE complex was shown to decrease as well. SNARE complex is a core complex protein that mediates granule fusion and insulin exocytosis from β-cell (Thurmond, 2007). This finding was supported by increasingly high toxicity of pancreatic β-cell. Several other proteins related to iron and β-cell function were also performed. Excessive iron accumulation affected the increase of iron storage protein, known as ferritin. This was also confirmed by an increase of intracellular iron content. This accumulation was also observed on one of the important iron transporters; DMT-1, which was increasingly expressive in pancreatic β-cell, MIN6 cells.

Perturbations caused by oxidative stress have been linked to chronic diseases. T2D has become one of metabolic diseases, which might result from the imbalance between the accumulation of ROS and biological systems that detoxify these reactive products (Pizzino et al., 2017). It has been established that iron is an essential nutrient involved in myriad biological processes, starting from normal function of cells to the energy production (Paul et a., 2017). However, as important as it is, iron contributes to several diseases due to its involvement in reactive products such as hydroxyl radicals. Particularly within pancreatic β-cell, oxidative damage is prone to occur due

to its lack of ability to possess enzymatic antioxidants that can effectively detoxify excessive concentrations of intracellular oxidative stress.

ROS have been established to be found in several locations intracellularly. Mitochondria are considered as the major source of these species within most mammalian cells and are formed as part of natural by-product of the mitochondrial metabolism (Zorov et al., 2014). Membrane potential is the force driving protons into the mitochondria (Perry et al., 2011). The current data suggested that excessive iron accumulation demonstrated decreased levels of mitochondrial membrane potential. The decrease or loss of mitochondrial membrane potential might be an early event in the apoptotic process (Ly et al., 2003). This outcome was supported by an extremely decreased mitochondrial OCR (Chapter 4), which was also observed on factors contributed to OCR include basal respiration, proton leak-linked respiration, ATP-linked respiration, maximal respiration, reserve capacity, and non-mitochondrial. Two reasons might be the cause of the decrease of this effect: the cells might be removed during the washing, or an interference between the positive charge of iron and protons within the matrix across the IMM into IMS.

Excessive iron accumulation mediated ROS generation might correlate to dysfunction of β-cell. As previously mentioned, iron contributes to the generation of the most dangerous free radical, which can attack essential components of the cells. Proteins, lipids, and nucleus are elements within the cells that are susceptible to this particular damage and can proceed to irreversible damages. It has been found that the secondary product of lipid peroxidation; MDA levels, were increased in the presence of high iron (Chapter 3). This data was supported by a result on β-cell cytotoxicity through increased formation of carbonyl groups on protein side chains as a form of cellular damage (Chapter 4).

Due to multiple damages which can be reversible or irreversible, myriad strategies and ideas have been developed. In this current thesis, antioxidant nanoformulation was optimised and observed using potato Dextrin and Modified Citrus Pectin. The experiment was performed on caco-2 cells to identify how effective the antioxidant coated by nanoformulations versus uncoated antioxidants. The current data showed that MCP was more stable and might be more effective in coating antioxidant nanoformulations (Chapter 5). This outcome might be amplified as a model to counter

oxidative stress due to excessive iron accumulation in pancreatic β-cell using pancreatic β-cell line, MIN6 cells.

6.2 Conclusions

The following findings are novel observations that have been observed to conclude this thesis:

- Excessive iron is involved in the higher expression of DMT1 on pancreatic β-cell line, MIN6 cells.
- Excessive iron has increased ferritin and intracellular iron content on MIN6 cells.
- Excessive iron contributes to the decrease of insulin secretion and increased insulin content chronically (24 h incubation).
- Excessive iron contributes to the decreased expression of one of insulin exocytosis machinery, called SNAP-25.
- Excessive iron may have increased β-cell viability.
- Excessive iron is associated with the increase of MDA levels as the result of lipid peroxidation.
- Excessive iron associates to the β-cell cytotoxicity through increased expression of carbonyl group formations on protein side chains as a form of cellular oxidative damage.
- Excessive iron contributes to the decrease of mitochondrial membrane potential levels.
- Excessive iron and glucose displayed opposite effects on OCR levels, which contribute to the decrease of OCR and vice versa, respectively.
- MCP is an effective and stable component of nanoformulations, which coated Hesperetin as an antioxidant to counter oxidative stress.

To summarise, the data presented in this thesis indicate that excessive iron and glucose accumulation, and consequent oxidative stress results in cellular membrane and mitochondrial damage and disruption. The perturbations in mitochondria

functionality correlate with diminishing of MIN6 β-cell insulin secretion, suggesting a mechanistic role for iron overload in the development and progression of type 2 diabetes. All nanocarrier formulations demonstrated high iron entrapment efficiency compared to $FeSO_4$ control and the ability to resist the inhibitory effect of a potent iron inhibitor highlight its potential as an iron delivery vehicle. These nanoformulations may be potentially used as a model to counter oxidative stress in pancreatic β-cell.

6.3 Future directions

Many strategies have emerged with practical applications in diseases caused by the overproduction of free radicals. One of the approaches that has been progressively explored is antioxidant therapeutics. β-cells are highly vulnerable to ROS owing to their low levels of antioxidant enzymes. They can be fortified with novel antioxidant formulations prepared using nanoformulation techniques that encapsulate potent antioxidants (e.g. hesperetin) in novel proteins, polysaccharides, and polymers. Such formulations need to be assessed to determine their stability and activity. Antioxidant activity can be evaluated with and without encapsulation, using the Ferric Reducing Antioxidant Power (FRAP) assay. The Cellular Antioxidant Activity (CAA) assay can also be used to compare the activity of free and encapsulated antioxidants within the cells. These findings can potentially contribute to antioxidant therapeutics for metabolic disorders.

As previously mentioned, proteins are considered to be the most vulnerable targets for oxidative stress; hence, protein identification must be applied in the future in addition to analysing the protein expression levels. This can be carried out using advanced mass spectrometry. Recognizing proteins corresponding to a particular type of cells might be one of the best strategies to achieve a discovery and devise treatments. In addition to analysing protein carbonylation in pancreatic β-cells, the proteins involved in mediating the secretion of insulin, a hormone that regulates blood glucose levels, need to be identified, e.g. proteins in the SNARE core complex and those that mediate insulin exocytosis. Two proteins that make up the SNARE core complex are syntaxin and synaptobrevin; studying them might provide wider insights to determine insulin mechanisms.

It has been established that low or moderate concentrations of ROS play many physiological roles. Investigating their major sources may contribute beneficial information. Studies have indicated that mitochondria are the sites where these species are produced, leading to cellular oxidative damage. It is noteworthy to understand the function of these organelles by isolating them from cells. This can be performed using an established technique called the mitochondria isolation assay. Further investigation on some specific enzymes related to excessive iron and glucose in the insulin secretory system can extend our knowledge on how extracellular iron is accumulated in these sites. Researchers have already identified one such protein, named calpain-10, using the traditional method of western blotting.

The parameters that need to be modified for further investigations on the OCR include the concentrations used for the nanoencapsulated drugs as well as various experimental timelines. Measurements of the oxygen consumption over several time courses using the Seahorse test can confirm the function of this organelle. Studying organelles (such as mitochondria) associated with multiple diseases linked to oxidative stress and the proteins involved in metabolism would contribute to reducing the occurrences of the diabetes mellitus disease. Moreover, the mechanisms of alterations and regulation of different intracellular processes that lead to other events would be important potential therapeutic targets to diminish the complexity of particular diseases. Furthermore, quantifying any consequences resulting from cellular oxidative damage, using confocal microscopy, can enhance our understanding by providing additional evidence.

The optimisation of nanoformulations in this study has provided useful results; nevertheless, additional experiments should be considered to ratify them. If MCPD's ability to bypass the effects of EGCG can be demonstrated, further work can be carried out to identify other forms of inhibitors that this formulation could potentially be resistant to. Moreover, this study could proceed in a human study level as our laboratory team has been working on several human studies related to curcumin. Thus, these collective data combine with antioxidant nanoformulations on human study might be used as a strategy to combat oxidative stress associated myriad diseases.

Appendix (i) – Graphs of flow cytometry result

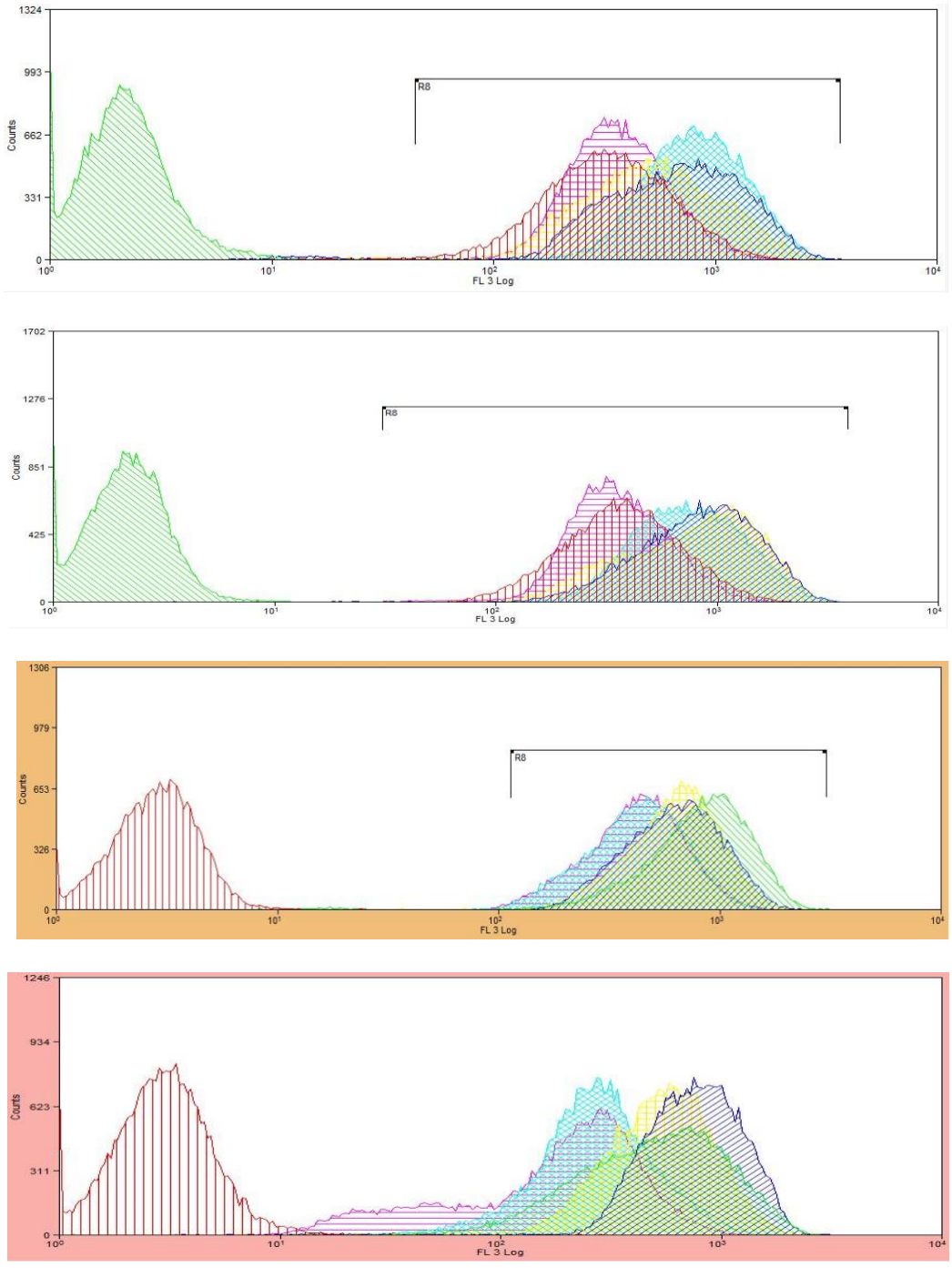

Fig. i. The overlay of all experimental conditions in estimating the changes of mitochondrial membrane potential performed by flow cytometry in four different periods (1, 2, 5, & 6 days) using fluorescent dye called Texas Red, (excitation ideally suited to the 561 or 594 nm laser lines). MIN6 cells were exposed by both iron and glucose present with various range of concentrations. Flow cytometry analysis of mitochondrial membrane potential level in application of median intensity (graphs), 6-well plates; n=3.

The above graph is an overlay looks of all different experimental conditions using a flow cytometry. The aim of this measurement is to estimate the levels of mitochondrial membrane potential on MIN6 cells that were exposed to variety concentrations of iron and glucose within four different incubation times.

Appendix (ii) – Graphs of oxygen consumption rate results

Below graphs are two different experiments on OCR analyses. OCR data on chapter 4 was a cumulative result from these graphs. Iron and glucose exposures on MIN6 cells displayed opposite results on OCR, which was the reason for the experiments to be performed separately.

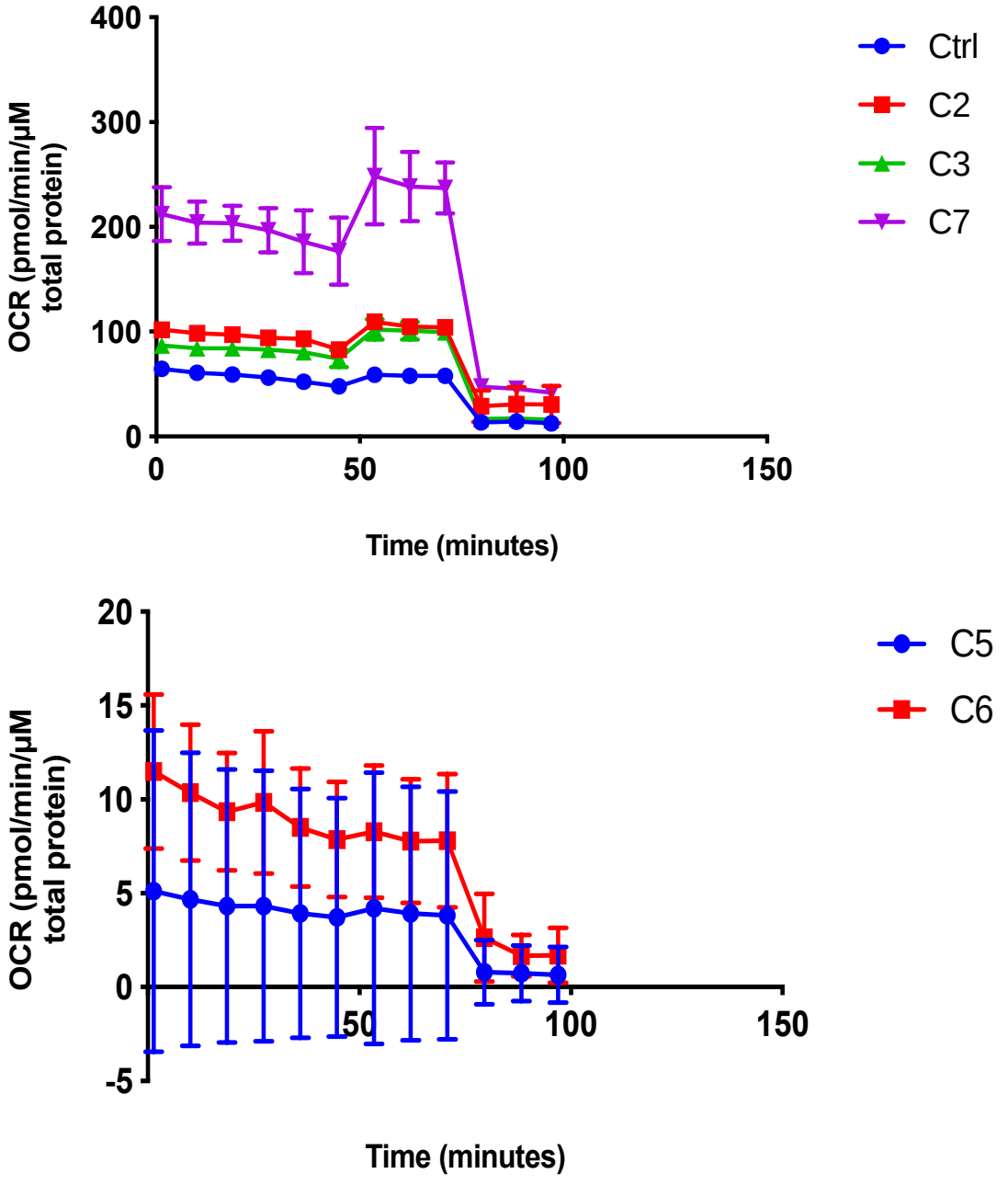

Fig. ii. Oxygen consumption profiles of pancreatic β-cells (MIN6) within a 24-h period in the presence of iron and glucose. Cells were plated at 50 x 10_4 cells/well in XF24 plates. The Seahorse experimental method was used along with the addition of several distinct agents involved in the electron transport chain in mitochondria, including oligomycin, FCCP, antimycin A, and rotenone. (A) OCR in the presence of glucose. (B) OCR in the presence of iron; n=5.

Appendix (iii) – Calculation of protein carbonyl

Prior to the loading of protein (cell lysate) on western blot, the amount of proteins (15 & 10 µg) needs to be calculated obtained from BCA assay.

A Raw Data (562)

	1	2	3	4	5	6	7	8	9	10	11	12
A	0.245	0.266	0.521	0.469	0.296	0.259	1.047	0.407	0.634	0.987	0.388	0.695
B	0.358	0.759	1.083	0.796	2.199	0.573	0.357	0.283	0.238	0.232	0.309	1.545
C	0.24	0.29	0.315	0.287	0.304	0.318	1.396	0.432	0.552	0.52	0.96	1.46
D	0.635	1.352	2.393	2.217	1.583	1.499	2.205	2.058	2.605	2.263	0.044	0.048
E	2.039	1.233	1.949	1.94	2.176	2.232	2.168	2.167	2.33	1.105	0.047	0.047
F	0.583	0.573	0.634	0.613	0.596	0.56	0.643	0.515	0.924	0.637	0.047	0.046
G	0.409	0.409	0.478	0.474	0.458	0.438	0.626	0.627	0.77	0.742	0.046	0.055
H	0.048	0.046	0.047	0.046	0.045	0.044	0.044	0.044	0.045	0.056	0.066	0.046

Fig. iiiA. A raw data of total protein using BCA assay. Absorbance was then measured at 562 nm using a microplate reader (BMG LABTECH, Germany).

B

Oxi
24 h

				y=0.001x + 0.0589		15	10
Ctrl	0.583	0.578	0.5775	518.6	12.965	28.9	19.3
	0.573						
C2	0.634	0.6235	0.623	564.1	14.1025	26.6	17.7
	0.613						
C3	0.596	0.578	0.5775	518.6	12.965	28.9	19.3
	0.56						
C5	0.643	0.579	0.5785	519.6	12.99	28.9	19.2
	0.515						
C6	0.924	0.7805	0.78	721.1	18.0275	20.8	13.9
	0.637						
48 h							
Ctrl	0.409	0.409	0.4085	349.6	8.74	42.9	28.6
	0.409						
C2	0.478	0.476	0.4755	416.6	10.415	36.0	24.0
	0.474						
C3	0.458	0.448	0.4475	388.6	9.715	38.6	25.7
	0.438						
C5	0.626	0.6265	0.626	567.1	14.1775	26.5	17.6
	0.627						
C6	0.77	0.756	0.7555	696.6	17.415	21.5	14.4
	0.742						

Fig. iiiB. Data on the amount of proteins loaded in each well for the purpose of SDS-PAGE analysis.

Appendix (iv) – Bands of protein carbonyl results

After proteins were estimated using BCA assay, the particular amount of proteins was ready to be loaded on the wells of SDS-PAGE chamber. The expression was estimated using a series of experiments, leading to the expression of bands, which could identify the level of protein expressions using image J application, version 1.52.

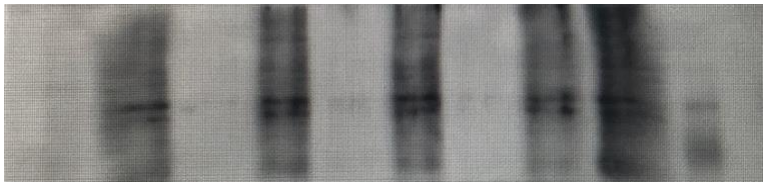

24-h incubation – Mw: 45 kDa

From left to right

Ctrl	165631.533
5.5 mM Glu	156690.395
11 mM Glu	55316.820
20 µM Fe	156674.838
100 µM Fe	8399.801

48-h incubation – Mw: 45 kDa

From left to right

Ctrl	12757.806
Ctrl	17409.492
5.5 mM Glu	23028.049
11 mM Glu	48772.361
20 µM Fe	13059.179
100 µM Fe	48784.432

Fig. iv. The estimation of carbonyl groups on the side chains of proteins was performed using OxyBlot™ Protein Oxidation kits in both 24- and 48-h periods. The protein was extracted and subjected to the western immunoblot technique using 10% agarose gel. The results shown above are: Different bands of protein expression in western blot after (A) 24- and (B) 48-h incubations. (C) Expression of protein oxidation in 24- and 48-h incubation times, demonstrated by the area under the curve (AUC). Gel loading was as follows (from top left): lane 1 - ctrl, lane 2 - negative ctrl of ctrl, lane 3 – normal glucose (C1), lane 4 - high glucose (C2), lane 5 - normal iron (C3), lane 6 - high iron (C4), lane 7 – neg ctrl of C1, lane 8 – neg ctrl of C2, lane 9 – neg ctrl of C3, lane 10 – neg ctrl of C4. (From bottom left): lane 1 - ctrl, lane 2 – C1, lane 3 - neg ctrl of C1, lane 4 – C2, lane 5 - neg ctrl of C2, lane 6 – C3, lane 7 - neg ctrl of C3, lane 8 – C4. The data represent mean ± SEM; n=3.

Appendix (v) – Data of cytotoxicity assessment

Below data were an example of how viability of cells was obtained and calculated. Firstly, raw data was obtained from a spectrophotometry, producing absorbance. The absorbance was calculated to find the level of MIN6 cytotoxicity due to exposure of iron and glucose within particular time incubations.

A

1. Raw Data (570 1)

	1	**2**	**3**	**4**
A	0.311	0.297	0.294	0.335
B	0.3	0.349	0.295	0.279
C	0.295	0.287	0.271	0.288

1. Raw Data (570 1)

	1	2	3	4
A	0.238	0.29	0.285	0.326
B	0.297	0.277	0.308	0.322
C	0.22	0.24	0.35	0.301

2. Raw Data (600 2)

	1	**2**	**3**	**4**
A	0.388	0.379	0.359	0.399
B	0.369	0.411	0.379	0.362
C	0.377	0.37	0.349	0.368

2. Raw Data (600 2)

	1	2	3	4
A	0.278	0.346	0.34	0.384
B	0.339	0.33	0.37	0.383
C	0.281	0.312	0.421	0.374

Fig. vA. A raw data of cytotoxicity assay using PrestoBlue® cell viability reagent. Absorbance was then measured at 560-590 nm using a microplate reader (BMG LABTECH, Germany).

A	570	600	O2*A1	O1*A2	R1*N2	R2*N1	G-H	I-J	K/L*100%
C1	0.311	0.388	36454.18	31267.37	65540.02	5128.2	5186.808	60411.82	85.86
	0.297	0.379	34813.15	30542.09	65540.02	5128.2	4271.058	60411.82	70.70
C2	0.294	0.359	34461.5	28930.37	65540.02	5128.2	5531.13	60411.82	91.56
	0.335	0.399	39267.36	32153.81	65540.02	5128.2	7113.546	60411.82	117.75
C3	0.3	0.369	35164.8	29736.23	65540.02	5128.2	5428.566	60411.82	89.86
	0.349	0.411	40908.38	33120.85	65540.02	5128.2	7787.538	60411.82	128.91
C4	0.295	0.379	34578.72	30542.09	65540.02	5128.2	4036.626	60411.82	66.82
	0.279	0.362	32703.26	29172.13	65540.02	5128.2	3531.132	60411.82	58.45
C5	0.295	0.377	34578.72	30380.92	65540.02	5128.2	4197.798	60411.82	69.49
	0.287	0.377	33640.99	29816.82	65540.02	5128.2	3824.172	60411.82	63.30
C6	0.271	0.349	31765.54	28124.51	65540.02	5128.2	3641.022	60411.82	60.27
	0.288	0.368	33758.21	29655.65	65540.02	5128.2	4102.56	60411.82	67.91
C7	0.238	0.278	27897.41	22402.91	65540.02	5128.2	5494.5	60411.82	90.95
	0.296	0.346	33992.64	27882.76	65540.02	5128.2	6109.884	60411.82	101.14
C8	0.285	0.345	33406.56	27399.24	65540.02	5128.2	6007.32	60411.82	99.44
	0.326	0.384	38212.42	30945.02	65540.02	5128.2	7267.392	60411.82	120.30
C9	0.297	0.339	34813.15	27318.65	65540.02	5128.2	7494.498	60411.82	124.06
	0.277	0.335	32468.83	26593.38	65540.02	5128.2	5875.452	60411.82	97.26
C10	0.308	0.378	36102.53	29816.82	65540.02	5128.2	6285.708	60411.82	104.05
	0.322	0.383	37743.55	30864.44	65540.02	5128.2	6879.114	60411.82	113.87

Fig. vB. Data on the calculations of cytotoxicity levels on MIN6 cells exposed to different levels of iron and glucose.

References

1. Abeti, R., Parkinson, M. H., Hargreaves, I. P., Angelova, P. R., Sandi, C., Pook, M. A., ... & Abramov, A. Y. (2017). 'Mitochondrial energy imbalance and lipid peroxidation cause cell death in Friedreich's ataxia'. *Cell death & disease*, *7*(5), e2237.
2. Adrian, T. E., Bloom, S. R., Hermansen, K., & Iversen, J. (1978). Pancreatic polypeptide, glucagon and insulin secretion from the isolated perfused canine pancreas. *Diabetologia*, *14*(6), 413-417.
3. AHRÉN, B., & TABORSKY JR, G. J. (1986). The mechanism of vagal nerve stimulation of glucagon and insulin secretion in the dog. *Endocrinology*, *118*(4), 1551-1557.
4. Aisen, P. (2004). Transferrin receptor 1. *The international journal of biochemistry & cell biology*, *36*(11), 2137-2143.
5. Alberti, K. G. M. M., & Zimmet, P. Z. (1998). Definition, diagnosis and classification of diabetes mellitus and its complications. Part 1: diagnosis and classification of diabetes mellitus. Provisional report of a WHO consultation. *Diabetic medicine*, *15*(7), 539-553.
6. Algren, D. A. (2010). Review of oral iron chelators (deferiprone and deferasirox) for the treatment of iron overload in pediatric patients. *World Health Organization [on line]*, 1-22.
7. Ames, B. N., Shigenaga, M. K., & Hagen, T. M. (1993). Oxidants, antioxidants, and the degenerative diseases of aging. *Proceedings of the National Academy of Sciences*, *90*(17), 7915-7922.
8. Andrews, N. C. (1999). Disorders of iron metabolism. *New England Journal of Medicine*, *341*(26), 1986-1995.
9. Andrews NC, Schmidt PJ. (2007). Iron Homeostasis. *Rev. Physiol*; 69: 69-85.
10. Araki, S., Tamori, Y., Kawanishi, M., Shinoda, H., Masugi, J., Mori, H., ... & Kasuga, M. (1997). Inhibition of the binding of SNAP-23 to syntaxin 4 by Munc18c. *Biochemical and biophysical research communications*, *234*(1), 257-262.
11. Aregbesola, A. O., Voutilainen, S., Virtanen, J. K., Mursu, J., & Tuomainen, T. P. (2013). Body iron stores and the risk of type 2 diabetes in middle-aged men. *European journal of endocrinology*, EJE-13.
12. Arora, S., & Kapoor, R. K. (2012). Iron Metabolism in Humans: An Overview. In *Iron Metabolism*. InTech.Buetler TM, Krauskopf A, Ruegg UT. (2004). Role of Superoxide as a Signaling Molecule. *News Physiol Sci*; 19: 120–123.
13. Aumelas, A., Serrero, A., Durand, A., Dellacherie, E., & Leonard, M. (2007). Nanoparticles of hydrophobically modified dextrans as potential drug carrier systems. *Colloids and Surfaces B: Biointerfaces*, *59*(1), 74-80.
14. Aziz, N., & Munro, H. N. (1987). Iron regulates ferritin mRNA translation through a segment of its 5'untranslated region. *Proceedings of the National Academy of Sciences*, *84*(23), 8478-8482.

15. Backe, M. B., Moen, I. W., Ellervik, C., Hansen, J. B., & Mandrup-Poulsen, T. (2016). Iron regulation of pancreatic beta-cell functions and oxidative stress. *Annual review of nutrition*, *36*, 241-273.
16. Barker, C. J., & Berggren, P. O. (2013). New horizons in cellular regulation by inositol polyphosphates: Insights from the pancreatic β-cell. *Pharmacological reviews*, *65*(2), 641-669.
17. Barnes, T. M., & Hodgkin, J. (1996). The tra-3 sex determination gene of Caenorhabditis elegans encodes a member of the calpain regulatory protease family. *The EMBO journal*, *15*(17), 4477-4484.
18. Bayrhuber, M., Meins, T., Habeck, M., Becker, S., Giller, K., Villinger, S., ... & Zeth, K. (2008). Structure of the human voltage-dependent anion channel. *Proceedings of the National Academy of Sciences*, *105*(40), 15370-15375.
19. Beinert, H. E. L. M. U. T., & Kennedy, M. C. (1993). Aconitase, a two-faced protein: enzyme and iron regulatory factor. *The FASEB journal*, *7*(15), 1442-1449.
20. Betteridge, D. J. (2000). What is oxidative stress?. *Metabolism*, *49*(2), 3-8.
21. Bratanova-Tochkova, T. K., Cheng, H., Daniel, S., Gunawardana, S., Liu, Y. J., Mulvaney-Musa, J., ... & Sharp, G. W. (2002). Triggering and augmentation mechanisms, granule pools, and biphasic insulin secretion. *Diabetes*, *51*(suppl 1), S83-S90.
22. Braulke, T., & Bonifacino, J. S. (2009). Sorting of lysosomal proteins. *Biochimica et Biophysica Acta (BBA)-Molecular Cell Research*, *1793*(4), 605-614.
23. Breuer, W., Shvartsman, M., & Cabantchik, Z. I. (2008). Intracellular labile iron. *The international journal of biochemistry & cell biology*, *40*(3), 350-354.
24. Brown, J. C., Mutt, V., & Pederson, R. A. (1970). Further purification of a polypeptide demonstrating enterogastrone activity. *The Journal of physiology*, *209*(1), 57-64.
25. Brownlee, M. (2005). The pathobiology of diabetic complications. *Diabetes*, *54*(6), 1615-1625.
26. Cabreiro, F., Picot, C. R., Friguet, B., & Petropoulos, I. (2006). Methionine sulfoxide reductases: relevance to aging and protection against oxidative stress. *Annals of the New York Academy of Sciences*, *1067*(1), 37-44.
27. Cairo, G., & Recalcati, S. (2007). Iron-regulatory proteins: molecular biology and pathophysiological implications. *Expert reviews in molecular medicine*, *9*(33), 1-13.
28. Canonne-Hergaux, F., Zhang, A. S., Ponka, P., & Gros, P. (2001). Characterization of the iron transporter DMT1 (NRAMP2/DCT1) in red blood cells of normal and anemic mk/mkmice. *Blood*, *98*(13), 3823-3830.
29. Carr, R. D., Larsen, M. O., Winzell, M. S., Jelic, K., Lindgren, O., Deacon, C. F., & Ahrén, B. (2008). Incretin and islet hormonal responses to fat and protein ingestion in healthy men. *American Journal of Physiology-Endocrinology and Metabolism*, *295*(4), E779-E784.

30. Cejvanovic, V., Asferg, C., Kjær, L. K., Andersen, U. B., Linneberg, A., Frystyk, J., ... & Jeppesen, J. (2016). Markers of oxidative stress in obese men with and without hypertension. *Scandinavian journal of clinical and laboratory investigation*, *76*(8), 620-625.
31. Chacko, B. K., Kramer, P. A., Ravi, S., Benavides, G. A., Mitchell, T., Dranka, B. P., ... & Hardy, R. W. (2014). The Bioenergetic Health Index: a new concept in mitochondrial translational research. *Clinical science*, *127*(6), 367-373.
32. Chen, Y. A., & Scheller, R. H. (2001). SNARE-mediated membrane fusion. *Nature reviews Molecular cell biology*, *2*(2), 98.
33. Cheng, K., Delghingaro-Augusto, V., Nolan, C. J., Turner, N., Hallahan, N., Andrikopoulos, S., & Gunton, J. E. (2012). High passage MIN6 cells have impaired insulin secretion with impaired glucose and lipid oxidation. *PloS one*, *7*(7), e40868.
34. Cheng, Zhiyong, and Michael Ristow. "Mitochondria and metabolic homeostasis." (2013): 240-242.
35. Cheung, C. L., Cheung, T. T., Lam, K. S., & Cheung, B. M. (2013). High ferritin and low transferrin saturation are associated with pre-diabetes among a national representative sample of US adults. *Clinical nutrition*, *32*(6), 1055-1060.
36. Choi, S. W., Gerencser, A. A., & Nicholls, D. G. (2009). Bioenergetic analysis of isolated cerebrocortical nerve terminals on a microgram scale: spare respiratory capacity and stochastic mitochondrial failure. *Journal of neurochemistry*, *109*(4), 1179-1191.
37. Cooksey, R. C., Jouihan, H. A., Ajioka, R. S., Hazel, M. W., Jones, D. L., Kushner, J. P., & McClain, D. A. (2004). Oxidative stress, β-cell apoptosis, and decreased insulin secretory capacity in mouse models of hemochromatosis. *Endocrinology*, *145*(11), 5305-5312.
38. Curry, D. L., Bennett, L. L., & Grodsky, G. M. (1968). Dynamics of insulin secretion by the perfused rat pancreas. *Endocrinology*, *83*(3), 572-584.
39. Dalle-Donne, I., Rossi, R., Giustarini, D., Milzani, A., & Colombo, R. (2003). Protein carbonyl groups as biomarkers of oxidative stress. *Clinica chimica acta*, *329*(1-2), 23-38.
40. Dalle-Donne, I., Scaloni, A., Giustarini, D., Cavarra, E., Tell, G., Lungarella, G., ... & Milzani, A. (2005). Proteins as biomarkers of oxidative/nitrosative stress in diseases: the contribution of redox proteomics. *Mass spectrometry reviews*, *24*(1), 55-99.
41. Davies, M. J. (1997). Radical-mediated protein oxidation. *" The pathology of protein oxidation"*, 207-218.
42. Davies, M. J. (2016). Protein oxidation and peroxidation. *Biochemical Journal*, *473*(7), 805-825.
43. De Domenico, I., Ward, D. M., & Kaplan, J. (2007). Hepcidin regulation: ironing out the details. *Journal of Clinical Investigation*,*117*(7), 1755. De Domenico, I., Ward, D. M., & Kaplan, J. (2007). Hepcidin regulation: ironing out the details. *Journal of Clinical Investigation*,*117*(7), 1755.

44. Deacon, C. F., Johnsen, A. H., & Holst, J. J. (1995). Degradation of glucagon-like peptide-1 by human plasma in vitro yields an N-terminally truncated peptide that is a major endogenous metabolite in vivo. *The Journal of Clinical Endocrinology & Metabolism*, *80*(3), 952-957.
45. Devasagayam, T. P. A., Boloor, K. K., & Ramasarma, T. (2003). Methods for estimating lipid peroxidation: an analysis of merits and demerits. *Indian journal of biochemistry & biophysics*, *40*(5), 300-308.
46. Diabetes UK. (2019). Type 2 Diabetes. https://www.diabetes.co.uk/type2-diabetes.html
47. Dillon, J. S., Tanizawa, Y., Wheeler, M. B., Leng, X. H., Ligon, B. B., Rabin, D. U., ... & Boyd 3rd, A. E. (1993). Cloning and functional expression of the human glucagon-like peptide-1 (GLP-1) receptor. *Endocrinology*, *133*(4), 1907-1910.
48. Divakaruni, A. S., & Brand, M. D. (2011). The regulation and physiology of mitochondrial proton leak. *Physiology*, *26*(3), 192-205.
49. Divakaruni, A. S., Paradyse, A., Ferrick, D. A., Murphy, A. N., & Jastroch, M. (2014). Analysis and interpretation of microplate-based oxygen consumption and pH data. In *Methods in enzymology* (Vol. 547, pp. 309-354). Academic Press.
50. Dodson, G., & Steiner, D. (1998). The role of assembly in insulin's biosynthesis. *Current opinion in structural biology*, *8*(2), 189-194.
51. Dranka, B. P., Benavides, G. A., Diers, A. R., Giordano, S., Zelickson, B. R., Reily, C., ... & Landar, A. (2011). Assessing bioenergetic function in response to oxidative stress by metabolic profiling. *Free Radical Biology and Medicine*, *51*(9), 1621-1635.
52. Dranka, B. P., Hill, B. G., & Darley-Usmar, V. M. (2010). Mitochondrial reserve capacity in endothelial cells: The impact of nitric oxide and reactive oxygen species. *Free Radical Biology and Medicine*, *48*(7), 905-914.
53. Dröge, W. (2002). Free radicals in the physiological control of cell function. *Physiological reviews*, *82*(1), 47-95.
54. Dunlop, R. A., Brunk, U. T., & Rodgers, K. J. (2009). Oxidized proteins: mechanisms of removal and consequences of accumulation. *IUBMB life*, *61*(5), 522-527.
55. Dunn, L. L., Rahmanto, Y. S., & Richardson, D. R. (2007). Iron uptake and metabolism in the new millennium. *Trends in cell biology*, *17*(2), 93-100.
56. Emori, Y., Kawasaki, H., Sugihara, H., Imajoh, S., Kawashima, S., & Suzuki, K. (1986). Isolation and sequence analyses of cDNA clones for the large subunits of two isozymes of rabbit calcium-dependent protease. *Journal of Biological Chemistry*, *261*(20), 9465-9471.
57. Erion, K. A., Ferrante, T., Corkey, B., & Deeney, J. (2013). Iron stimulates insulin secretion in clonal pancreatic β-cells and dissociated rat islets. *The FASEB Journal*, *27*(1 Supplement), 1010-13.
58. Evan, G. I., & Vousden, K. H. (2001). Proliferation, cell cycle and apoptosis in cancer. *Nature*, *411*(6835), 342.

59. Facchini, F. S. (1998). Effect of phlebotomy on plasma glucose and insulin concentrations. *Diabetes care*, *21*(12), 2190-2190.
60. Fairweather-Tait, S. J. (2004). Iron nutrition in the UK: getting the balance right. *Proceedings of the Nutrition Society*, *63*(4), 519-528.
61. Fedtke, N., Boucheron, J. A.,, Walker, V. E., & Swenberg, J. A. (1990). Vinyl chloride-induced DNA adducts. 2. Formation and persistence of 7-2'-oxoethylguanine and n2,3-ethenoguanine in rat-tissue DNA. *Carcinogenesis, 11*, 1287-1292.
62. Fehmann, H. C., Goke, R., & Goke, B. (1995). Cell and molecular biology of the incretin hormones glucagon-like peptide-I and glucose-dependent insulin releasing polypeptide. *Endocrine reviews*, *16*(3), 390-410.
63. Fink, S. L., & Cookson, B. T. (2005). Apoptosis, pyroptosis, and necrosis: mechanistic description of dead and dying eukaryotic cells. *Infection and immunity*, *73*(4), 1907-1916.
64. Fink, S. P., Reddy, G. R., & Marnett,. L. J. (1997). Mutagenicity in *Escherichia coli* of the major DNA adduct derived from the endogenous mutagen malondialdehyde. *Proc. Natl. Acad. Sci. U.S.A., 94*, 8652-8657.
65. Finkel, T. (2003). Oxidant signals and oxidative stress. *Current opinion in cell biology*, *15*(2), 247-254.
66. Fleming, M. D., Su, M. A., Foernzler, D., Beier, D. R., Dietrich, W. F., & Andrews, N. C. (1997). Microcytic anaemia mice have a mutation in Nramp2, a candidate iron transporter gene. *Nature genetics*, *16*(4), 383-386.
67. Ford, E. S., & Cogswell, M. E. (1999). Diabetes and serum ferritin concentration among US adults. *Diabetes care*, *22*(12), 1978-1983.
68. Forman, H. J., & Azzi, A. (1997). On the virtual existence of superoxide anions in mitochondria: thoughts regarding its role in pathophysiology. *The FASEB Journal, 11*(5), 374-375.
69. Frank, J. (1832). Classis V, Ordo I. *Genus II. De Curandis Hominum Morbis*.
70. Frohnert, B. I., & Bernlohr, D. A. (2013). Protein carbonylation, mitochondrial dysfunction, and insulin resistance. *Advances in nutrition*, *4*(2), 157-163.
71. Ganz, T. (2003). Hepcidin, a key regulator of iron metabolism and mediator of anemia of inflammation. *Blood*, *102*(3), 783-788.
72. Ganz, T., & Nemeth, E. (2006). Iron imports. IV. Hepcidin and regulation of body iron metabolism. *American Journal of Physiology-Gastrointestinal and Liver Physiology*, *290*(2), G199-G203.
73. Ganz, T., & Nemeth, E. (2012). Hepcidin and iron homeostasis.*Biochimica et Biophysica Acta (BBA)-Molecular Cell Research*,*1823*(9), 1434-1443.
74. Gao, X., Campian, J. L., Qian, M., Sun, X. F., & Eaton, J. W. (2009). Mitochondrial DNA damage in iron overload. *Journal of Biological Chemistry*, *284*(8), 4767-4775.
75. Giniatullin, A. R., Darios, F., Shakirzyanova, A., Davletov, B., & Giniatullin, R. (2006). SNAP25 is a pre-synaptic target for the depressant action of reactive oxygen species on transmitter release. *Journal of neurochemistry*, *98*(6), 1789-1797.

76. Gremlich, S., Porret, A., Cherif, D., Vionnet, N., Froguel, P., & Thorens, B. (1995). Cloning, functional expression, and chromosomal localization of the human pancreatic islet glucose-dependent insulinotropic polypeptide receptor. *Diabetes*, *44*(10), 1202-1208.
77. Grodsky, G. M. (2000). Kinetics of insulin secretion: underlying metabolic events in diabetes mellitus. *Diabetes Mellitus: A Fundamental and Clinical Text. LeRoith D, Taylor SI, Olefsky JM, Eds. Philadelphia, Lippicott Williams & Wilkins*, 2-11.
78. Guerra, D. D., & Callis, J. (2012). Ubiquitin on the move: the ubiquitin modification system plays diverse roles in the regulation of endoplasmic reticulum-and plasma membrane-localized proteins. *Plant physiology*, *160*(1), 56-64.
79. Gunshin, H., Mackenzie, B., Berger, U. V., Gunshin, Y., Romero, M. F., Boron, W. F., … & Hediger, M. A. (1997). Cloning and characterisation of a mammalian prton-coupled metal ion-transporter. *Nature*, *388*(6641), 482.
80. Gutteridge, J. M. (1995). Lipid peroxidation and antioxidants as biomarkers of tissue damage. *Clinical chemistry*, *41*(12), 1819-1828.
81. Halliwell, B. (1993). The role of oxygen radicals in human disease, with particular reference to the vascular system. *Pathophysiology of Haemostasis and Thrombosis*, *23*(Suppl. 1), 118-126.
82. Hansen, A. M. K., Bödvarsdottir, T. B., Nordestgaard, D. N. E., Heller, R. S., Gotfredsen, C. F., Maedler, K., ... & Karlsen, A. E. (2011). Upregulation of alpha cell glucagon-like peptide 1 (GLP-1) in Psammomys obesus—an adaptive response to hyperglycaemia?. *Diabetologia*, *54*(6), 1379-1387.
83. Hansen, J. B., Moen, I. W., & Mandrup-Poulsen, T. (2014). Iron: the hard player in diabetes pathophysiology. *Acta Physiologica*,*210*(4), 717-732.
84. Havel, P. J., Akpan, J. O., Curry, D. L., Stern, J. S., Gingerich, R. L., & Ahren, B. (1993). Autonomic control of pancreatic polypeptide and glucagon secretion during neuroglucopenia and hypoglycemia in mice. *American Journal of Physiology-Regulatory, Integrative and Comparative Physiology*, *265*(1), R246-R254.
85. Hentze, M. W., & Kühn, L. C. (1996). Molecular control of vertebrate iron metabolism: mRNA-based regulatory circuits operated by iron, nitric oxide, and oxidative stress. *Proceedings of the National Academy of Sciences*, *93*(16), 8175-8182.
86. Hibino, H., Inanobe, A., Furutani, K., Murakami, S., Findlay, I. A. N., & Kurachi, Y. (2010). Inwardly rectifying potassium channels: their structure, function, and physiological roles. *Physiological reviews*, *90*(1), 291-366.
87. Holz, G. G. (2004). Epac: a new cAMP-binding protein in support of glucagon-like peptide-1 receptor-mediated signal transduction in the pancreatic β-cell. *Diabetes*, *53*(1), 5-13.
88. Hopkins Medicine. 2001. Retrieved from https://www.hopkinsmedicine.org/gastroenterology_hepatology/_pdfs/liver/hemochromatosis.pdf.

89. Huang, S., & Czech, M. P. (2007). The GLUT4 glucose transporter. *Cell metabolism*, *5*(4), 237-252.
90. Hudson, D. M., Curtis, S. B., Smith, V. C., Griffiths, T. A., Wong, A. Y., Scudamore, C. H., ... & MacGillivray, R. T. (2010). Human hephaestin expression is not limited to enterocytes of the gastrointestinal tract but is also found in the antrum, the enteric nervous system, and pancreatic β-cells. *American Journal of Physiology-Gastrointestinal and Liver Physiology*, *298*(3), G425-G432.
91. Hutton, J. C., & Malaisse, W. J. (1980). Dynamics of O 2 consumption in rat pancreatic islets. *Diabetologia*, *18*(5), 395-405.
92. Ikeda, Y., Suehiro, T., Yamanaka, S., Kumon, Y., Takata, H., Inada, S., ... & Hashimoto, K. (2006). Association between serum ferritin and circulating oxidized low-density lipoprotein levels in patients with type 2 diabetes. *Endocrine journal*, *53*(5), 665-670.
93. International Diabetes Federation. IDF Diabetes Atlas, 6th edn. (2017). http://www.idf.org/diabetesatlas.
94. Iron disorders institute. 2009. Retrieved from http://www.irondisorders.org/iron-overload.
95. Ishihara, H., Asano, T., Tsukuda, K., Katagiri, H., Inukai, K., Anai, M., ... & Oka, Y. (1993). Pancreatic β-cells line MIN6 exhibits characteristics of glucose metabolism and glucose-stimulated insulin secretion similar to those of normal islets. *Diabetologia*, *36*(11), 1139-1145.
96. Ito, H., Kurokawa, H., Hirayama, A., Indo, H. P., Majima, H. J., & Matsui, H. (2017). Cancer cell-specific mitochondrial reactive oxygen species promote non-heme iron uptake and enhance the proliferation of gastric epithelial cancer cell. *Journal of clinical biochemistry and nutrition*, *61*(3), 183-188.
97. Jahn, R., & Scheller, R. H. (2006). SNAREs—engines for membrane fusion. *Nature reviews Molecular cell biology*, *7*(9), 631.
98. Jain D. Endocrine pancreas. PathologyOutlines.com website. http://www.pathologyoutlines.com/topic/pancreasendocrine.html. Accessed January 6th, 2020.
99. Janbon, M., Chaptal, J., Vedel, A., & Schaap, J. (1942). Accidents hypoglycémiques graves par un sulfamidothiodiazol (le VK 57 ou 2254 RP). *Montpellier med*, *441*, 21-22.
100. Jewell, J. L., Oh, E., & Thurmond, D. C. (2010). Exocytosis mechanisms underlying insulin release and glucose uptake: conserved roles for Munc18c and syntaxin 4. *American Journal of Physiology-Regulatory, Integrative and Comparative Physiology*, *298*(3), R517-R531.
101. Ježek, P., & Hlavatá, L. (2005). Mitochondria in homeostasis of reactive oxygen species in cell, tissues, and organism. *The international journal of biochemistry & cell biology*, *37*(12), 2478-2503.
102. Jiang, R., Manson, J. E., Meigs, J. B., Ma, J., Rifai, N., & Hu, F. B. (2004). Body iron stores in relation to risk of type 2 diabetes in apparently healthy women. *Jama*, *291*(6), 711-717.

103. Jonkers, J., Meuwissen, R., van der Gulden, H., Peterse, H., van der Valk, M., & Berns, A. (2001). Synergistic tumor suppressor activity of BRCA2 and p53 in a conditional mouse model for breast cancer. *Nature genetics*, *29*(4), 418.
104. Jun, H. S., Bae, H. Y., Lee, B. R., Koh, K. S., Kim, Y. S., Lee, K. W., ... & Yoon, J. W. (1999). Pathogenesis of non-insulin-dependent (type II) diabetes mellitus (NIDDM)–genetic predisposition and metabolic abnormalities. *Advanced drug delivery reviews*, *35*(2), 157-177.
105. Kadenbach, B. (2003). Intrinsic and extrinsic uncoupling of oxidative phosphorylation. *Biochimica et Biophysica Acta (BBA)-Bioenergetics*, *1604*(2), 77-94.
106. Kahn, S. E., Cooper, M. E., & Del Prato, S. (2014). Pathophysiology and treatment of type 2 diabetes: perspectives on the past, present, and future. *The Lancet*, *383*(9922), 1068-1083.
107. Kajimoto, Y., & Kaneto, H. (2004). Role of Oxidative Stress in Pancreatic β-Cell Dysfunction. *Annals of the New York Academy of Sciences*, *1011*(1), 168-176.
108. Kalra, S., Zargar, A. H., Jain, S. M., Sethi, B., Chowdhury, S., Singh, A. K., ... & Malve, H. (2016). Diabetes insipidus: The other diabetes. *Indian journal of endocrinology and metabolism*, *20*(1), 9.
109. Kasuga, M. (2006). Insulin resistance and pancreatic β cell failure. *The Journal of clinical investigation*, *116*(7), 1756-1760.
110. Keating, D. J. (2008). Mitochondrial dysfunction, oxidative stress, regulation of exocytosis and their relevance to neurodegenerative diseases. *Journal of neurochemistry*, *104*(2), 298-305.
111. Kehrer, J. P. (2000). The Haber–Weiss reaction and mechanisms of toxicity. *Toxicology*, *149*(1), 43-50.
112. Kim, S., & Kim, H. (2018). Inhibitory Effect of Astaxanthin on Oxidative Stress-Induced Mitochondrial Dysfunction-A Mini-Review. *Nutrients*, *10*(9), 1137.
113. Kimball, C. P., & Murlin, J. R. (1923). Aqueous extracts of pancreas III. Some precipitation reactions of insulin. *Journal of Biological Chemistry*, *58*(1), 337-346.
114. Koch, R. O., Zoller, H., Theuri, I., Obrist, P., Egg, G., Strohmayer, W., ... & Weiss, G. (2003). Distribution of DMT 1 within the human glandular system. *Histology and histopathology*, *18*(4), 1095-1101.
115. Koeslag, J. H., Saunders, P. T., & Terblanche, E. (2003). A reappraisal of blood glucose homeostat which complrehensively explains the type 2 diabetes mellitus-syndrome X complex. *The Journal of Physiology, 549*(2), 333-346.
116. Komatsu, M., Takei, M., Ishii, H., & Sato, Y. (2013). Glucose-stimulated insulin secretion: A newer perspective. *Journal of diabetes investigation*, *4*(6), 511-516.

117. Kramer, P. A., Ravi, S., Chacko, B., Johnson, M. S., & Darley-Usmar, V. M. (2014). A review of the mitochondrial and glycolytic metabolism in human platelets and leukocytes: implications for their use as bioenergetic biomarkers. *Redox biology*, *2*, 206-210.
118. Lane, D. J. R., Merlot, A. M., Huang, M. H., Bae, D. H., Jansson, P. J., Sahni, S., ... & Richardson, D. R. (2015). Cellular iron uptake, trafficking and metabolism: key molecules and mechanisms and their roles in disease. *Biochimica et Biophysica Acta (BBA)-Molecular Cell Research*, *1853*(5), 1130-1144.
119. Lasocki, S., Gaillard, T., & Rineau, E. (2014). Iron is essential for living!. *Critical Care*, *18*(6), 678.
120. Lawlor, N., George, J., Bolisetty, M., Kursawe, R., Sun, L., Sivakamasundari, V., ... & Stitzel, M. L. (2017). Single-cell transcriptomes identify human islet cell signatures and reveal cell-type–specific expression changes in type 2 diabetes. *Genome research*, *27*(2), 208-222.
121. Lees, J. A., Messa, M., Sun, E. W., Wheeler, H., Torta, F., Wenk, M. R., ... & Reinisch, K. M. (2017). Lipid transport by TMEM24 at ER–plasma membrane contacts regulates pulsatile insulin secretion. *Science*, *355*(6326), eaah6171.
122. Lenzen, S. (2008). Oxidative stress: the vulnerable β-cell.
123. Levine, M., Rumsey, S. C., Daruwala, R., Park, J. B., & Wang, Y. (1999). Criteria and recommendations for vitamin C intake. *Jama*, *281*(15), 1415-1423.
124. Liebler, D. C. (2007). Protein damage by reactive electrophiles: targets and consequences. *Chemical research in toxicology*, *21*(1), 117-128.
125. Lill, R., & Mühlenhoff, U. (2006). Iron-sulfur protein biogenesis in eukaryotes: components and mechanisms. *Annu. Rev. Cell Dev. Biol.*, *22*, 457-486.
126. Liu, Y., Fiskum, G., & Schubert, D. (2002). Generation of reactive oxygen species by the mitochondrial electron transport chain.*Journal of neurochemistry*, *80*(5), 780-787.
127. Longnecker, D. (2014). Anatomy and histology of the pancreas. *Pancreapedia: Exocrine Pancreas Knowledge Base*, DOI: 10.3998/panc.2014.3
128. Ly, J. D., Grubb, D. R., & Lawen, A. (2003). The mitochondrial membrane potential (Δψm) in apoptosis; an update. *Apoptosis*, *8*(2), 115-128.
129. Ma, H., Fukiage, C., Kim, Y. H., Duncan, M. K., Reed, N. A., Shih, M., ... & Shearer, T. R. (2001). Characterization and expression of calpain 10 a novel ubiquitous calpain with nuclear localization. *Journal of Biological Chemistry*, *276*(30), 28525-28531.
130. Ma, Z. A., Zhao, Z., & Turk, J. (2011). Mitochondrial dysfunction and β-cell failure in type 2 diabetes mellitus. *Experimental diabetes research*, *2012*.
131. MacDonald, P. E., Wang, G., Tsuk, S., Dodo, C., Kang, Y., Tang, L., ... & Lotan, I. (2002). Synaptosome-associated protein of 25 kilodaltons modulates Kv2. 1 voltage-dependent K+ channels in neuroendocrine islet β-

cells through an interaction with the channel N terminus. *Molecular endocrinology*, *16*(11), 2452-2461.

132. Machado, V. M., Morte, M. I., Carreira, B. P., Azevedo, M. M., Takano, J., Iwata, N., ... & Araújo, I. M. (2015). Involvement of calpains in adult neurogenesis: implications for stroke. *Frontiers in Cellular Neuroscience*, *9*, 22.
133. Maechler, P. (2013). Mitochondrial function and insulin secretion. *Molecular and cellular endocrinology*, *379*(1), 12-18.
134. Malaisse, W. J. (1992). Insulin biosynthesis and secretion in vitro. *International Textbook of Diabetes Mellitus. KGMM Alberti, editor. John Wiley & Sons, Inc., New York*
135. Malmgren, S., Nicholls, D. G., Taneera, J., Bacos, K., Koeck, T., Tamaddon, A., ... & Sharoyko, V. V. (2009). Tight coupling between glucose and mitochondrial metabolism in clonal beta-cells is required for robust insulin secretion. *Journal of Biological Chemistry*, jbc-M109.
136. Marchetti, P., Lupi, R., Bugliani, M., Kirkpatrick, C. L., Sebastiani, G., Grieco, F. A., ... & Boggi, U. (2012). A local glucagon-like peptide 1 (GLP-1) system in human pancreatic islets. *Diabetologia*, *55*(12), 3262-3272.
137. Marivin, A., Berthelet, J., Plenchette, S., & Dubrez, L. (2012). The inhibitor of apoptosis (IAPs) in adaptive response to cellular stress. *Cells*, *1*(4), 711-737.
138. Marshall, C., Hitman, G. A., Partridge, C. J., Clark, A., Ma, H., Shearer, T. R., & Turner, M. D. (2005). Evidence that an isoform of calpain-10 is a regulator of exocytosis in pancreatic β-cells. *Molecular endocrinology*, *19*(1), 213-224.
139. McKenna, T. (2009). *Oxidative stress on mammalian cell cultures during recombinant protein expression* (Doctoral dissertation, Linköping University Electronic Press).
140. Miyazaki, J. I., Araki, K., Yamato, E., Ikegami, H., Asano, T., Shibasaki , Y., … & YAMAMURA, K. I. (1990). Establishment of pancreatic β cell line that retains glucose-inducible insulin secretion: special reference to expression of glucose transporter isoforms. *Endocrinology*, *127*(1), 126-132.
141. Nagamatsu, S., Nakamichi, Y., Watanabe, T., Matsushima, S., Yamaguchi, S., Ni, J., ... & Ishida, H. (2001). Localization of cellubrevin-related peptide, endobrevin, in the early endosome in pancreatic beta cells and its physiological function in exo-endocytosis of secretory granules. *Journal of cell science*, *114*(1), 219-227.
142. Nagamatsu, S., Nakamichi, Y., Yamamura, C., Matsushima, S., Watanabe, T., Ozawa, S., ... & Ishida, H. (1999). Decreased expression of t-SNARE, syntaxin 1, and SNAP-25 in pancreatic beta-cells is involved in impaired insulin secretion from diabetic GK rat islets: restoration of decreased t-SNARE proteins improves impaired insulin secretion. *Diabetes*, *48*(12), 2367-2373.
143. Namazi, H., Fathi, F., & Heydari, A. (2012). Nanoparticles based on modified polysaccharides. In *The delivery of nanoparticles*. InTech.

144. Nangia-Makker, P., Hogan, V., Honjo, Y., Baccarini, S., Tait, L., Bresalier, R., & Raz, A. (2002). Inhibition of human cancer cell growth and metastasis in nude mice by oral intake of modified citrus pectin. *Journal of the National Cancer Institute*, *94*(24), 1854-1862.
145. Nathan, D. M., Buse, J. B., Davidson, M. B., Ferrannini, E., Holman, R. R., Sherwin, R., & Zinman, B. (2009). Medical management of hyperglycemia in type 2 diabetes: a consensus algorithm for the initiation and adjustment of therapy. *Diabetes care*, *32*(1), 193-203.
146. National Institute of Diabetes and Digestive and Kidney Diseases. 2015. Retrieved from https://www.niddk.nih.gov/health-information/kidney-disease/diabetes-insipidus
147. National Institute of Health. 1998. Retrieved from https://www.ncbi.nlm.nih.gov/books/NBK22223/pdf/Bookshelf_NBK22223.pdf.
148. Nemeth, E., & Ganz, T. (2009). The role of hepcidin in iron metabolism. *Acta haematologica*, *122*(2-3), 78.
149. NHS UK. 2019, November 14. Retrieved from https://www.nhs.uk/conditions/haemochromatosis/treatment/.
150. Nicholls, D. G. (2008). Forty years of Mitchell's proton circuit: From little grey books to little grey cells. *Biochimica et Biophysica Acta (BBA)-Bioenergetics*, *1777*(7-8), 550-556.
151. Nicolas, G., Bennoun, M., Devaux, I., Beaumont, C., Grandchamp, B., Kahn, A., & Vaulont, S. (2001). Lack of hepcidin gene expression and severe tissue iron overload in upstream stimulatory factor 2 (USF2) knockout mice. *Proceedings of the National Academy of Sciences*, *98*(15), 8780-8785.
152. Palit, S., Kar, S., Sharma, G., & Das, P. K. (2015). Hesperetin induces apoptosis in breast carcinoma by triggering accumulation of ROS and activation of ASK1/JNK pathway. *Journal of cellular physiology*, *230*(8), 1729-1739.
153. Panter, S. S. (1994). [32] Release of iron from hemoglobin. *Methods in enzymology*, *231*, 502-514.
154. Ohara-Imaizumi, M., Fujiwara, T., Nakamichi, Y., Okamura, T., Akimoto, Y., Kawai, J., ... & Nagamatsu, S. (2007). Imaging analysis reveals mechanistic differences between first-and second-phase insulin exocytosis. *The Journal of cell biology*, *177*(4), 695-705.
155. Papanikolaou, G., & Pantopoulos, K. (2005). Iron metabolism and toxicity. *Toxicology and applied pharmacology*, *202*(2), 199-211.
156. Papaspyros, N. S. (1964). *The history of diabetes mellitus* (Vol. 1964). G. Thieme.
157. Paradkar, P. N., Zumbrennen, K. B., Paw, B. H., Ward, D. M., & Kaplan, J. (2009). Regulation of mitochondrial iron import through differential turnover of mitoferrin 1 and mitoferrin 2. *Molecular and cellular biology*, *29*(4), 1007-1016.
158. Patterson, J. N., Cousteils, K., Lou, J. W., Fox, J. E. M., MacDonald, P. E., & Joseph, J. W. (2014). Mitochondrial metabolism of pyruvate is essential for regulating glucose-stimulated insulin secretion. *Journal of Biological Chemistry*, *289*(19), 13335-13346.

159. Paul, B. T., Manz, D. H., Torti, F. M., & Torti, S. V. (2017). Mitochondria and Iron: current questions. *Expert review of hematology*, *10*(1), 65-79.
160. Perry, S. W., Norman, J. P., Barbieri, J., Brown, E. B., & Gelbard, H. A. (2011). Mitochondrial membrane potential probes and the proton gradient: a practical usage guide. *Biotechniques*, *50*(2), 98.
161. Pfanner, N., & Geissler, A. (2001). Versatility of the mitochondrial protein import machinery. *Nature reviews Molecular cell biology*, *2*(5), 339.
162. Picard, M., Shirihai, O. S., Gentil, B. J., & Burelle, Y. (2013). Mitochondrial morphology transitions and functions: implications for retrograde signaling?. *American Journal of Physiology-Regulatory, Integrative and Comparative Physiology*, *304*(6), R393-R406.
163. Pizzino, G., Irrera, N., Cucinotta, M., Pallio, G., Mannino, F., Arcoraci, V., ... & Bitto, A. (2017). Oxidative stress: harms and benefits for human health. *Oxidative medicine and cellular longevity*, *2017*.
164. Ramos, C. L., Pou, S., Britigan, B. E., Cohen, M. S., & Rosen, G. M. (1992). Spin trapping evidence for myeloperoxidase-dependent hydroxyl radical formation by human neutrophils and monocytes. *Journal of Biological Chemistry*, *267*(12), 8307-8312.
165. Ren, J., Jin, P., Wang, E., Liu, E., Harlan, D. M., Li, X., & Stroncek, D. F. (2007). Pancreatic islet cell therapy for type I diabetes: understanding the effects of glucose stimulation on islets in order to produce better islets for transplantation. *Journal of translational medicine*, *5*(1), 1.
166. Riemer, J., Hoepken, H. H., Czerwinska, H., Robinson, S. R., & Dringen, R. (2004). Colorimetric ferrozine-based assay for the quantitation of iron in cultured cells. *Analytical biochemistry*, *331*(2), 370-375.
167. Rizo, J., & Südhof, T. C. (2002). Snares and Munc18 in synaptic vesicle fusion. *Nature Reviews Neuroscience*, *3*(8), 641.
168. Roglic, G. (2016). WHO Global report on diabetes: A summary. *International Journal of Noncommunicable Diseases*, *1*(1), 3.
169. Rose, S., Frye, R. E., Slattery, J., Wynne, R., Tippett, M., Pavliv, O., ... & James, S. J. (2014). Oxidative stress induces mitochondrial dysfunction in a subset of autism lymphoblastoid cell lines in a well-matched case control cohort. *PloS one*, *9*(1), e85436.
170. Rouzes, C., Leonard, M., Durand, A., & Dellacherie, E. (2003). Influence of polymeric surfactants on the properties of drug-loaded PLA nanospheres. *Colloids and Surfaces B: Biointerfaces*, *32*(2), 125-135.
171. Roy, C. N., & Enns, C. A. (2000). Iron homeostasis: new tales from the crypt. *Blood*, *96*(13), 4020-4027.
172. Schmidt, W. E., Siegel, E. G., & Creutzfeldt, W. (1985). Glucagon-like peptide-1 but not glucagon-like peptide-2 stimulates insulin release from isolated rat pancreatic islets. *Diabetologia*, *28*(9), 704-707.
173. Schröder, D., & Zühlke, H. (1982). Gene technology, characterization of insulin gene and the relationship to diabetes research. *Endokrinologie*, *79*(2), 197-209.

174. Harris, S. (1946). *Banting's miracle: The story of the discovery of insulin*. Dent.
175. Shaaban, M. A., Dawod, A. E. A., & Nasr, M. A. (2016). Role of iron in diabetes mellitus and its complications. *Menoufia Medical Journal*, *29*(1), 11.
176. Shaw, G. C., Cope, J. J., Li, L., Corson, K., Hersey, C., Ackermann, G. E., ... & Trede, N. S. (2006). Mitoferrin is essential for erythroid iron assimilation. *Nature*, *440*(7080), 96.
177. Sheth, S., & Brittenham, G. M. (2000). Genetic disorders affecting proteins of iron metabolism: clinical implications. *Annual review of medicine*, *51*(1), 443-464.
178. Siah, C. W., Ombiga, J., Adams, L. A., Trinder, D., & Olynyk, J. K. (2006). Normal iron metabolism and the pathophysiology of iron overload disorders. *Clinical Biochemist Reviews*, *27*(1), 5.
179. Siems, W. G., Grune, T., & Esterbauer, H. (1995). 4-Hydroxynonenal formation during ischemia and reperfusion of rat small intestine. *Life sciences*, *57*(8), 785-789.
180. Singh, R. P., Sharad, S., & Kapur, S. (2004). Free radicals and oxidative stress in neurodegenerative diseases: relevance of dietary antioxidants. *J Indian Acad Clin Med*, *5*(3), 218-225.
181. Skelin, M., Rupnik, M., & Cencič, A. (2010). Pancreatic beta cell lines and their applications in diabetes mellitus research. *ALTEX-Alternatives to animal experimentation*, *27*(2), 105-113.
182. Smotra S, Kudyar RP. Relationship between serum ferritin and type-2 diabetes mellitus. Journal Knowledge Science, published in Jammu and Kashmir, 2008;10:170-4.
183. Soejima, A., Inoue, K., Takai, D., Kaneko, M., Ishihara, H., Oka, Y., & Hayashi, J. I. (1996). Mitochondrial DNA is required for regulation of glucose-stimulated insulin secretion in a mouse pancreatic β-cells line, MIN6. *Journal of Biological Chemistry*,*271*(42), 26194-26199.
184. Sola, D., Rossi, L., Schianca, G. P. C., Maffioli, P., Bigliocca, M., Mella, R., ... & Derosa, G. (2015). Sulfonylureas and their use in clinical practice. *Archives of medical science: AMS*, *11*(4), 840.
185. Stadtman, E. R. (1990). Metal ion-catalyzed oxidation of proteins: biochemical mechanism and biological consequences. *Free Radical Biology and Medicine*, *9*(4), 315-325.
186. Stadtman, E. R., & Levine, R. L. (2003). Free radical-mediated oxidation of free amino acids and amino acid residues in proteins. *Amino acids*, *25*(3-4), 207-218.
187. Stankowski, J. N., Codreanu, S. G., Liebler, D. C., & McLaughlin, B. (2011). Analysis of protein targets by oxidative stress using the oxyblot and biotin–avidin-capture methodology. In *Cell Culture Techniques* (pp. 365-381). Humana Press.

188. Stehling, O., & Lill, R. (2013). The role of mitochondria in cellular iron–sulfur protein biogenesis: mechanisms, connected processes, and diseases. *Cold Spring Harbor perspectives in biology*, *5*(8), a011312.
189. Takenouchi, T., Sekiyama, K., Tsukimoto, M., Iwamaru, Y., Fujita, M., Sugama, S., ... & Hashimoto, M. (2015). Role of Autophagy in P2X7 Receptor-Mediated Maturation and Unconventional Secretion of IL-1β in Microglia. In *Autophagy: Cancer, Other Pathologies, Inflammation, Immunity, Infection, and Aging* (pp. 211-222). Academic Press.
190. Thurmond, D. C. (2007). Regulation of insulin action and insulin secretion by SNARE-mediated vesicle exocytosis. In *Mechanisms of Insulin Action* (pp. 52-70). Springer, New York, NY.
191. Tsukiyama, K., Yamada, Y., Yamada, C., Harada, N., Kawasaki, Y., Ogura, M., ... & Udagawa, N. (2006). Gastric inhibitory polypeptide as an endogenous factor promoting new bone formation after food ingestion. *Molecular Endocrinology*, *20*(7), 1644-1651.
192. Turrens, J. F. (2003). Mitochondrial formation of reactive oxygen species. *The Journal of physiology*, *552*(2), 335-344.
193. Tyler, D. D. (1992). *The mitochondrion in health and disease*. VCH.
194. Type 2 Diabetes. 2017, August 13. Retrieved from http://www.diabetes.co.uk/type2-diabetes.html
195. Ungar, D., & Hughson, F. M. (2003). SNARE protein structure and function. *Annual review of cell and developmental biology*, *19*(1), 493-517.
196. Unger, R. H. (2003). Minireview: weapons of lean body mass destruction: the role of ectopic lipids in the metabolic syndrome. *Endocrinology*, *144*(12), 5159-5165.
197. Valko, M., Leibfritz, D., Moncol, J., Cronin, M. T., Mazur, M., & Telser, J. (2007). Free radicals and antioxidants in normal physiological functions and human disease. *The international journal of biochemistry & cell biology*, *39*(1), 44-84.
198. Valko, M., Rhodes, C., Moncol, J., Izakovic, M. M., & Mazur, M. (2006). Free radicals, metals and antioxidants in oxidative stress-induced cancer. *Chemico-biological interactions*, *160*(1), 1-40.
199. Wang, J., & Wang, H. (2017). Oxidative stress in pancreatic beta cell regeneration. *Oxidative medicine and cellular longevity*, *2017*.
200. Wang, X., & Robbins, J. (2014). Proteasomal and lysosomal protein degradation and heart disease. *Journal of molecular and cellular cardiology*, *71*, 16-24.
201. Weir, G. C. (1994). Pathogenesis of non-insulin-dependent (type II) diabetes mellitus. *Joslin's Diabetes Mellitus*.
202. Wild, S. H., Roglic, G., Green, A., Sicree, R., & King, H. (2004). Global prevalence of diabetes: estimates for the year 2000 and projections for 2030: response to Rathman and Giani. *Diabetes care*, *27*(10), 2569-2569.

203. Willis, M. S., & Patterson, C. (2013). Proteotoxicity and cardiac dysfunction—Alzheimer's disease of the heart?. *New England Journal of Medicine*, *368*(5), 455-464.
204. World Health Organization. (2008). Worldwide prevalence of anaemia 1993-2005: WHO global database on anaemia.
205. World Health Organization. (2014). Global health estimates: Deaths by cause, age, sex and country, 2000-2012. *Geneva, WHO*, *9*.
206. Wu, M., Neilson, A., Swift, A. L., Moran, R., Tamagnine, J., Parslow, D., ... & Chomicz, S. (2007). Multiparameter metabolic analysis reveals a close link between attenuated mitochondrial bioenergetic function and enhanced glycolysis dependency in human tumor cells. *American Journal of Physiology-Cell Physiology*, *292*(1), C125-C136.
207. Yamada, C., Yamada, Y., Tsukiyama, K., Yamada, K., Udagawa, N., Takahashi, N., ... & Inagaki, N. (2008). The murine glucagon-like peptide-1 receptor is essential for control of bone resorption. *Endocrinology*, *149*(2), 574-579.
208. Yang, L., Kuang, J., Li, Z., Zhang, B., Cai, X., & Zhang, L. M. (2008). Amphiphilic cholesteryl-bearing carboxymethylcellulose derivatives: self-assembly and rheological behaviour in aqueous solution. *Cellulose*, *15*(5), 659-669.
209. Yusoff, A. A. M. (2015). Role of mitochondrial DNA mutations in brain tumors: A mini-review. *Journal of cancer research and therapeutics*, *11*(3), 535.
210. Zander, M., Madsbad, S., Madsen, J. L., & Holst, J. J. (2002). Effect of 6-week course of glucagon-like peptide 1 on glycaemic control, insulin sensitivity, and β-cell function in type 2 diabetes: a parallel-group study. *The Lancet*, *359*(9309), 824-830.
211. Zhang, N., Wardwell, P. R., & Bader, R. A. (2013). Polysaccharide-based micelles for drug delivery. *Pharmaceutics*, *5*(2), 329-352.
212. Zorov, D. B., Juhaszova, M., & Sollott, S. J. (2014). Mitochondrial reactive oxygen species (ROS) and ROS-induced ROS release. *Physiological reviews*, *94*(3), 909-950.